USP-2
00-26

Towards the real-time use of Quikscat winds

A. Stoffelen
J. de Vries
A. Voorrips

BCRS 00-26 MD

MISSIE REMOTE SENSING

Towards the real-time use of Quikscat winds

A. Stoffelen
J. de Vries
A. Voorrips

Royal Netherlands Meteorological Institute
(KNMI)

USP-2 report 00-26
USP-2 project 1.1/DE-04
ISBN 90 54 11 330 8

February 2001

This report describes a project carried out in the framework of the User Support Programme
(USP-2) under responsibility of the Netherlands Remote Sensing Board (BCRS)

EXECUTIVE SUMMARY

ERS scatterometer observations have proven important for the forecasting of dynamical weather, such as tropical cyclones. Recently, SeaWinds scatterometer measurements from QuikScat have become available. SeaWinds on QuikSCAT provides great coverage over the oceans. However, quality monitoring, rain contamination, wind direction noise characteristics, and wind direction ambiguity selection need further study to allow routine use in weather forecasting.

We describe our work on QuikScat product validation and inversion of the backscatter data to winds. A new procedure to quality control (QC) SeaWinds scatterometer observations, in particular to screen out rain-contaminated Wind Vector Cells (WVC), and a new procedure to assimilate QuikScat observations are developed at KNMI. The QC method is based on a methodology that was used to screen anomalous ERS and NSCAT backscatter triplets or quadruplets respectively. The methodology checks whether the consistency of the backscatter measurements at a particular WVC is compatible with the consistency as predicted by the Geophysical Model Function (GMF). Rain contaminated points are screened out effectively thus opening the way to effective wind information assimilation.

The noise in the 25-km SeaWinds wind direction has detrimental effects on usefulness of the winds. We attempted to reduce the noise by providing a coarser resolution product. We made checks that the inversion at 100-km resolution is performed without systematic biases in the winds, and verified the better spatial consistency and at this resolution for low winds (tropics). However, further optimisation and validation of the GMF and the inversion process are recommended, in particular for the higher wind speeds. Improved spatial consistency is beneficial for a successful ambiguity removal. 100-km SeaWinds first-rank solution appear much better as the 25-km winds.

The ERS scatterometer two-dimensional variational ambiguity removal procedure, called 2D-VAR, is generalised to deal with ambiguous solution sets with more than two solutions of varying probability and quality. ERS provides two ambiguities with about the same quality and probability. Extension of the assimilation procedure is essential to deal with the average 83% probability of the first rank SeaWinds solution and the occurrence of occasional high-probability third and fourth rank solutions. Moreover, it opens the way to the assimilation of the SeaWinds backscatter data in those WVC where the wind vector is not well determined, in particular the outer swath where only two azimuth looks are available. The on average high rank-one probability makes the ambiguity removal successful in many cases even though third and fourth rank solutions are often present.

2D-VAR products were validated both objectively and subjectively. The objective validation resulted in a skill comparable to the JPL product. Refined objective tests are recommended to highlight differences between the schemes. KNMI meteorologists subjectively evaluated selected cases where SeaWinds deviates substantially from the numerical weather prediction reference wind field. It is found that the SeaWinds products are reliable in the so-called sweet parts of the swath, but of more variable quality in the nadir region; the outer swath was not considered here. Further subjective evaluation is ongoing to help evaluate the tuning of the processing system.

The real-time use of SeaWinds data can only be reliable if appropriate quality monitoring and control routines are operated. The quality information should be available and provided at the same time as the winds. As was found for ERS, the WVC quality control rejection rate, the normalised inversion residual and the wind speed bias and wind direction standard deviation against a NWP model provide effective instrument and processing monitoring parameters. They can be used to provide guidance as to whether the real-time SeaWinds wind vector data are of nominal quality.

The SeaWinds quality control, inversion, monitoring, and 2D-VAR as described here are an excellent preparation for the assimilation of scatterometer winds in variational meteorological analyses, such as 3D-VAR in HIRLAM or 4D-VAR at ECMWF, since the methodologies are the same and the main challenge in the assimilation of scatterometer winds lies in the ambiguity removal. At the current level of processing, variational analysis quality control schemes may become slightly more active than in case of ERS scatterometer data, although we did not include any of the common gross quality checks in 2D-VAR. Moreover, the 2D-VAR product is useful for operational meteorologists in nowcasting or short-range forecasting, and for use with OI data assimilation. As such, we expect that the work described here paves the way to the successful use of SeaWinds for meteorological forecasts and analyses.

PREFACE

The work in this report was funded by the BCRS in the context of the Netherlands Remote Sensing Programme (NRSP). The objective of the work described in this report is the timely development of a good quality near-real time wind product from SeaWinds guaranteed in the time frame between now and the METOP mission. The well-established scatterometer user community at large benefits from this activity, providing high-coverage scatterometer wind data in time. Here, we in particular demonstrate its benefit for NWP in Europe, and for the direct use by meteorologists at KNMI. KNMI has much experience on wind extraction from scatterometer data involving many projects. Within the Ocean and Sea Ice SAF the wind processing for ASCAT on METOP is prepared using ERS scatterometer data, serving the European user community at large. By using scatterometer winds with larger coverage such as SeaWinds, this preparation for ASCAT could be made more optimal. With the help of a EUMETSAT fellowship, KNMI participates in the work on the validation and interpretation of QuikScat data. In this work, KNMI collaborated with NASA and other European entities, such as the ECMWF, to demonstrate the methodology for the interpretation of QuikSCAT data, including aspects such as data validation, data quality control, and wind retrieval. In the NWP SAF KNMI collaborates with ECMWF and the Meteorological Office of the UK to develop a methodology for assimilation and monitoring of SeaWinds observations.

CONTENTS

1 INTRODUCTION

ERS scatterometer winds have proven to be very useful for the forecasting of dynamic weather (Isaksen and Stoffelen, 2000). Increased coverage, such as from tandem ERS-1 and ERS-2 measurements, clearly improve the forecasts of extreme events (e.g., Stoffelen and Beukering, 1998; Le Meur et al, 1997). Improved coverage from the Ku-band scatterometers NSCAT and SeaWinds have thus great potential (Atlas and Hoffman, 2000). See also figures 1.2-3. Preliminary attempts to assimilate SeaWinds data have been carried out with mixed success and improved data characterisation and assimilation procedures are needed (Leidner and Isaksen, 2000).

Severe storms that hit Europe often originate over the North Atlantic Ocean, where sparse meteorological observations are available. As a consequence, the initial stage of severe storms is often poorly analysed and their development poorly predicted (ESA, 1999, WMO, 2000). The SeaWinds data coverage is such that developing storms are likely hit, thus depicting their position and amplitude. For example, the Netherlands was hit by a storm in late May 2000 when three people were killed. Appropriate storm warnings for the public were issued by KNMI a day before the storm occurred. However, the meteorologist on duty had little observational evidence of the precise position and amplitude of the meteorological disturbance leading to the storm and furthermore the available meteorological models were not consistent. SeaWinds data were available on the critical location and time and could have provided more confidence on the necessity to issue storm warnings. However, the SeaWinds product as available from NOAA was contaminated by serious ambiguity removal errors and did not provide any meteorological guidance, as depicted in figure 1.1. In such cases, SeaWinds product improvement as described in this report is essential.

The SeaWinds on QuikSCAT mission from NASA is a "quick recovery" mission to fill the gap created by the loss of data from the NASA Scatterometer (NSCAT) after the ADEOS-1 satellite lost power in June 1997. QuikSCAT was launched from Vandenberg Air Force Base (USA) in June 19, 1999. A similar version of the SeaWinds instrument will fly on the Japanese ADEOS-II satellite currently scheduled for launch in late 2001. SeaWinds on QuikSCAT and on ADEOS-II in late 2001 may provide a bridge between the ERS and METOP missions in case that the ERS-2 scatterometer instrument fails and then provide a continuous scatterometer data availability to suit the well-established meteorological user community. Furthermore, the wide swath of SeaWinds is a potentially large resource for near-surface wind information.

Because of the fortuitous antenna configuration of the ERS scatterometers, a practical and straightforward solution for the inversion problem exists (Stoffelen, 1998). In case of NSCAT, the antenna geometry is less ideal, but this is compensated by the use of a fourth measurement in horizontal polarisation for the mid beam; ERS uses only vertical polarisation measurements. The SeaWinds instrument is a conically scanning pencil-beam scatterometer, which in comparison with the NSCAT fan-beam scatterometer has the following advantages: higher signal-to-noise ratio, smaller in size, and superior coverage. On the other hand, the SeaWinds scanning scatterometer concept poses new challenges to an effective extraction of wind information. QuikSCAT has an antenna illumination pattern that is dependent on node number or cross-track location, due to its circular scans on the ocean. The skill of the wind retrieval algorithm depends very much on the number of measurements and their polarization (horizontal HH or vertical VV) and azimuth diversity, where "azimuth diversity" is defined as the spread of the azimuth looks among the measurements in the WVC. The nadir region has fore and aft looks of both beams (HH and VV) nearly 180° apart. At the edges of the swath the outer VV beam fore and aft looks are nearly in the same direction and no inner HH beam information is available. In both areas, the skill of the wind

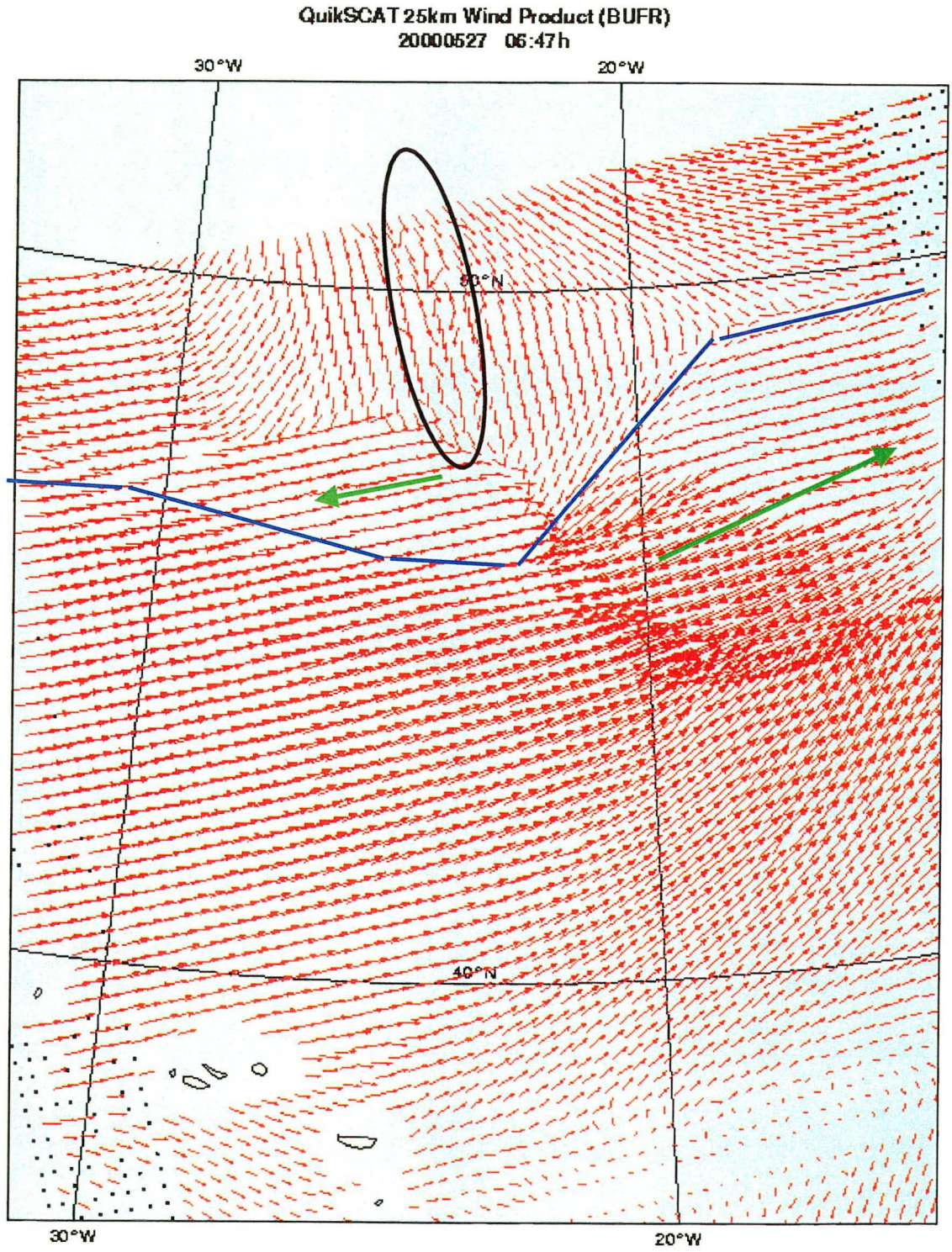

Figuur 1.1: QuikScat winds on 27 May around 45N and 20W in an area where a damaging storm is developing. The blue line depicts the polar front on the basis of meteorological information from the ECMWF model and available real-time observations. The green arrows denote areas where the QuikScat Ambiguity removal has resulted in a solution opposite to that expected. The back circle denotes very noisy winds. The near-real time QuikScat winds from NOAA constitute a poor product in this case.

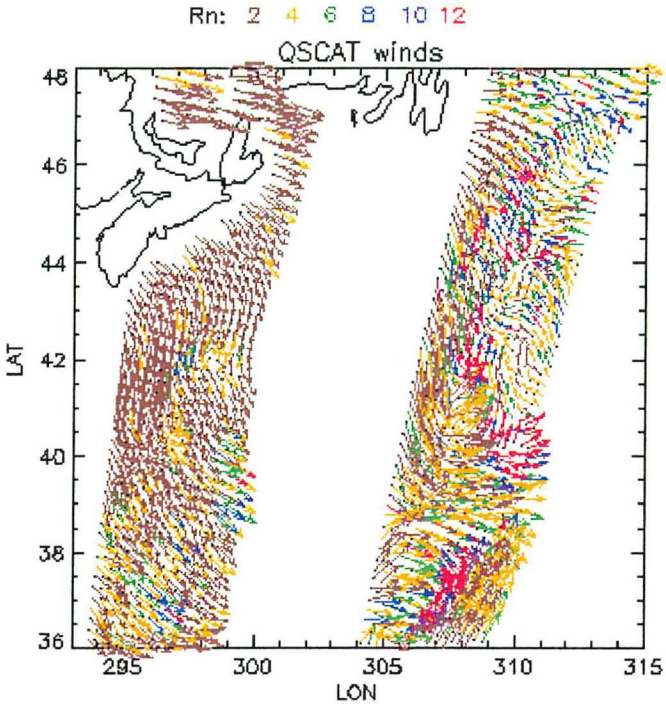

Figure 2.1: QuikScat winds in the Atlantic in the development zone of the devastating storms that hit Western Europe during Christmas 1999. Date and time of observation are December 24 22 GMT. The inversion residual is normalised as a function of speed and WVC, such that a number Rn results with an expectation value of one. Rn values for good quality winds between 2 and 4 are thus unlikely, and winds at values above 4 are verified to be generally of bad quality (Portabella and Stoffelen, 2000). The colour code for the Rn values is shown above the plot. Anomalous winds have generally Rn > 4. For Rn < 4 large areas remain that depict relevant and important mesoscale features of the wind field.

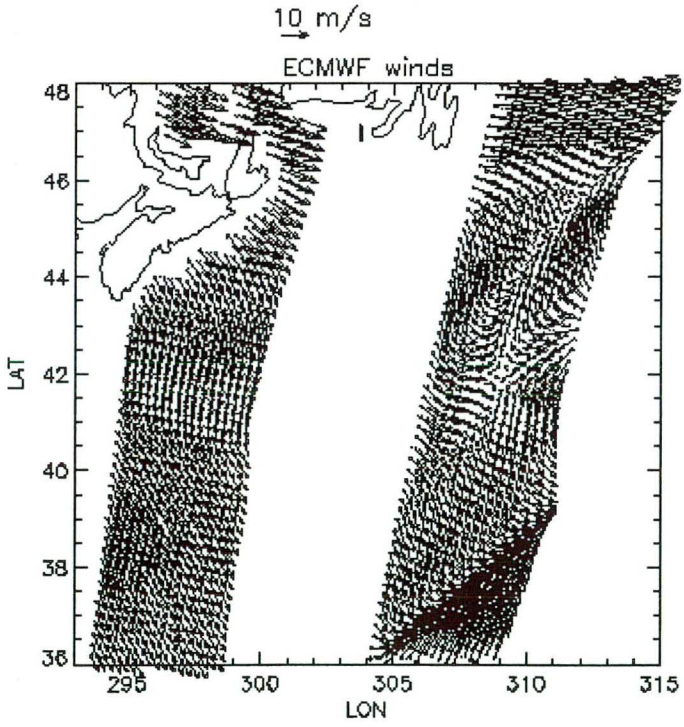

Figure 1.3: As figure 1.2, but ECMWF winds. Dynamical features particularly appearing in the right SeaWinds swath are not well represented in the ECMWF first guess, for example the through orientation and position, and the low at 308E and 41N.

retrieval algorithm is decreased with respect to the rest of the swath (called the sweet zone) where there are four measurements (fore-HH, fore-VV, aft-HH and aft-VV) with enough azimuth diversity.

To demonstrate the capabilities of QuikSCAT, we will focus on that part of the swath, 1100 km wide, where four backscatter measurements are available, with different azimuth and/or polarisation. In that case the interpretation problem is similar to NSCAT and a quality-assured wind product can be developed. The inversion software based on the ERS scatterometer processing

(Stoffelen, 1998) modified by Figa (Figa and Stoffelen, 1999) for NSCAT has been adapted for QuikSCAT. In was verified to closely mimic JPL's inversion (Portabella and Stoffelen, 2000) and is used throughout this report. SeaWinds simulations confirm a higher standard deviation of speeds and directions in the outer and nadir parts compared to the sweet zone of the swath. No significant bias is seen in any part of the swath.

1.1 APPROACH

To demonstrate SeaWinds on QuikSCAT the following steps need to be taken:

- ocean backscatter calibration and validation (e.g., Stoffelen, 1999; Stoffelen and Anderson, 1998; Stoffelen, 1997; Stoffelen and Beukering, 1997; and Figa and Stoffelen, 1999);
- wind retrieval algorithm (e.g., Stoffelen and Anderson, 1998 and 1993; Figa and Stoffelen, 1999);
- wind and radar backscatter quality control algorithms (Stoffelen and Anderson, 1998 and 1997; Stoffelen and Beukering, 1997;
- including rain detection (Figa and Stoffelen, 2000; Portabella and Stoffelen, 2000);
- ambiguity removal (Stoffelen and Anderson, 1997; de Vries and Stoffelen, 2000); and
- monitoring methodology (Stoffelen, 1998b; Le Meur et al, 1998);

After ocean calibration and noise characterisation of the backscatter measurements as reported in section 2, the existing wind retrieval methodology can be applied over that part of the swath with sufficient azimuth and polarisation coverage. Section 3 discusses a better way of scatterometer wind validation. Section 5 discusses the implications of retrieving winds at 100-km resolution. The residual of the retrieval is used for ambiguity solution selection and (geophysical) quality control, as described in sections 4 and 6 respectively. It is a generalisation of what is being applied in PreScat at KNMI and ECMWF or as was developed for NSCAT at KNMI (Figa and Stoffelen, 2000; Portabella and Stoffelen, 2000). In particular rain elimination is very critical for SeaWinds (section 4). After the quality control and selection of potential solutions at each node, the ambiguity removal scheme is run. 2D-VAR (de Vries and stoffelen, 2000) is applied here as detailed in section 7. The performance of the processing scheme is validated both objectively and subjectively as discussed in section 8, whereafter in section 9 we discuss monitoring in near-real time, and a recommendation for operational implementation is made in the conclusive section 10 of the report.

1.2 QUIKSCAT DATA

For the simulations we used Seawinds BUFR data that had been disseminated by NOAA/NESDIS in near real time on March 1st and March 2nd 2000. The data was retrieved from the MARS archive at ECMWF.

Seawinds BUFR data has a record structure. A BUFR record contains observed Earth-located radar backscatter measurements and retrieved wind vector information, available at the time of processing, collocated in 25 x 25-km wind vector cells (WVC's). Each BUFR record consists of a row of between 1 and 76 WVC's depending on the number of observations present. If there are no observations the row is not stored. A row of WVC's corresponds to a single cross-track cut of the Seawinds instrument measurement swath and is uniquely identified by its row number and orbit number. In addition each WVC has a unique cell number. An orbit that covers the circumference of the Earth contains 1624 rows.

The backscatter measurements in the BUFR data are WVC-composites that are appropriately averaged finer grained σ^0 data. The finer grained σ^0 data can be either whole radar pulses or "eggs" or egg slices, which are range resolution elements of an egg. Per WVC four "flavours" of backscatter measurements (beams) can be present. Based on the antenna geometry we distinguish between a for-inner, fore-outer, aft-inner and aft-outer beam. For each WVC the antenna geometry is different so additional parameters/flags are present describing the measurement conditions. Described are beam geometry, σ^0-location, antenna polarisation, noise characteristics, the Earth's surface condition and σ^0-quality. Here we report generally on data from WVC's 13-28 and 49-64, corresponding to the "sweet part" of the swath.

2 BACKSCATTER DOMAIN

2.1 VISUALISATION

It is useful to visualise sets of measured σ^0 observations for (Stoffelen and Anderson, 1997a)

- checking the validity of the geophysical model function (GMF) that is used in the inversion;
- a visual check of the data to characterise noise and to identify outliers;
- depicting the geometry of the inversion problem

The most fruitful visualisation of the backscatter measurement (phase) space that was applied for ERS scatterometer data was to make a selection of $\sigma^0_{\text{fore}} + \sigma^0_{aft} \approx$ constant, and to plot $\sigma^0_{\text{fore}} - \sigma^0_{aft}$ against σ^0_{mid}. Why this is fruitful can be understood by elaborating on a rough expression of the GMF

$$\sigma^0(V,\phi;\theta,\alpha,p) = A_0 + A_1\cos(\phi-\alpha) + A_2\cos(2\phi-2\alpha) \tag{2.1}$$

where V is wind speed, ϕ wind direction with respect to the mid beam pointing direction, p the polarisation, θ the incidence angle, and α the azimuth look direction with respect to the mid beam pointing direction; $A_i = A_i(V,\theta,p)$, and, particularly for V-polarisation, $A_i << A_2$.. If, as for the ERS scatterometers, we further realise $\alpha_{\text{fore}} = -\alpha_{aft}$ we find

$$\begin{aligned} \sigma^0_{\text{fore}} + \sigma^0_{aft} &= 2A_0 + 2A_2\cos 2\alpha\cos 2\phi \\ \sigma^0_{\text{fore}} - \sigma^0_{aft} &= \quad 2A_2\sin 2\alpha\sin 2\phi \end{aligned} \tag{2.2}$$

where α is really α_{fore}. Since for ERS $\alpha_{\text{fore}} = 45^o$ and $\alpha_{mid} = 0^o$ we find the three independent coordinates

$$\begin{aligned} \sigma^0_{\text{fore}} + \sigma^0_{aft} &= 2A_0 \\ \sigma^0_{\text{fore}} - \sigma^0_{aft} &= 2A_2\sin 2\phi \\ \sigma^0_{\text{mid}} &= A^m_0 + A^m{}_2\cos 2\phi \end{aligned} \tag{2.3}$$

This means that taking a cross-section $\sigma^0_{\text{fore}} + \sigma^0_{aft}$ = constant, comes down to keeping the wind speed (almost) constant. Therefore, in such a cross-section where the axes are determined by the other two coordinates, one can easily draw the GMF curve that (almost) describes a double elliptical shape for varying ϕ, together with the measurement points, and hence simply check the validity of the GMF or the relative calibration of the fore and aft beams. Note that A_0 and A_2 increase with increasing wind speed such that in three dimensions the GMF describes a cone-like surface (Stoffelen, 1998).

The NASA scatterometer, NSCAT, on board the Japanese ADEOS-I was tested in a similar way. Here, a complication lies in the fact that in addition to vertical polarisation, horizontal polarisation is used on the mid fan beam, where no longer $A_i << A_2$ applies. The second complication is that the mid beam is at $\alpha_{mid} = 25^o$. Nevertheless, Figa and Stoffelen (1999) found a

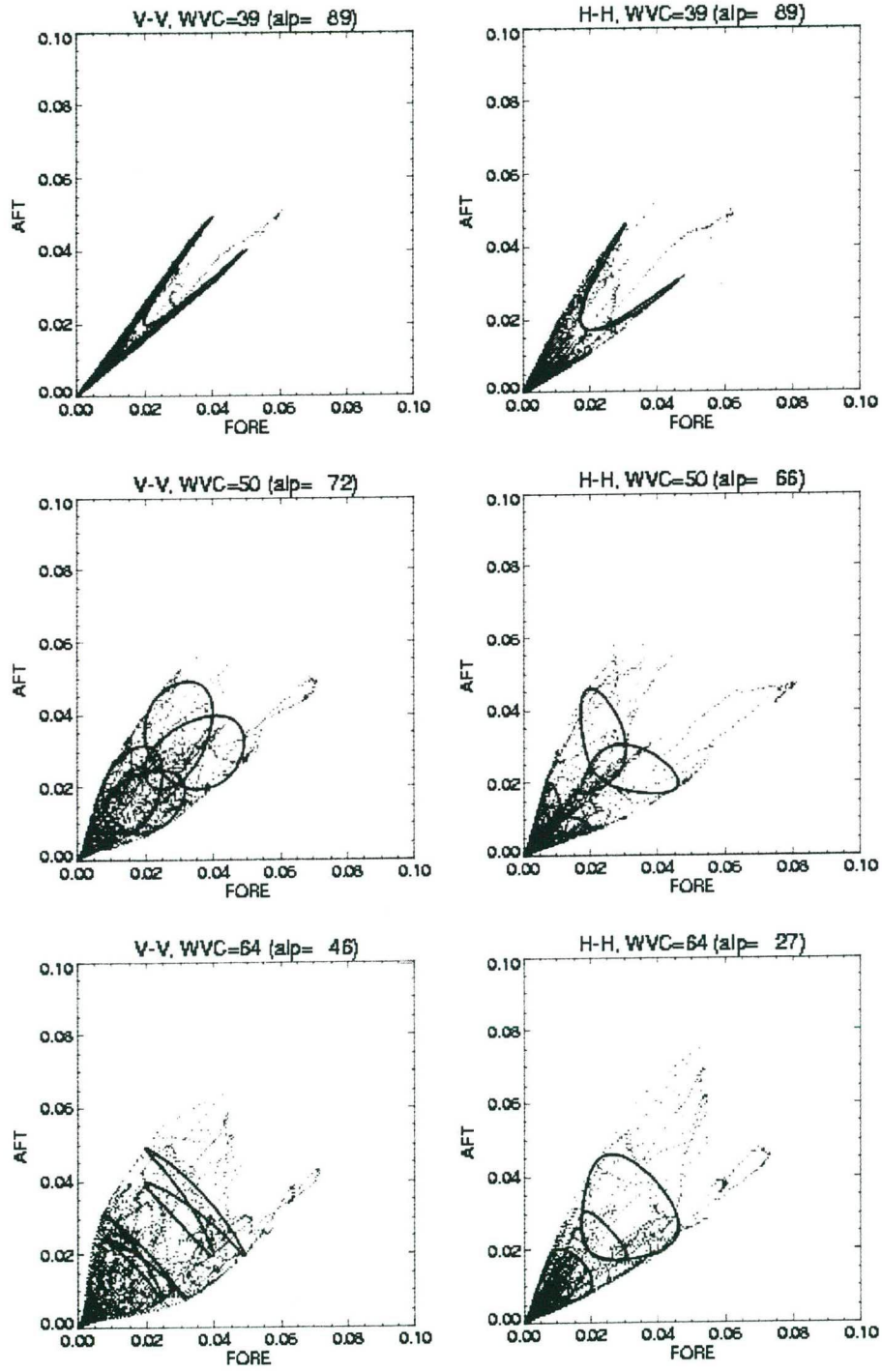

Figure 2.1: Scatter plot of backscatter values for the outer beam (left panels) and the inner beam (right panels), for simulated measurements without noise. Results are shown for WVC 39 (upper panels), 50 (middle), and 64 (lower panels). In the plot titles, the azimuth angle α of the antenna is given. The Lissajous-type figures correspond to the NSCAT-2 GMF for 10 and 15 m/s (a curve at 5 m/s has been drawn, but is lost in the cloud of points).

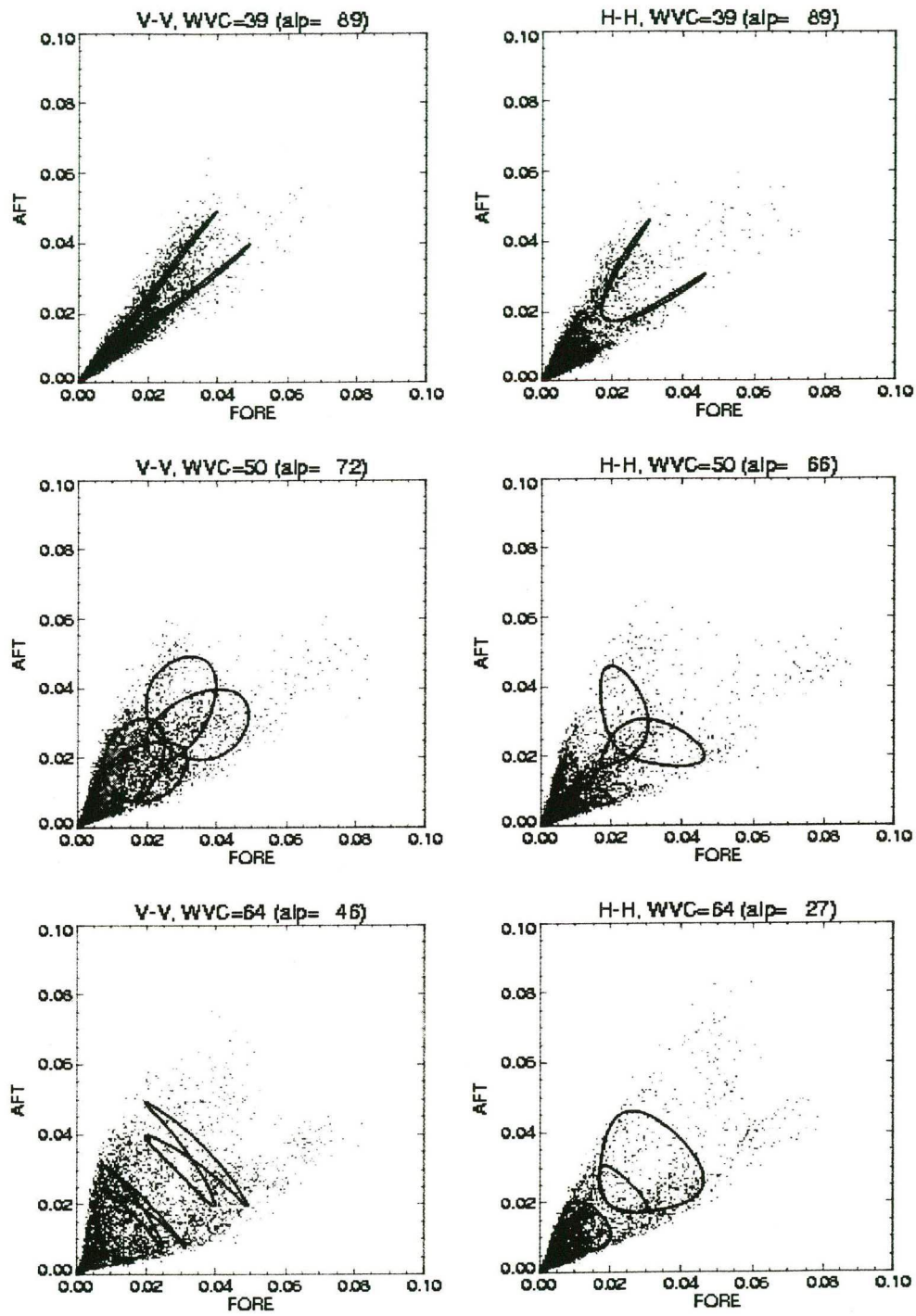

Figure 2.2: As figure 2.1, but now for simulated measurements with noise added.

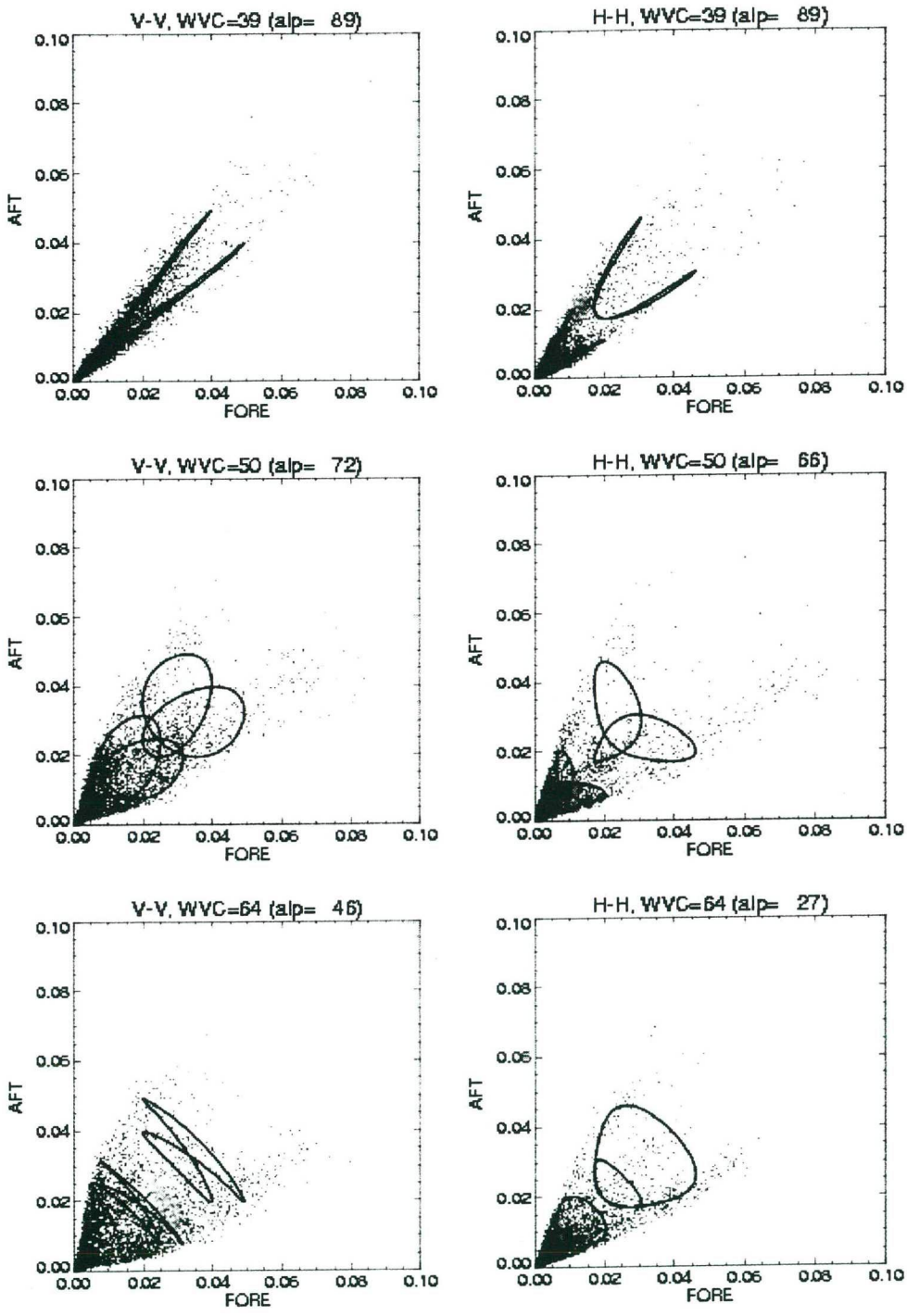

Figure 2.3: As figure 2.1, but now for real measurements.

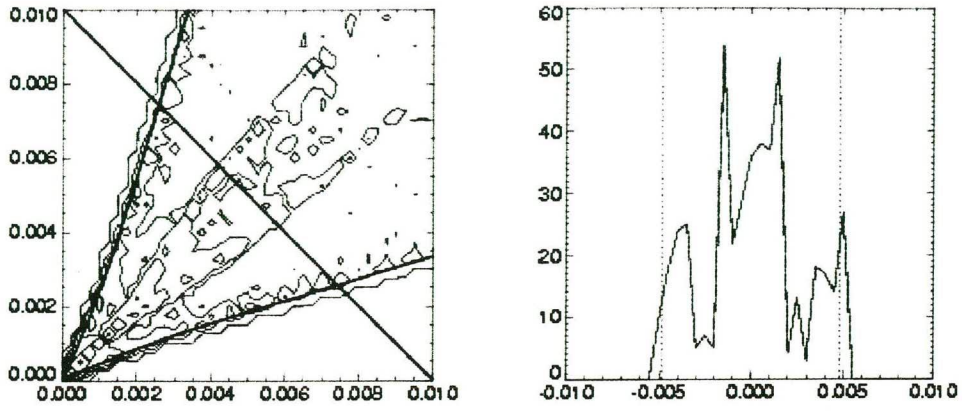

Figure 2.1: Left: Density-contoured scatter plot of backscatter values for the outer beam for simulated SeaWinds data at WVC 50 with nominally 142 degrees separation between fore and aft look. The scatter plot is build up from Lissajous-type curves that follow an inner revolution and an outer revolution as wind direction changes. The boundary of the outer revolution is shown by the thick lines from the origin outward produced using the NSCAT-2 GMF. Right: Number density along the cross-diagonal thick line of the left plot. The boundaries of the outer and inner Lissajous revolutions are now clearly discernible. Cross sections of this type are being used to validate aspects of the GMF definition.

convenient transformation, revealing relevant properties of the GMF. The transformation has however not been extensively tested in the inversion procedure.

For QuikScat the situation is more complicated, because α is varying with the distance from the satellite ground track and hence with WVC number. In fact, it is not clear what would be a sensible cut through the (2- or 4-dimensional) cone. Alternatively, we can simply plot σ^0_{fore} against σ^0_{aft} for all quadruplets, but separated for VV and HH. Examples are shown in figures 2.1-3. Figure 2.1 shows scatter plots for simulated data, without noise, for various parts of the swath. The Lissajous-type curves represent NSCAT-2 curves for constant wind speed and varying wind direction. It is clear that the form of these curves depends very much on the azimuth angle α. Note that for $\alpha = 45^o$ in the lower-left panel, the modulation of $\sigma^0_{\text{fore}} + \sigma^0_{aft}$ for given wind speed is indeed small. Already it is clear that the outer edge of these curves should coincide with the outer edge of the cloud of measurements, if the NSCAT-2 GMF is perfect and the measurements contain no noise. Also clear is that, due to the geometry of the GMF, the desity of points increases when the Lissajous curves are parallel to the diagonal. Figures 2.2-3 show the same scatter plots, but respectively with noise added according to the K_p values in the measurement files, and for the actual observed data. It is clear that the picture is blurred compared to the no-noise curves, and also that the density jumps associated with the diagonal direction of the Lissajous curves are less clear. But already we can conclude that the QuikScat measurements follow the NSCAT-2 GMF to a fair degree over the whole swath, and with a noise level that is realistically estimated from the observed data. This is, figures 2.2 and 2.3 appear very similar.

Figure 2.4 shows a refined analysis of the above, where twodimensional log-density contoured histograms are made of the scatter plots, and sections through these are plotted. In the contour plot (left) we have added for reference the theoretical outer edge of the Lissajous curves as shown before in figures 2.1-3, allowing easier comparison with the data points. In the right panel, the section through the contour plot shows nicely this outer edge. Moreover, an inner edge is observed at the

other location where the Lissajous curves are parallel to the diagonal and the data density peaks. One can infer that the inner distribution limited by the inner edges is mainly due to points with $\phi \in (-90^0, 90^o)$, and that the rest of the distribution with the outer edge peaks correspondsto all other ϕ. As such, this type of plot allows a more detailed analyses of the quality of the QuikScat GMF. Approaches include the separate plotting of points with $\phi \in (-90^0, 90^o)$ and those with all other values of ϕ, and compare the expected distributions with the real ones. We note that all WVC obey to the same GMF with only different α; the combination of cross-sections for all WVC thus reveals in principle sufficient relevant information on the wind speed and direction dependency of the GMF.

3 WIND VALIDATION

Figures 3.1 and 3.2 contain simple examples of twodimensional log-density contoured histograms that are used to intercompare JPL inverted, KNMI inverted, and NWP wind velovities. They show common examples of wind speed and direction comparisons that are usually accompanied by the associated wind component plots, presenting the same information in a transformed manner (Stoffelen, 1998). In this section we illustrate advanced methods of assessing scatterometer wind direction skill, thereby taking into account the ambiguous nature of these observations.

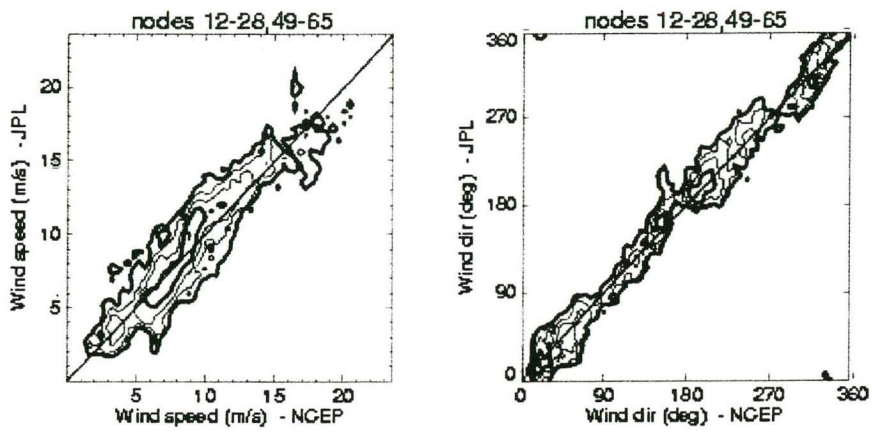

Speed		
N	=	19159
mean X	=	9.63 m/s
mean Y	-	9.82 m/s
mean Y-X	=	0.19 m/s
STD Y-X	=	2.08 m/s
Cor XY	=	0.87

Direction		
N	=	17166
mean X	=	171.25 deg
mean Y	-	173.04 deg
mean Y-X	=	1.78 deg
STD Y-X	=	18.67 deg
Cor XY	=	0.98

Figure 3.1: Example of joint distribution of the JPL inverted and NCEP wind speeds (left) and directions (right). Directions are with respect to the cross-track direction and JPL's closest to NCEP is used.

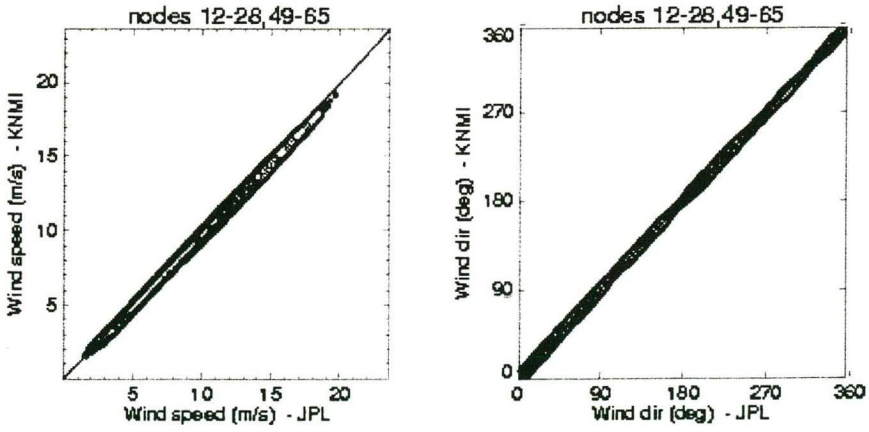

Speed		
N	=	19182
mean X	=	9.77 m/s
mean Y	-	9.47 m/s
mean Y-X	=	-0.30 m/s
STD Y-X	=	0.33 m/s
Cor XY	=	1.00

Direction		
N	=	17721
mean X	=	155.70 deg
mean Y	-	155.76 deg
mean Y-X	=	0.06 deg
STD Y-X	=	5.54 deg
Cor XY	=	1.00

Figure 3.2: Joint distribution of the JPL inverted and KNMI inverted wind speeds (left) and directions (right). Directions are with respect to the cross-track direction and KNMI's closest to JPL is used.

3.1 WIND DIRECTION SKILL

As illustrated in figure 3.1, one can validate the inverted wind directoion against a reference wind direction, such as from NWP models or buoys, by taking the closest to the reference, and computing the RMS difference. However, it is clear that the more ambiguous solutions are provided by the inversion, the *smaller* the RMS will be, because the chance that one of the solutions will be close to the wind reference will increase. In the limite of an infinite amount of observations, the RMS will even be zero, while the information content of the set of solutions in reality *decreases* with an increasing number of solutions, because there is no a priori way to say which of the solutiuons is the correct one. To avoid this problem, one can validate the selected (by AR) or the rank-1 solutions, but since both rank-1 skill and AR skill are not perfect, these approaches reveal a pessimistic view on the inherent information content of the scatterometer regarding wind direction. One may expect that the rank-1 skill and the AR skill generally decrease with an increasing number of solutions.

Therefore, we attempt here to define a "normalised" RMS (NRMS) difference, which reflects in a fair way the quality of the closest solution. This NRMS contains a normalisation factor which is equal to the expected value in the case that there is no skill in the system

$$NRMS = RMS\left(\frac{\phi^C - \phi^T}{\left\langle \left(\phi^C - \phi^T\right)^2 \right\rangle^{1/2}} \right) \tag{3.1}$$

where ϕ^T is the true wind direction, ϕ^C is the solution closest to the true solution, and $\langle\ \rangle$ denotes the expected value in case that there is no skill. This is in the case ϕ^C is randomly distributed with respect to ϕ^T, or vice versa ϕ^T is randomly distributed with respect to ϕ^C. Of course always $\left|\phi^C - \phi^T\right| \le \pi$.

To define the NRMS, we have to specify the denominator. We followed two approaches.

1) Suppose that we have N solutions, sorted such that $0 \le \phi_1 < \phi_2 ..... < \phi_N < 2\pi$. We compute the a priori expected variance of this solution pattern in case of no wind direction skill. For convenience, we define $\phi_0 \equiv \phi_N - 2\pi, \phi_{N+1} \equiv \phi_1 + 2\pi$. The boundaries between the solutions, which define their angular sector of representation, are defined by

$$\phi_i^{\ B} = \frac{\phi_{i-1} + \phi_i}{2}, \qquad i = \{1,....N+1\} \tag{3.2}$$

We take the case of no skill in the solutions as a random probability of ϕ^T with respect to the solutions, i.e., $p\left(\phi^T\right) = (2\pi)^{-1}$. Then we get

$$\left\langle \left(\phi^C - \phi^T\right)^2 \right\rangle = \int_0^{2\pi} \left(\phi^C - \phi^T\right)^2 p\left(\phi^T\right) d\phi^T = \frac{1}{2\pi} \sum_{i=1}^{N} \int_{\phi_i^B}^{\phi_{i+1}^B} \left(\phi^C - \phi^T\right)^2 d\phi^T = \frac{1}{24\pi} \sum_{i=1}^{N} \left(\phi_{i+1} - \phi_i\right)^3 \tag{3.3}$$

where, in the last equality the boundaries as defined before have been substituted.

The variance expression thus obtained depends on the number and on the distribution of the solutions. Some appealing features of this definition can be easily derived. The first one is that the variance decreases with an increasing number of solutions, hence giving a higher "penalty"in the NRMS. For instance, if the solutions are regularly distributed such that $\phi_{i+1} - \phi_i = 2\pi / N$, we find $\left\langle \left(\phi^C - {}^T\right)^2 \right\rangle_\phi = \pi^2 / 3N^2$. Another and nice property is that, in the case that artificial "double minima" solutions are produced by the inversion procedure, such that $\phi_{j+1} - \phi_j \approx 0$ for certain j, this will have no effect on the normalisation.

2) Now let us first select the solution closest to the reference and then compute the expected variance in case of no skill. Using the above equations and if we first order the solutions such that always $\phi_1 = \phi^C$ we can define

$$p(\phi^T) = \begin{cases} \left(\phi_2^B - \phi_1^B\right)^{-1} & \text{if } \phi_1^B \le \phi^T \le \phi_2^B \\ 0 & \text{otherwise} \end{cases} \tag{3.4}$$

Then we find

$$\left\langle \left(\phi^C - {}^T\right)^2 \right\rangle_\phi = \frac{\left[(\phi_2 - \phi_1)^3 + (\phi_1 - \phi_0)^3\right]}{12(\phi_2 - \phi_0)} \tag{3.5}$$

For $N = 1$ and $N = 2$, the variance expression yields the same as before, i.e., the knowledge of which solution is selected is irrelevant. Also in the case that the solutions are regularly spaced this is the case, as one may expect. However, in other cases, the variances computed by both methods are different.

The most important difference is that the first approach yields a method that is only dependent on the distribution of solutions, whereas the second approach yields a variance that only depends on what turns out to be closest solution and its neighbour solutions. If the solution pattern is random with respect to ϕ^T then both equations work very similarly. However, imagine the simplest case that we get three solutions with $\phi_1 = -\phi, \phi_2 = 0, \phi_3 = \phi, 0 \le \phi \le \pi$. In figure 3.3 the expected variances by both approaches are plotted after carefully evaluating the expressions. We note that as long as the angular sectors are not too small, both approaches yield a very similar result, and the same at $\phi = \pi / 3$. However, if the sector of the closest solution approaches zero, i.e., in this case when $\phi^C = \phi_2$ if ϕ goes to zero, then the second approach provides an expected variance that goes to zero. In practise this is not a problem because also the term $\phi^C - \phi^T$ goes to zero, and $\phi = 0$ corresponds to a case with one solution.

Using the above example, let us examine a pathetic case to better understand the differences between both approaches. We assume that we always have three solutions with $\phi_1 = -\phi, \phi_2 = 0, \phi_3 = \phi, 0 \le \phi \le \pi$. In case of no skill both methods provide the same skill over a large data sample, since the computed "no skill" variance is by definition equal to the denominator of the NRMS. However, in the other extreme, the high skill case, a difference occurs. Let us assume that $\phi^C = \phi_2$ and that $SD(\phi^C - \phi^T) = \varepsilon$ with $\varepsilon << \phi$. This means that the orientation of the solution

pattern is closely correlated with ϕ^T. Figure 3.4 depicts the resulting NRMS for a case with relatively large ϕ and small ϕ. Approach 1) gives a relatively low NRMS when the three solutions are close together (small ϕ), whereas approach 2) give a relatively high NRMS in this case. The reason for this, is that approach 2) takes into account the correlation of the orientation of the solution pattern with ϕ^T, whereas approach 1) does not take this into account. In scatterometer data one often observes that the solution pattern and its orientation depend on ϕ^T. As such, including the skill of the orientation of the solution pattern with respect to ϕ^T seems most appropriate generally and therefore approach 2) is recommended.

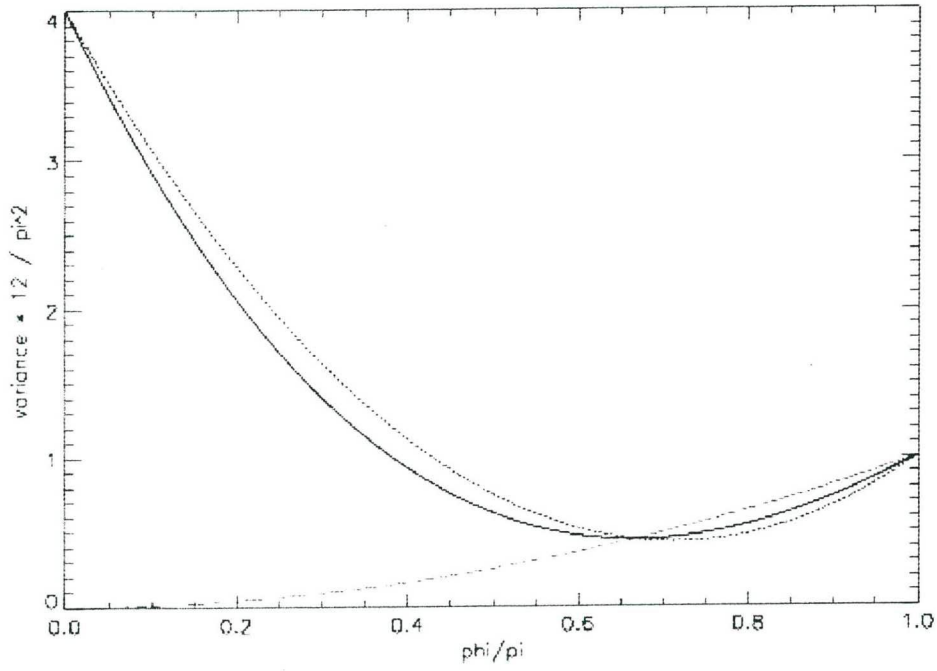

Figure 3.3: Variance $\langle(\phi^C - \phi^T)^2\rangle$ *for the case* $N = 3$ *with solutions* $\phi_1 = -\phi, \phi_2 = 0, \phi_3 = \phi, 0 \leq \phi \leq \pi$, *as a function of* ϕ. *The solid line gives the results obtained with approach 1); the dotted line is approach 2) with* $\phi^C = \phi_2$, *and the dotted line appraoch 2) with either of the two other solutions.*

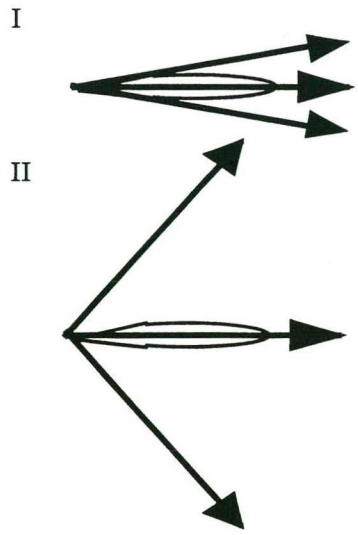

Approach	$\langle(\phi^C - \phi^T)^2\rangle$	NRMS
1)	I > II	II > I
2)	II > I	I > II

Figure 3.4: Illustration of case with fixed solution pattern as provided in figure 3.3 for a narrow true wind vector distribution depicted by the thin contour line. Example I (top) and II (bottom) are such that $\phi = \phi_I < \phi_{II}$. *The table (right) compares the a priori "no skill" variance* $<(\phi^C - \phi^T)^2>$ *and the NRMS of the two examples for the two approaches discussed in this section.*

4 QUALITY CONTROL AND RAIN ELIMINATION

In contrast with C-band scatterometers such as on ERS and ASCAT, Ku-band scatterometers are sensitive to rain and procedures need to be developed to screen out rain-contaminated measurements. Besides rain elimination, geophysical anomalies exist in 1 or 2 % of cases and where the retrieved winds are detrimentally affected in case of the ERS scatterometers.

A quality control procedure has been developed for SeaWinds based on the QC methodology for the ERS scatterometer (Stoffelen and Anderson, 1997; Stoffelen, 1998). In addition to a screening similar to ERS, the procedure acts to remove rain contaminated points (Figa and Stoffelen, 2000; Portabella and Stoffelen, 2000). The methodology checks whether the consistency of the backscatter measurements at a particular Wind Vector Cell (WVC) is compatible with the consistency as predicted by the Geophysical Model Function (GMF). A measure of this consistency is provided by the inversion residual or MLE (Maximum-Likelihood Estimator). A limitation of this approach is obviously that anomalous geophysical conditions that are still compatible with the GMF are not screened out, such as a few rain points that appear as 15-20 m/s winds. Such points should ideally be rejected by the standard QC procedures of NWP data assimilation systems.

Alternatively, one could use the backscatter polarisation ratio, but this has the same limitation and is more restricted (Wentz, 1999), i.e., the polarisation ratio discrimination is implicitly included in the MLE check. Particularly in those parts of the SeaWinds swath where azimuth view diversity or polarisation coverage is lacking, notably around nadir and in the far swath, the wind vector may be underdetermined and QC by a consistency check, such as in the above-described methodology, impossible. The part of the swath where this occurs is limited fortunately.

Another alternative is to use the SeaWinds passive noise measurement to detect rain, though this has low accuracy (of 13 K) and a relatively large footprint (> 75 km; Jones, 1999). Combining MLE information and the passive noise measurement JPL developed a rain elimination routine that has recently been implemented in the near-real time product. Vadidation of this QC flag is ongoing at KNMI. SeaWinds on ADEOS-II may profit from AMSR for rain elimination, when all parts of the swath may be checked for rain. Work remains to be done to develop procedures to extract the wind information in those swath parts with poor azimuth or polarisation diversity.

In the QuikScat processing used throughout this report, we implemented the KNMI rain elimination algorithm (Portabella and Stoffelen, 2000).

5 OBSERVATION SMOOTHING

SeaWinds data are nominally provided with a sampling of 25 km, whereas most NWP models use observations at at least a 100-km density. The small-scale structures observed by a scatterometer cannot be fitted well by the relatively broad spatial structure functions, and statistical noise in the analyses results. For many observing systems data thinning procedures are in use (see e.g., Rohn et al, 1999; Anderson et al, 1999; Leidner and Isaksen, 2000, McNally, 2000). The size of the spatial structure functions used in meteorological analysis for spatial extrapolation of the observed variables is mainly determined by the poor observation of the upper air flow (ESA, 1999). For scatterometer data, in order to reduce systematic wind retrieval errors it is better to reduce noise and average backscatter measurements, σ^0, to lower resolution before the non-linear wind retrieval process. For ERS and ASCAT observations the same applies, but where as a first step it has been shown that averaged winds compare better to the HIRLAM (2000) first guess than thinned data (Stoffelen and Beukering, 1998). In a second step, de Vries and Stoffelen (2000) applied observation grouping in one location, whereby the ambiguity patterns of all individual 50-km ERS scatterometer wind observations are kept, but still a spatial averaging effect in 2D-VAR was achieved thereby avoiding small-scale noise and phase errors in the 2D-VAR analysis and ambiguity removal.

The above problem of numerically analysing small-scale weather patterns provides an important motivation to present scatterometer wind data to operational meteorologists for nowcasting and short-range forecasting purposes (see e.g. figure 1.1-3). However, still appropriate quality of the retrieved winds and ambiguity removal has to be achieved in order to present a reliable product. The cases presented in figures 1.1-3 indicate that this is not achieved in the 25-km near-real time QuikSCAT BUFR product. In order to improve quality and reliability we investigate here the effect of spatial smoothing of the backscatter data.

A procedure is tested and incorporated in the inversion module to average backscatter measurements in a resolution cell of varying size, a so-called Super WVC or SWVC. In line with the requirements for NWP we first assess QuikSCAT wind quality at 100 km resolution.

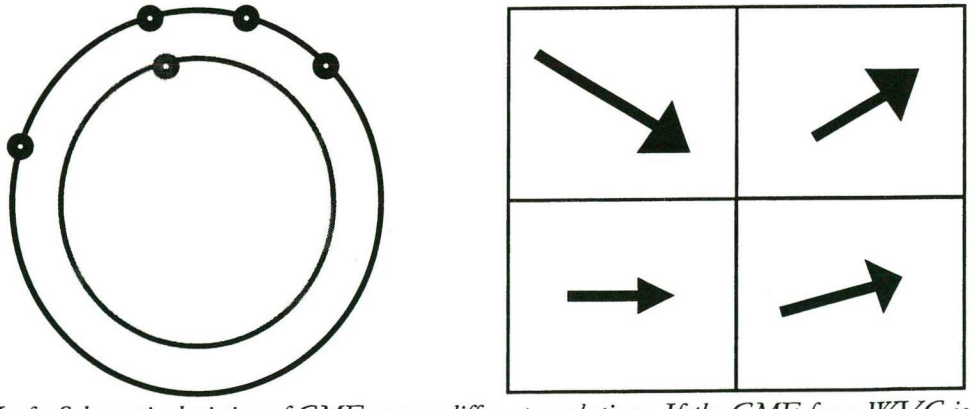

Figure 5.1: Left: Schematic depiction of GMF at two different resolutions. If the GMF for a WVC is defined by the black line, the GMF for a SWVC is better defined by the grey line. if the typical wind variability is taken into account. The four black dots represent backscatter data at four WVC, and the grey dot is their average representative for a SWVC. Right: Variation of the wind by WVC in a SWVC.

5.1 BACKSCATTER DATA AT 100 KM

We address first how from the given backscatter observations at 25 km resolution (σ^0_{25}) composites at 100 km resolution (σ^0_{100}) can be derived as an intermediate step, where there are several issues to take into consideration

1. GMF definition: Figure 5.1 depicts four WVC constituting one super WVC or SWVC. The mean wind in a WVC is $\boldsymbol{V}_{\mathrm{WVC}} = \boldsymbol{V}_{\mathrm{SWVC}} + \delta\boldsymbol{V}$ where $\boldsymbol{V}_{\mathrm{SWVC}}$ is the mean wind in the SWVC and $\delta\boldsymbol{V}$ an increment vector drawn from a normal distribution in the wind components u and v with zero mean and standard deviation of variance $\sigma = \sigma_u = \sigma_v$.. σ^2 is the integral of the expected wind component variability density spectrum from the scale of the WVC to that of the SWVC. Note that by this definition the dynamic range of winds is increased by increasing resolution (see also Stoffelen, 1998b). The WVC backscatter quadruplet data corresponding to these winds relate to them in a harmonic and non-linear way. The SWVC quadruplet does thus not obey the same internal consistency as the WVC quadruplets do, as depicted in figure 5.1. In other words, the GMF at WVC resolution is not identical to the GMF at SWVC resolution. We investigate the first order magnitude of this effect in a simulation experiment, where we compare the backscatter distributions at 25 and 100 km for diverse wind conditions. The resulting mean difference is used in a calibration experiment to assess its importance on the retrieved winds.
2. Noise: Moreover, the statistical distributions of σ^0_{25} and σ^0_{100} differ due to the level of instrument noise and geophysical noise (due to wind variability). The instrument (speckle) noise is reduced by a factor of four, i.e., the same factor as by which resolution is reduced. Reduced noise will result in more accurate retrieved winds. The effect of geophysical noise will however counteract the effect of reduced instrument noise. We thus need to investigate noise effects in the averaging process and 100-km wind retrieval. We do this in a simulation experiment.

5.2 SIMULATION

The true wind reference for the simulation was chosen as follows:

1. The NOAA BUFR product 25-km rank-1 wind field was assumed to be truth. We assume that this field results in a realistic backscatter field spatial variability and consistency. One could argue that the variability is too high, since the QuikScat data contain noise beyond the geophysical variations. This means that the geophysical noise effect on the GMF and the inversion is somewhat exaggerated in the simulation. If we would use NWP fields as truth there would have been no variability whatsoever on scales between 25 and 100 km, making the simulations meaningless.
2. We used the rank-1 wind vector solution (WVS) fom the JPL inversion of the WVC closest to the centroid of the super cell for validation. The fact that the rank-1 wind field is not always spatially and meteorologically consistent is thought to have little effect on the simulations.

Having chosen a true wind reference we subsequently simulated a backscatter measurement ($\sigma^0_{25\,S}$) using the NSCAT-2 GMF. We added Gaussian noise to the backscatter measurement to obtain $\sigma^0_{25\,N}$. We considered three scenarios regarding the wind retrieval in each SWVC:

1) Simply use per beam the up to 16 $\sigma^0_{25\,N}$ values and the observed noise values of $K_{p\alpha}, K_{p\beta}, K_{p\gamma}$, azimuth and incidence angle from the WVC's for the valid data in the BUFR product.

2) Construct a K_p-averaged backscatter value per beam representative for the super cell from the up to 16 $\sigma^0_{25\,N}$, i.e.

$$\left\langle \mathrm{var}\,\sigma^0_{25} \right\rangle = K_{p\alpha}\sigma^{0\,2}_{25\,N} + K_{p\beta}\sigma^0_{25\,N} + K_{p\gamma} \tag{5.1}$$

$$\left\langle \mathrm{var}\,\sigma^0_{100} \right\rangle = \frac{1}{\sum_{i=1}^{N} \frac{1}{\left\langle \mathrm{var}\,\sigma^0_{25} \right\rangle_i}} \tag{5.2}$$

$$\sigma^0_{100\,N} = \left\langle \mathrm{var}\,\sigma^0_{100} \right\rangle \cdot \sum_{i=1}^{N} \sigma^0_{25\,N\,i} \Big/ \left\langle \mathrm{var}\,\sigma^0_{25} \right\rangle_i \tag{5.3}$$

The value of $\left\langle \mathrm{var}\,\sigma^0_{100} \right\rangle$ is passed to the inversion by appropriately setting the values

$$K^{100}_{p\alpha} = \frac{\left\langle \mathrm{var}\,\sigma^0_{100} \right\rangle}{\left(\sigma^0_{100\,N}\right)^2},\quad K^{100}_{p\beta} = K^{100}_{p\gamma} = 0 \tag{5.4}$$

The values of the azimuth and incidence angle are averaged per flavour for the 16 WVC's. With this scenario we emphasise the importance of accuracy in the backscatter measurements and hypothesise that noise variability within a 100-km SWVC has a significant effect on the wind retrieval, especially at low wind speed.

3) The same as scenario 2 except that we take the geometric mean of the 16 $\sigma^0_{25\,N}$ values as the backscatter value representative for the super cell, i.e.

$$\sigma^0_{100\,N} = \overline{\sigma^0_{25\,N}} = \frac{1}{N}\sum_{i=1}^{N} \sigma^0_{25\,N\,i} \tag{5.5}$$

5.3 CALIBRATION

In section 5.1 it was explained that normal wind component variability on scales between 25 and 100 km causes the GMF to be different at 25 and 100 km resolutions. For example, for a low value of σ^0_{25}, it is probable that neighbours exhibit higher σ^0_{25} and as a result the associated σ^0_{100} is probably higher. For low σ^0_{25} we expect thus $\sigma^0_{100} > \sigma^0_{25}$. However, we only have a GMF and $\sigma^0_{25\,N}$ data processing scheme tuned (by e.g., $\sigma^0_{25\,N}$ calibration) to deal with 25-km data. A difference in σ^0 distribution due to resolution may result in a systematically wrong mapping of backscatter values the wind domain with less favourable wind error characteristics like a high degree

of skewness or wind direction aliasing. In particular at low σ^0 and thus wind speed this problem is accute. A possible method to overcome this inconsistency to first order, is to map the SWVC $\sigma^0_{100\ N}$ distribution onto the WVC $\sigma^0_{25\ N}$ distribution. In a calibration experiment we investigated whether a change in the mean of the distribution of $\sigma^0_{100\ N}$ compared to that of $\sigma^0_{25\ N}$ needs correcting for. We used simulation scenario three for the test described here.

The 100km-minus-25km difference was obtained by comparing the closest to centroid $\sigma^0_{25\ N}$ from $\sigma^0_{100\ N}$. As a reference we used the closest to centroid simulated backscatter values $\sigma^0_{25\ S}$.

Figures 5.2 and 5.3 show the noise characteristics for the inner beams (fore and aft) and outer beams. In the upper panels of these figures the separate contributions are shown. The noise characteristic at 25-km resolution (green line) is basically the zero mean Gaussian noise that was added in the simulations. The lower panels show that the wind variability gives rise to a fairly constant but small bias for low values of σ^0, corresponding to low wind speeds. This bias is different for inner and outer beams. We did not find a noticeable difference in the bias between fore and aft beams. The erratic behaviour for backscatter values upward of –20 dB is due to lack of data.

Based on the result of figures 5.2 and 5.3, we applied a proportional σ^0 bias correction to $\sigma^0_{100\ N}$. For the inner beams $\sigma^0_{100\ N}$ was reduced by a factor of 0.9998 and for the outer beams by a factor 0.9997. This correction is aimed to reduce the bias for low backscatter values. However this correction did not have an impact on the wind statistics as they are shown in next section. Therefore we may conclude that a bias correction for the noise is not necessary. To verify whether the selected simulation was representative for real data we determined the 100-km and 25-km backscatter distributions after repeating scenario 3 with the observed backscatter measurements from the BUFR product instead of simulated ones. Figure 5.4 shows the results and verifies the minor effect found with the simulated data.

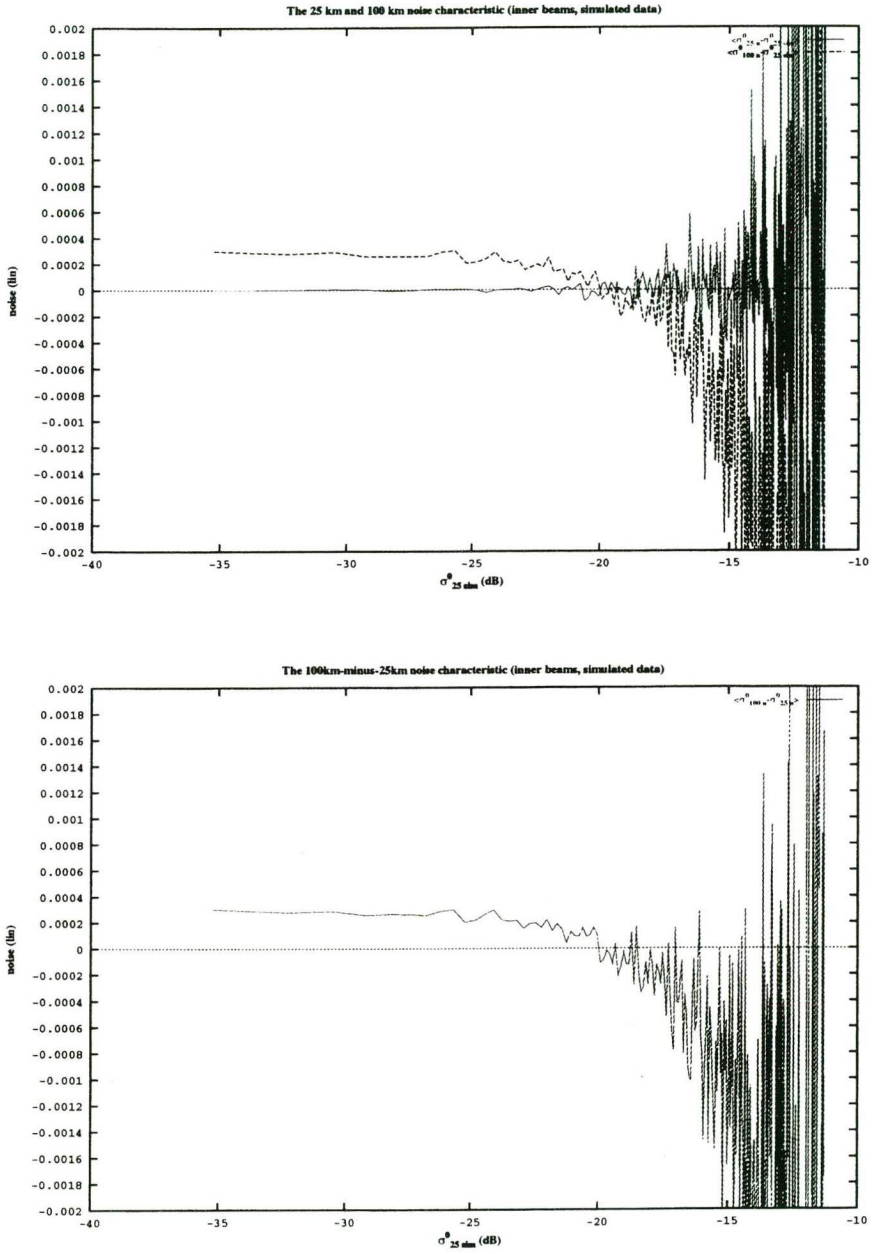

Figure 5.2: Noise characteristics inner beam, simulated data

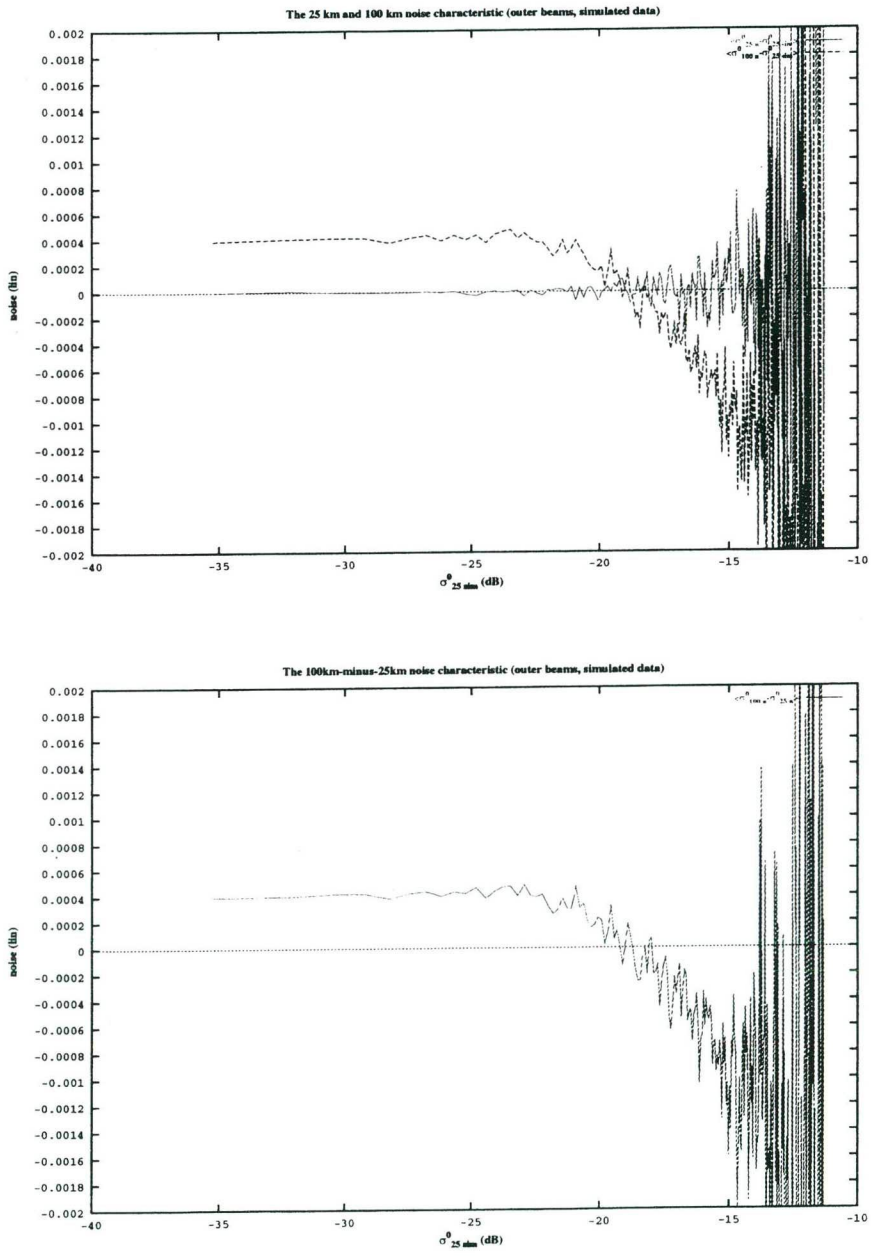

Figure 5.3 : Noise characteristics outer beam, simulated data.

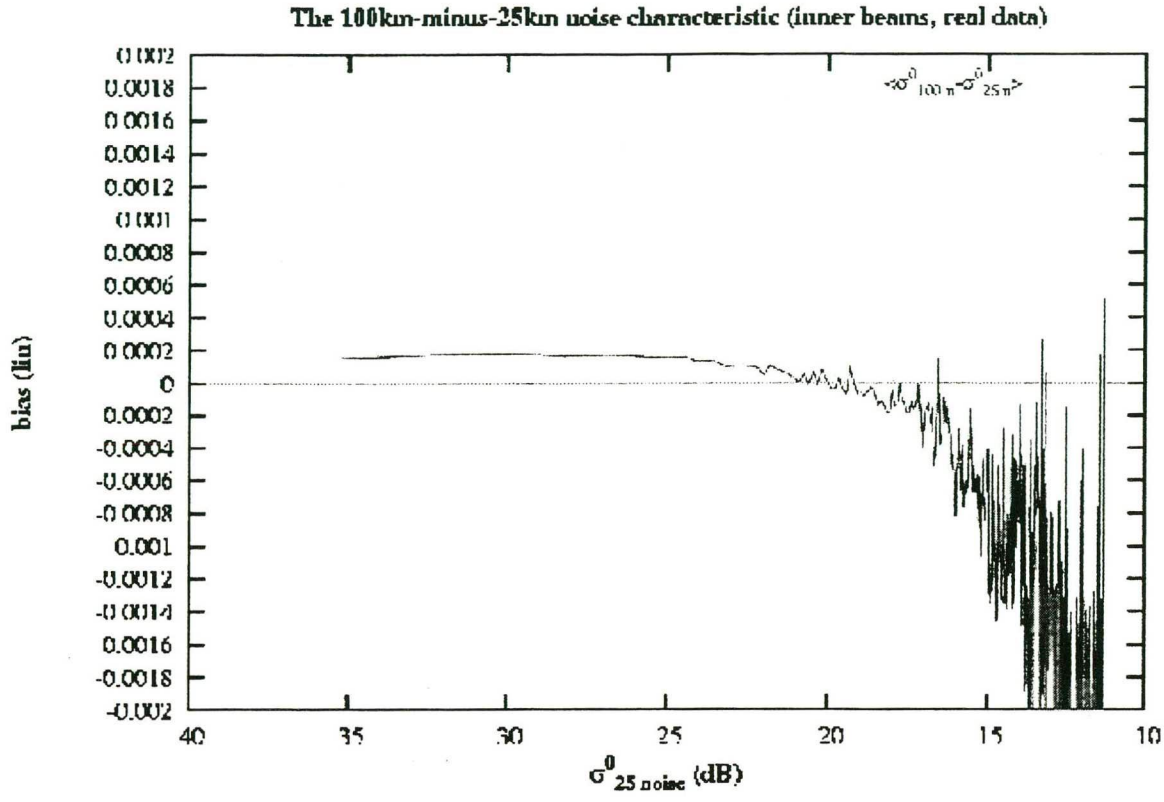

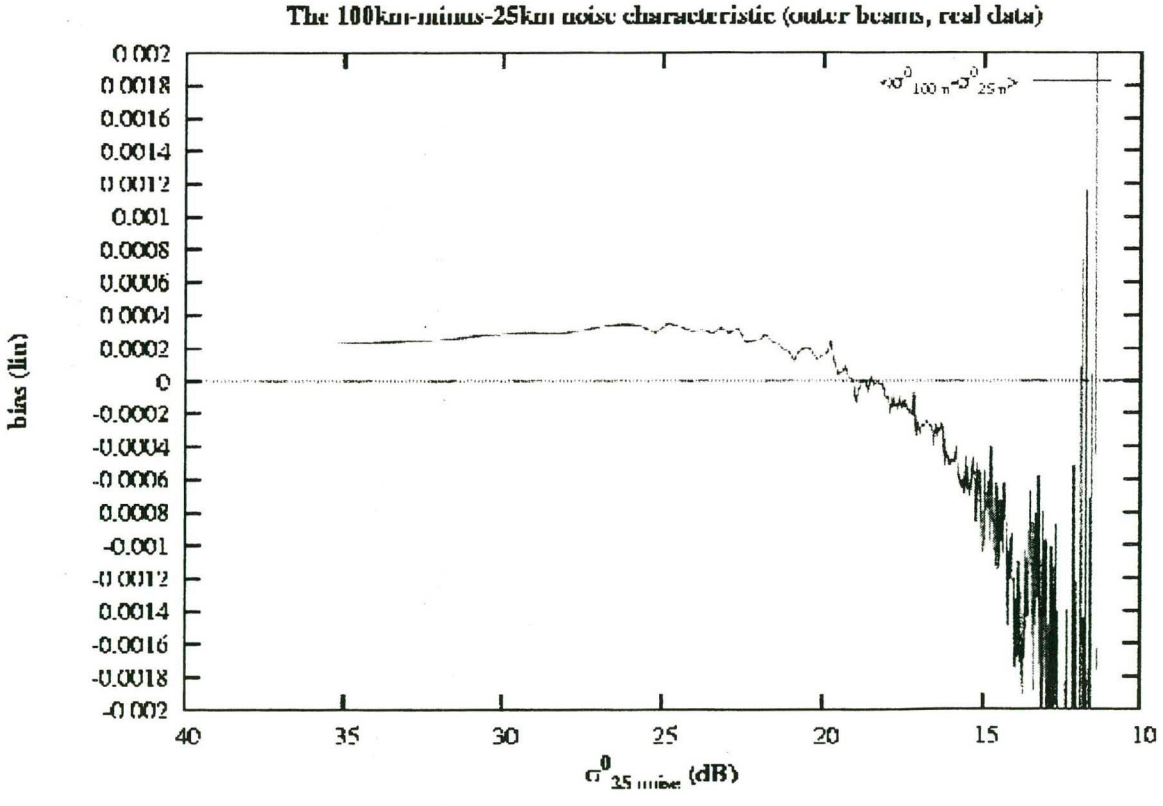

Figure 5.4: Noise characteristics for inner and outer beam, real data

5.4 INVERSION

After the inversion we compared the retrieved rank 1 wind solution and the closest-to- truth wind solution with the true wind. The comparison gives insight into the systematic and random errors produced in the different scenarios when going from 25 km to 100 km. We can also determine the 1st rank skill for each scenario. We define the 1st rank skill as the percentage of WVC's for which the rank 1 ambiguity is the one closest to the true wind. The 1st rank skill depends on signal-to-noise (SNR) ratio, wind speed, and relative azimuths of the radar beam with respect to the local wind direction and polarisation.

In figures 5.5-7, log-density contoured two-dimensional histograms are shown for the simulated versus Seawinds rank 1 (true) wind comparison. In the histograms the highest valued contour is equal to the maximum value reduced by a factor 0.9, followed by lower contour levels that are half the value each time.

Figures 5.5 presents the wind statistics for the scenario of using 16 $\sigma^0_{25\,N}$ in the wind inversion, which is scenario 1 of section 1.2. The wind speed distribution exhibits a positive bias for speeds between 1 and 15 m/s with simulated wind speeds higher than the true wind speeds. This shows that scenario 1 overestimates the mean strength of the backscatter signal in the SWVC (i.e., $\sigma^0_{100\,S}$). The wind direction distribution is not uniform for all directions. Peaks around 90 and 270 degrees suggest the sampling of winds with persistent direction over significant parts of the globe, such as the westerlies or the trade winds. The distributions in the upper left and lower right part of the histogram are caused by the periodicity of the wind direction domain.

Figure 5.6 shows the result when using K_p-averaged σ^0's in the wind retrieval. We can see that in the wind speed distribution the simulated wind speed is biased low between 5 and 15 m/s, with a skew wind speed error distribution. The presence of this bias is also found in the wind component distribution in the form of a distinct S-shape curvature. At high speeds the contouring is erratic due to lack of data. The wind direction distribution furthermore shows a wave-like curvature indicating directional biases. At low speeds the wind speed distribution is somewhat positively biased with estimated wind speeds higher than the true wind speed.

Figure 5.7 shows the results of the simulations with a geometric mean σ^0. The symmetry in the wind speed distribution from 5 to 15 m/s shows a good and symmetric fit between the true wind and the simulated wind. Evidence of this is also found in the wind component distributions. Above 15 m/s the distributions become erratic due to lack of data and it is difficult to make a statement for the fit at higher speeds. At low speeds in the wind speed distribution the simulated wind speed is biased slightly high. However, such wind speed effect can be easily taken out in a wind calibration, e.g. as in Stoffelen (1999). The directional distribution lies tighter on the diagonal than in figures 5.5-6, resulting in a lower wind direction error standard deviation.

Comparing the results of the different scenarios we can conclude that a SWVC mean σ^0 based on the geometric mean of the backscatter values of the individual WVC's (scenario 3) gives the best fit between simulated winds and the truth. In line with this, the statistics in the legend of the histograms show that the standard deviation of the difference (STD) and bias are smallest for scenario 3.

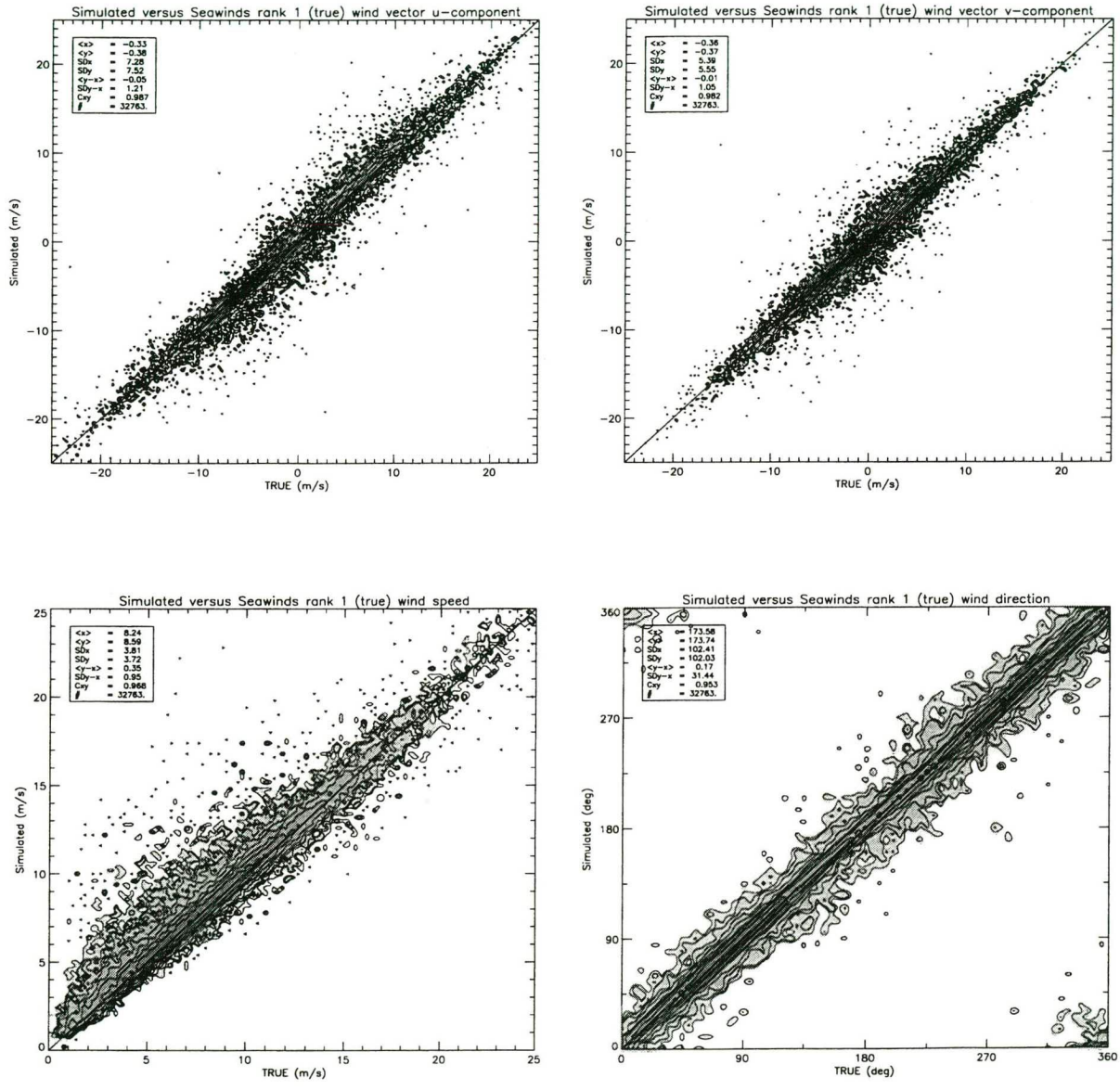

Figure 5.5 : Bi-dimensional histogram for the simulations with 16 backscatter values per beam in the wind retrieval

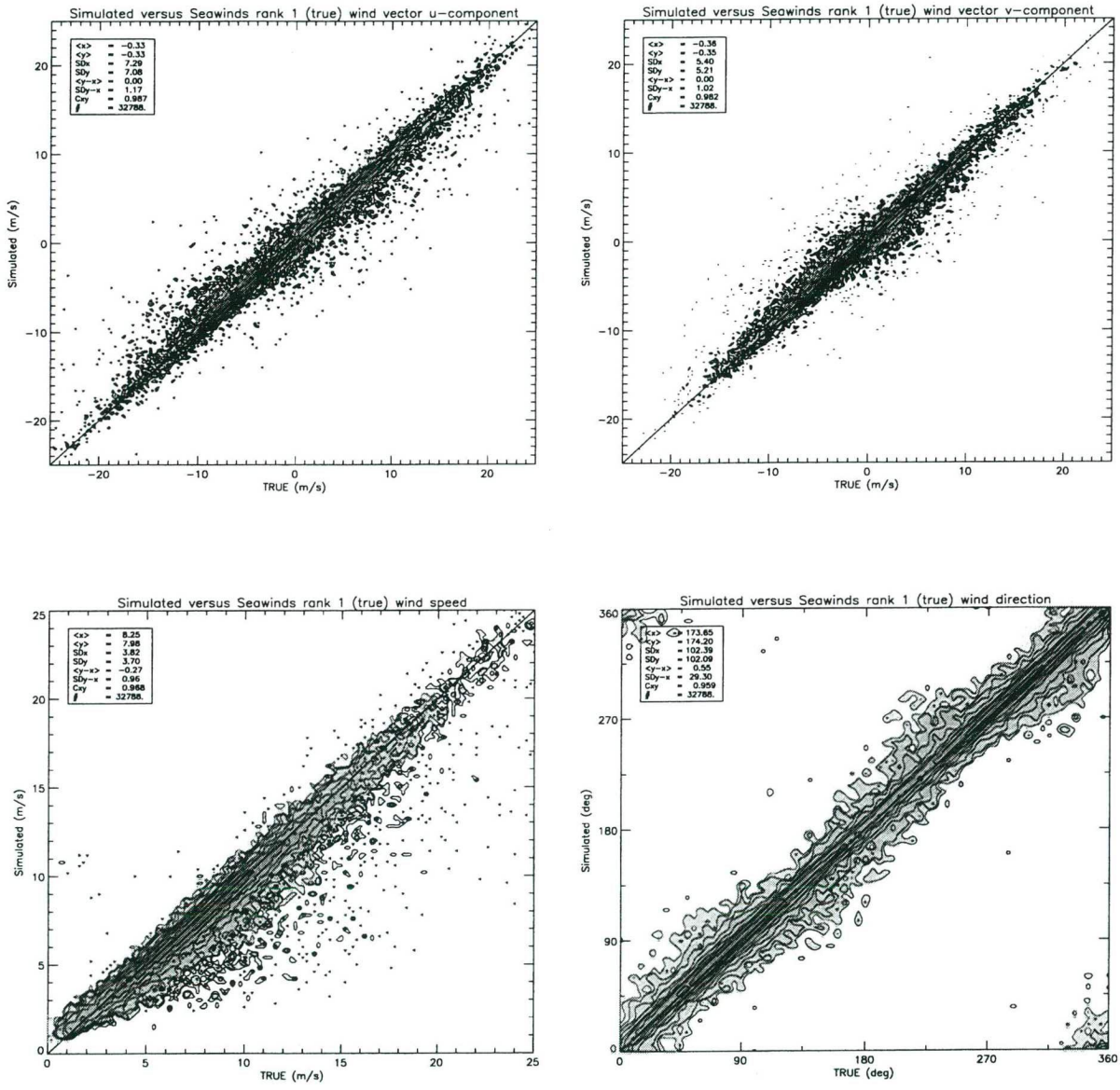

Figure 5.6: Bi-dimensional histogram of the wind statistics resulting from the simulations with Kp-averaged backscatter values in the wind retrieval.

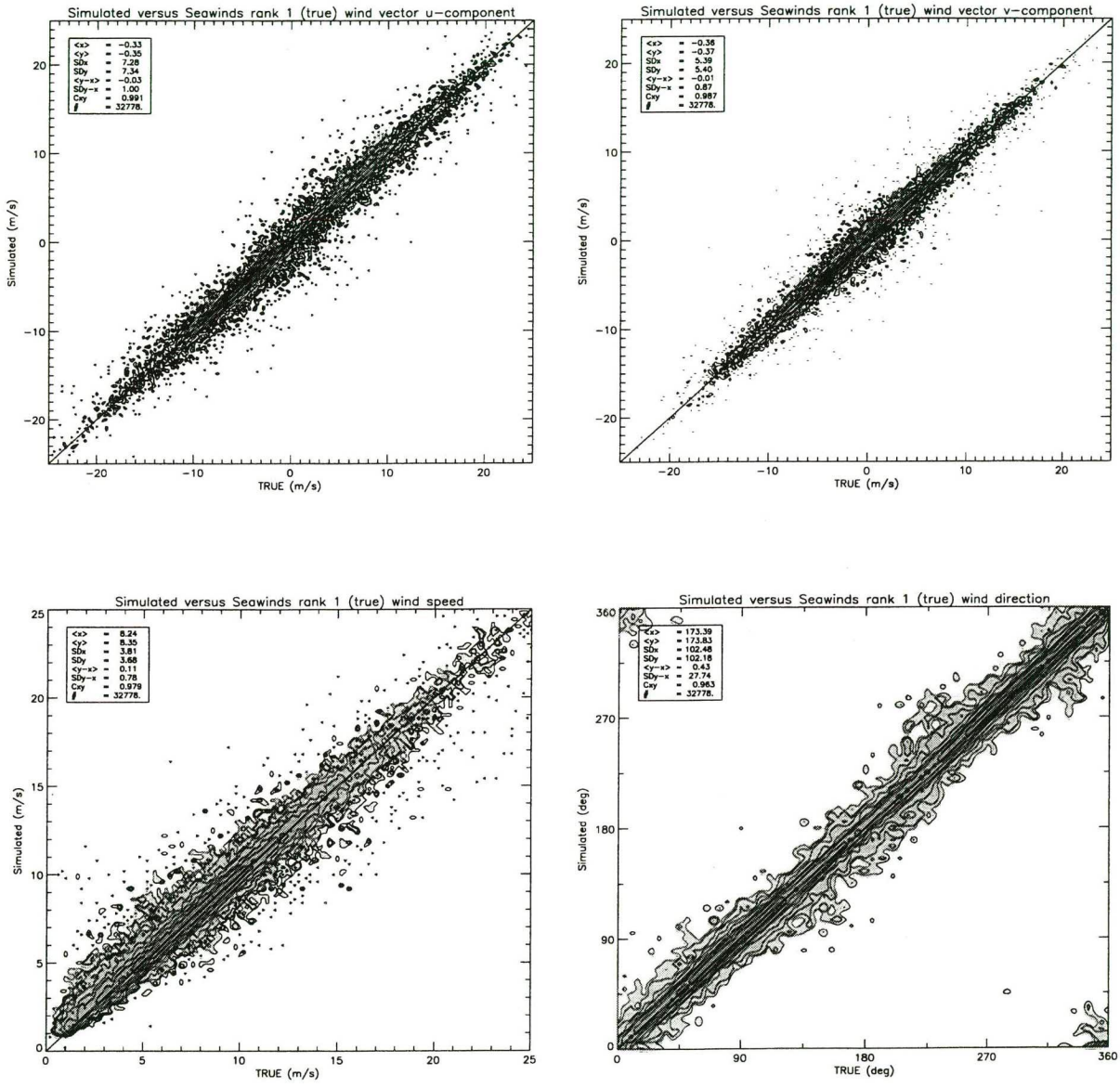

Figure 5.7: Bi-dimensional histogram of wind statistics for wind retrieval with super cell mean backscatter values.

6 SEAWINDS ASSIMILATION

Lorenc (1988) provides a detailed and comprehensive description of the problem of data assimilation. He derives the equations for "optimal" nonlinear objective analysis that form the basis of many current variational data assimilation schemes, using maximum probability as the major constraint. Stoffelen (1998a; chapter VI) describes the problem of the analysis of variables that are related in a non-linear way to the NWP model variables, such as scatterometer backscatter measurements. He suggests that normal distributed noise can introduce systematic biases when constraining a minimum variance or maximum probability solution, if the relationship that is used in the analysis between observed and model variable is not linear. If the goal in data assimilation is to achieve an unbiased estimate of the model state then the term "optimal" for a maximum probability solution in combination with the phrase nonlinear appears misleading.

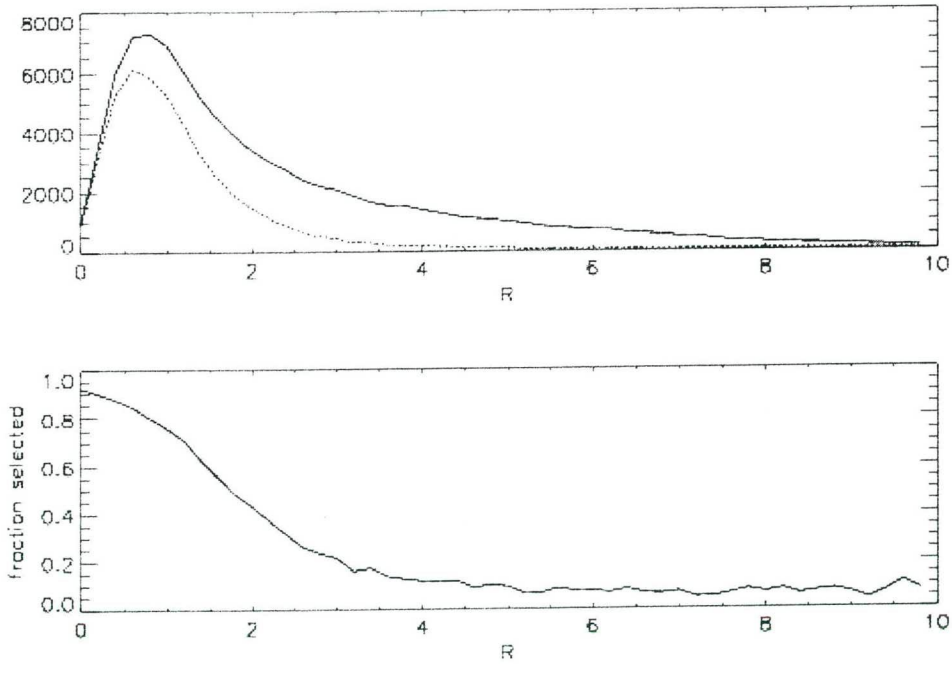

Figure 6.1: In the upper panel, number of inversion solutions occurring (solid line) and number of solutions closest to the NCEP wind velocity (dashed line) as a function of normalised residual R, for five orbits of data and for the sweet part of the swath. In the lower panel the ratio of these two quantities is plotted.

As the most practical solution for the assimilation of scatterometer data, Stoffelen (1998) suggests to assimilate retrieved scatterometer winds. This approach is further pursued here for SeaWinds scatterometer observations. Scatterometer winds can be retrieved accurately, since backscatter noise is generally small for all scatterometer systems. Backscatter-only noise results in a wind vector uncertainty of only about 0.5 m/s after the non-linear inversion. As such, the biases are limited. However, the interpretation of a radar backscatter measurement, that is most directly related to the anisotropic roughness of the ocean topography on the cm-scale, as a wind at 10m height introduces a much larger uncertainty that can be well modelled by a normal wind component error distribution (Stoffelen, 1998b). Wind vector measurements from a scatterometer have an estimated accuracy of about 2 m/s. This larger uncertainty in the wind domain makes the assimilation of retrieved winds more attractive than the direct assimilation of backscatter measurements.

Moreover, in the direct assimilation of backscatter observations, one would transform the first guess errors and the uncertainty in the Geophysical Model Function (GMF) in a non-linear way to the backscatter space, resulting in a biased and skew error distribution in this space. The first guess vector error is about 1.5 m/s (Stoffelen, 1998). The precise form of the σ^0 error distribution would depend on wind speed, wind direction, and view configuration. The maximum probability in a skew distribution does generally not overlap with the mean of the distribution, nor has the maximum symmetric properties. In line with this, the assumptions made to derive a quadratic cost function in variational data assimilation (2D-VAR, 3D-Var, 4D-Var) that

1. a priori all states of the control variable are equally likely; and that
2. the deviation between true state and background can be described by a Gaussian distribution;

are invalid in the backscatter space. The optimal observation cost function and observation operator is not a priori clear in such a case and requires considerable thought (Stoffelen, 1998; chapters V and VI). By assimilating retrieved winds this problem disappears, since the above assumptions do hold by approximation in this domain.

NSCAT and SeaWinds use horizontal and vertical polarisation measurements, whereas ERS or ASCAT are solely based on vertical polarisation. This in combination with a varying measurement geometry results in a different wind direction ambiguity structure than for ERS or ASCAT.

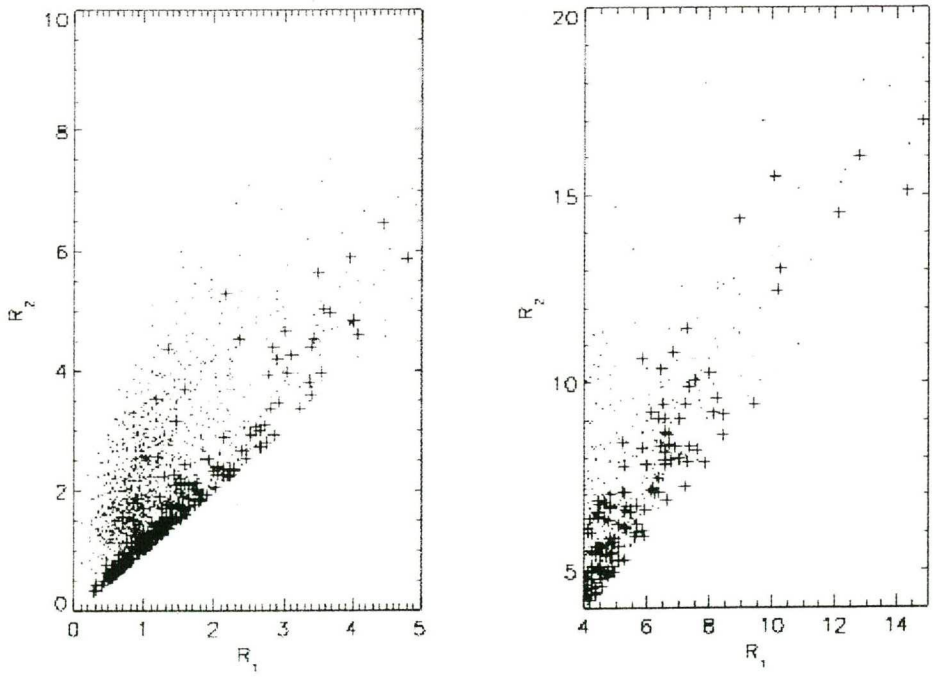

Figure 6.2: Scatter plot of first rank normalised inversion residual R_1 against second rank solution residual R_2 only for cases with two solutions. Dots indicate pairs where the first rank is the one closest to the NWP wind velocity; plusses are pairs where the second rank is selected. The left panel highlights only the lower range residuals of a total of 1,500 pairs, whereas the right panel only shows higher range pairs of a total of 15,000 pairs. For $R_1 < 3$ the first rank is almost always selected, unless $R_1 \approx R_2$. For higher R_1 either rank may be selected, indicating less predictive skill in the residual. Note however that all points in the right panel are screened by our QC. As such, SeaWinds ranking information appears to be an excellent predictor.

6.1 A GENERIC SCATTEROMETER DATA ASSIMILATION APPROACH

The ERS scatterometer cost function may be generalised to be able to cope with all scatterometer data. All scatterometer data can be characterised by multiple wind vector ambiguities that each have different probability and accuracy. A procedure is described here that estimates this probability and accuracy and as such provides the input for a general scatterometer cost function. The working of the cost function for ambiguity removal is tested and documented in next chapter.

Generally data assimilation systems constrain to a background or first guess field and to observations (e.g., Lorenc, 1988; and Courtier, 1999) in a minimisation problem of the objective function

$$J = J_b + J_o \tag{6.1}$$

where J_o is the observation cost function and J_b the background field cost term.

The observation term consists of a contribution from each observation and is related to the probability of a meteorological state, given the measurements. For scatterometer data we write

$$J_o^{SCAT} = -2\ln\{p(\sigma_O^0 \mid \mathbf{v})\} \tag{6.2}$$

where, for a set of scatterometer data, $\sigma^0{}_O$ we may write for the probability of the surface wind $\boldsymbol{V}$

$$p(\sigma_O^0 \mid \mathbf{v}) = \sum_{i=1}^{N} w\{p_i^p\, p_i(R_i)\} N(\mathbf{v}_i, \varepsilon_i) \tag{6.3}$$

where p_i^p is the prior probability of a solution i, $i \in [1, N]$, i.e., without knowledge of R. It is solely dependent on the wind direction sector that a solution represents and only relevant in case of more than two solutions, i.e., $N > 2$. For NSCAT or SeaWinds, the prior probability p_i^p just depends on the azimuths of the solutions (Figa and Stoffelen, 2000) and with equation (3.3) we define

$$p_i^p = \frac{\phi^B{}_{i+1} - \phi_i^B}{2\pi} \tag{6.4}$$

$p_i(R_i)$ is the probability of a solution based on the normalised residual of the solution i. We further discuss the combination of these probabilities and the formulation of the weight w in section 6.2.

$N(\mathbf{v}_i, \varepsilon_i)$ is a normal distribution with maximum at the wind solution $\mathbf{v}_i$ and error width ε_i. For ERS scatterometer data (Stoffelen, 1998) the values $N = 2$, $p_i^p = 0.5$, $p_i(Rn_i) = 1$, $w = 0.5$, and $\varepsilon_i = (\varepsilon_U, \varepsilon_V)$ with $\varepsilon_U = \varepsilon_V = 1.5$ m/s are used.

Stoffelen (1998) discussed at length the concept of measurement (phase) space. In this space a 2D surface, called cone, exists spanned by the two wind vector variables (u,v) or (V, ϕ). R is then denoted "distance-to-the-cone" and is a measure of how well a particular measured triplet fits the wind surface in the measurement space. Thus, a measured backscatter triplet is transformed into three independent variables, i.e., R, u, and v. In the formulation above, the three variables $p(R)$, ε_U, and ε_V determine the quality or information content of these three parameters. It thus appears logical to assume $(\varepsilon_U, \varepsilon_V)$ independent of R, since these represent the independent wind variables.

The generalised methodology presented here may also be adopted for those parts of the swath where the wind vector cannot be fully determined, because of limited azimuth or polarisation coverage, and where the ambiguity pattern can be of greater complexity. However, in these parts of the swath the solution minima may be less well defined than in the sweet zone, because of the wind

vector underdeterminacy. In that case, the width of the minimum can be decomposed into two independent wind components, e.g., along the wind vector solution and across, or any other orthogonal set that models the likely anisotropy of the retrieval solution minimum width. ε_i is then determined by the retrieval widths and the isotropic geophysical interpretation error of about 1.5 m/s in a component. Another limitation is that for some parts of the swath QC may be difficult and assimilation therefore more risky (see section 2 above). AMSR on ADEOS-II is likely to ease this problem.

6.2 *R* DEPENDENCE OF THE COST FUNCTION

In the case of QuikScat, the number of solutions ranges from 1 to 4 (as JPL, we truncate at four in this report with R strongly varying from one solution to the next. Since

$$R \approx -2\ln\left\{p\left(\mathbf{v} \mid \sigma_O^0\right)\right\} \tag{6.5}$$

is a measure of the distance of a measurement from the wind cone (Stoffelen and Anderson, 1997a), it seems reasoneable to assume that with increasing R, the probability decreases that a certain solution is the selected solution, i.e., the one closest to the true wind velocity. To get a first impression of this we plotted figure 6.1. Here, the distribution of JPL inversion solutions is plotted as a function of normalised R together with the number of solutions closest to the NWP estimate♣. It can be seen that the fraction of selected (i.e., here taken as that closest to NCEP) decrease rapidly with increasing R indicating that R is a good measure of the probability of a solution.

The result of figure 6.1 prompted us to look for a way to determine the weights w_I on the basis of R_I. To do this, we formulate the following

Assumption: *There exists a function $p_s(x)$ such that, if we have a set of inversion solutions $\mathbf{V}_i$ with normalised residual R_i, then the probability that rank j is the one closest to the true wind, denoted here by $s=j$, is given by*

$$P(s = j \mid R_i, i \in \{1, N\}) = \frac{p_s(R_j)}{\sum_{i=1}^{N} p_s(R_i)} \tag{6.6}$$

To determine $p_s(x)$, we concentrate first on only those cases which have exactly two solutions. Figure 6.2 shows a scatter plot of those cases. It can be seen again that in the left panel rank 1 is the selected one most of the time and rank 2 is only chosen if R_2 is close to R_1. For large residuals, as in the right panel, the difference between R_2 and R_1 is a less good predictor for selection. However, note that $R_1 > 4$ corresponds to cases that we reject by our QC (section 4).

By taking many more points than those shown in figure 6.2, we can construct a twodimensional histogram showing the relative probability of selecting either the first or the second rank, as a function of R_2 and R_1. But according to our assumption, by applying (6.6) with $N = 2$, we find that the probability of selecting rank 1 is given by

$$P(s = 1 \mid R_1, R_2) = \frac{p_s(R_1)}{p_s(R_1) + p_s(R_2)} = \left\{1 + p_s(R_2)/p_s(R_1)\right\}^{-1} \tag{6.7}$$

♣ R is defined as in section 4 but with the NCEP wind velocity taken in the normalisation function in stead of the retrieved velocity. However, the results presented here do not depend strongly on the normalisation.

Hence, the two-dimensional histogram gives us an estimate of $p_s(R_2)/p_s(R_1)$ for every combination of R_2 and R_1. Figure 6.3, left panel, shows such experimentally determined ratios as a function of R_2 - R_1. As can be seen, for not too high values of R_1 the ratio seems to be a fairly constant function of R_2 - R_1, suggesting that $p_s(x)$ is a decaying exponential function of R_2 - R_1 when R_1 increases. Therefore, we have attempted to fit the function

$$p_s(x) = \exp\left[-\left(\frac{x}{a_1 + a_2 x}\right)\right] \tag{6.8}$$

to the data. This function has the nice asymptotical property that for large R_2 and R_1 the probabilities for selecting rank 1 and rank 2 become equal, which is the behaviour suggested in figure 6.2. We found a reasonable fit (figure 6.3, right panel) and for the values a_1 a value of 0.30 and for a_2

$$a_2 = \begin{cases} 0.03 & ; \quad x \le 2.5 \\ 0.03 + 0.015(x - 2.5) & ; \quad 2.5 < x \le 4.5 \\ 0.06 & ; \quad x > 4.5 \end{cases} \tag{6.9}$$

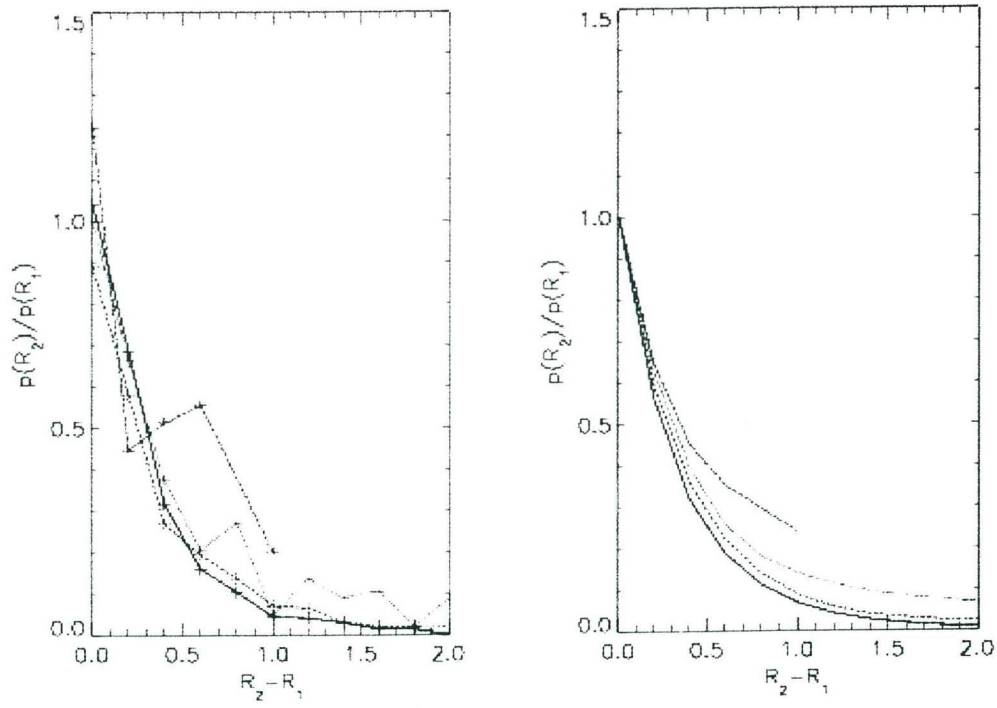

Figure 6.3: Ratio of the number of realisations of R_2 *and the number of realisations of* R_1 *as a function of* $R_2 - R_1$*, and for values of* R_1 *= 0.5 (solid),* R_1 *= 1.1 (dashed),* R_1 *= 1.7 (dotted), and* R_1 *= 2.1 (dash-dot). The left plot is based on real data and the right plot is constructed using an exponential relationship* $p_s(R)$*. The normalised residual can be well explained in terms of a wind solution probability.*

All data				
	Number of solutions			
	2	3	4	All
M	45,407	32,881	47,872	126,160
Rank 1	88 (89)	77 (76)	71 (73)	79 (79)
Rank 2	12 (11)	18 (19)	19 (20)	16 (17)
Rank 3	-	5 (5)	7 (5)	4 (3)
Rank 4	-	-	3 (2)	1 (1)

$R_2 - R_1 \leq 1$				
	Number of solutions			
	2	3	4	All
M	14,742	18,980	33,905	67,627
Rank 1	70 (69)	65 (63)	62 (65)	65 (65)
Rank 2	30 (31)	27 (28)	26 (26)	27 (28)
Rank 3	-	8 (8)	8 (6)	6 (6)
Rank 4	-	-	3 (3)	2 (1)

$R_2 - R_1 > 1$				
	Number of solutions			
	2	3	4	All
M	30,665	13,901	13,967	58,533
Rank 1	97 (98)	94 (92)	93 (92)	95 (95)
Rank 2	3 (2)	5 (6)	4 (5)	4 (4)
Rank 3	-	1 (2)	2 (2)	1 (1)
Rank 4	-	-	1 (1)	0 (0)

Table 6.1: Distribution in % of the "selected" rank, i.e., the solution closest to NCEP wind, over all ranks ranked in increasing order of R. Data are stratified with respect to the total number of solutions with columns of 2, 3, 4, and all solution cases. M is the number of cases in each column. The percentages between brackets are the actual observed distributions in 5 orbits of data; numbers without brackets are the predicted distributions using equations (6.6-9). The top table shows statistics over all data, the middele table over data with $R_2 - R_1 \leq 1$, and the lower table over data with $R_2 - R_1 > 1$.

We can now use the formulation of $p_s(x)$ to predict how often a certain solution rank corresponds to the "true" solution for a varying number of solutions, and for varying distributions of R_i. Table 6.1 compares the predicted distribution over the different ranks with the one actually observed in a sample of five orbits. Results are presented for all cases and for cases stratified using the conditions $R_2 - R_1 \leq 1$ and $R_2 - R_1 > 1$. The correspondance is striking. Therefore, we can conclude that our assumption in the beginning of this section is a useful one, and that equation (6.8) can be used to determine the weights w_i in the scatterometer observation cost function in equation (6.3).

We now determine how to combine the two probabilities that determine w in equation (6.3). We assume that the solution pattern V_i and the solution probabilities $p(R_i)$ are two independent pieces of information that help to determine the probability w_i of each solution. A straightforward way to combine them is given by

$$P(s = j \mid \phi_i, R_i; i \in \{1, N\}) = \frac{p_s(R_j)p_j^P}{\sum_{i=1}^{N} p_s(R_i)p_i^P} \tag{6.10}$$

It turns out that the sizes of the angular sectors are over a large data sample evenly distributed over the various ranks; hence, a table like 6.1 calculated on the basis of equation (6.10) in stead of (6.6) gives equal probabilities for all ranks, and a table based on (6.10) gives almost exactly the same results as a table based on (6.6). Nevertheless, equation (6.10) is likely the better choice as the basis for the cost function, since it, for each particular wind solution pattern, takes into account the a posteriori probability of solution selection. Doing so, this results in a spatially consistent solution pattern and probability field (Figa and Stoffelen, 2000).

The effect of using residual and sector information on J_O^{SCAT} is shown in figures 6.4a and 6.4b. The contour values used in the figures are identical. In figure 6.4a it can be seen that the lower probability solution of the two closely spaced wind vector solutions is narrower than in figure 6.4b, and therefore indeed less likely. Also the minimum for the isolated wind vector solution is deeper and has a larger "region of influence" in figure 6.4a compared to 6.4b. Region of influence can be understood as that part of the wind domain where the gradient points away from a particular solution (note the shift of the contour lines around the origin). The region of influence of a particular solution should be proportional to its probability.

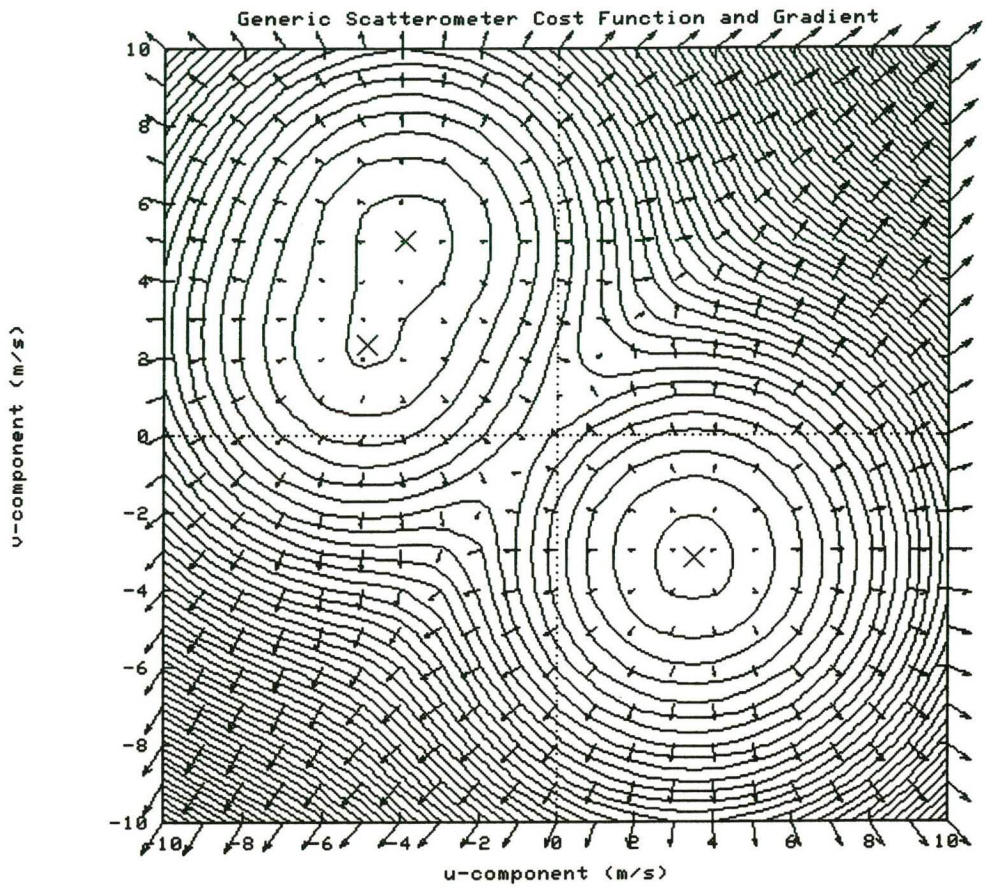

Figure 7.3a : Plot of the scatterometer cost function with inversion residual and wind direction sector representation appropriately included.

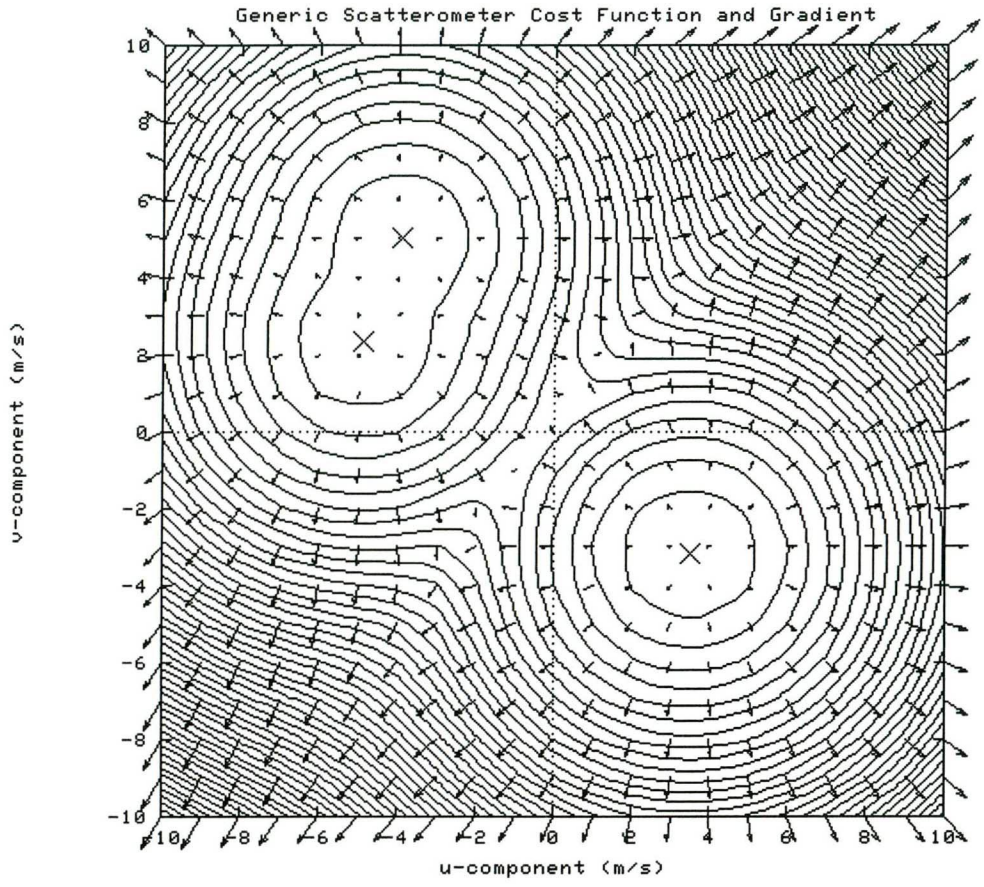

Figure 7.3b : Plot of the scatterometer cost function and gradient without accounting for direction sector and inversion residual.

6.3 OPTIMAL FORMULATION

Equations (6.2-10) provide equations that can be used to formulate a generic cost function for scatterometer data. However, Stoffelen and Anderson (1997c) report the following features of this formalism for ERS data in case that V is smaller than ε_s

- Not quadratic in the minumum; and
- No minimum at either of the solutions, but at $V = 0$.

These authors provide an alternative formulation that cures these features

$$J_o^{SCAT} = \left(\frac{\prod_{i=1}^{N} K_i}{\sum_{i=1}^{N} K_i} \right)^{1/P} \tag{6.11}$$

where they use $P = 4$ and we redefine

$$K_i = \left[\left(\frac{u - u_i}{\varepsilon_u} \right)^2 + \left(\frac{v - v_i}{\varepsilon_v} \right)^2 - 2 \ln P_i \right]^P \tag{6.12}$$

In case of more than two solutions, such as with NSCAT or SeaWinds, there will be more occasions when two solutions are close together, i.e., $|\mathbf{V}_i - \mathbf{V}_j| < \varepsilon_s$. As such, it becomes more important which formulation to use. Here we will elaborate on this issue.

Figure 7.4 shows a simple illustration of the different behaviour of equations (6.2-10) and (6.11-12). It represents a case where the scatterometer observes a wind speed of 2 m/s on the ocean surface with 180 degree ambiguity. Using equations (6.2-10) result in a cost that is minimum at zero wind speed, indicating that this is the most likely wind speed. Physically speaking, this is certainly not right; the ocean capillary-gravity waves will correspond quite well with 2 m/s. If we would systematically use this cost function formulation for these cases, we would get a wind speed that is lower than 2 m/s, i.e., a bias with respect to the scatterometer observation. Apparently, the maximum probability solution that we adopt is biased. Stoffelen (1998; chapter 6) shows that in case of non-linear problems, it is not clear what objective results in the best analysis, since a zero bias, minimum variance, or maximum probability constraint can all result in a different answer.

If we adopt the approach that we want to minimise systematic error in the wind domain, it will be better to have a minimum in the cost function at or very near the wind solutions that are retrieved. In figure 7.4 it is illustrated that the cost function of equations (6.11-12) has these properties. In fact, in case one solution is the most likely at a particular wind then it will dominate the cost function, i.e., the formulation acts much like a solution selection algorithm.

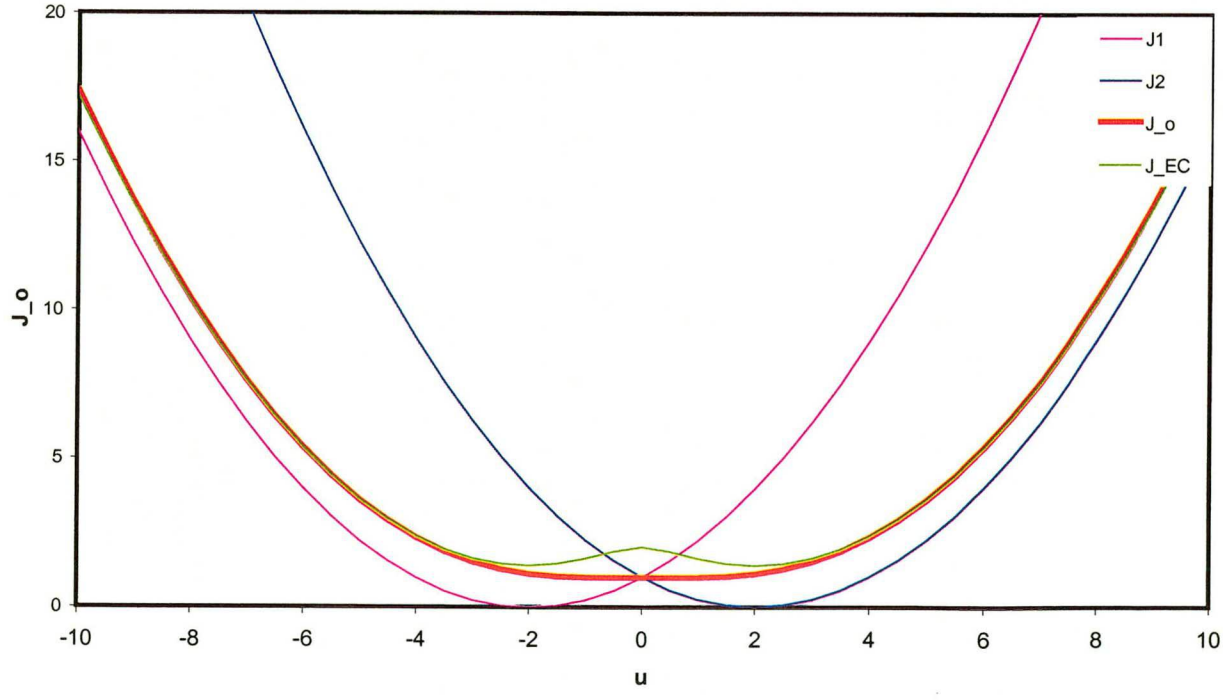

Figure 7.4: Plot of the generic scatterometer cost function formulation in u for an one-dimensional section along u with solutions $-u_1 = u_2 = \varepsilon_s = 2$ m/s, and $P_1 = P_2 = 0.5$. J1 and J2 present the quadratic contribution of the two solutions respectively, whereas J_o is the total cost using equations (6.2-10) and J_EC when using the alternative formulation of equations (6.11-12). In the latter case both solutions are kept as minima.

Often observation cost is used to monitor the RMS fit of the assimilation model control variables to the observations. To make such diagnostic more realistic for scatterometer data when using the above formulations, one could add for example 2 ln $P_{s=j}$ for each observation to the total cost.

Either equations (6.11-12) or (6.2-10) can be used to allow variational quality control. In that case, one needs to add a solution with let us say $\varepsilon_s >> 100$ and P_i equal to the expected gross error rate. For the nadir and far swath parts this could be a way to use the winds, but with more stringent QC. This needs to be further explored in the near future.

Based on the above discussion we recommend the use of equations (6.11-12).

7 AMBIGUITY REMOVAL

Ambiguity removal (AR) is the process of selecting the wind vector solution at each observation point in a way that results in a spatially and meteorologically consistent wind field. AR is required when the 1st rank skill is not 100%.

In section 7.1 we give a short description of the 2D-VAR method and the changes that are incorporated for Seawinds. For more details on 2D-VAR see (de Vries and Stoffelen, 2000). Section 7.3 shows some validation of the approach.

7.1 DESCRIPTION OF 2D-VAR

In line with chapter 6, in 2D-VAR ambiguity removal is formulated as a minimisation problem of the objective function.

$$J = J_b + J_o^{scat} \tag{7.1}$$

where J_o is the observation cost function and J_b the background field cost term. 2D-VAR is based on the analysis of wind increments with the control variable defined as

$$\delta \underline{x} = (\underline{x} - \underline{x}_b) = \begin{pmatrix} u \\ v \end{pmatrix} \tag{7.2}$$

where $\underline{x}$ is the control state, $\underline{x}_b$ is the background state, u the west-to-east component of the wind, v and the south-to-north component. For the minimization a conjugate gradients method is used.

The background term J_b in the cost function is based on a maximum probability formulation and the assumption that errors in the background field have a statistical distribution, which is Gaussian around the wind vector components. The background term quantifies the spatial context of background field errors and determines the spreading of observational information. It is expressed as

$$J_b = \delta \underline{x}^T B^{-1} \delta \underline{x} \tag{7.3}$$

The wind increment components in the background term are cross-correlated leading to a full error covariance matrix B. Given the size of B in practice, direct inversion makes the minimisation proces expensive if not intractable. To circumvent direct inversion we assume that the background error covariances are homogenous and isotropic i.e. a function of separation distance only. This allows for the efficient diagonalisation of the background error covariance matrix in the spectral domain by means of a unitary similarity transform. The similarity transform is in fact a rotation of the frame of reference that results in the wind being expressed in terms of longitudinal and transverse wind components (figure 7.1), i.e.

$$l = u\cos\theta + v\sin\theta \tag{7.4}$$

$$t = -u\sin\theta + v\cos\theta \tag{7.5}$$

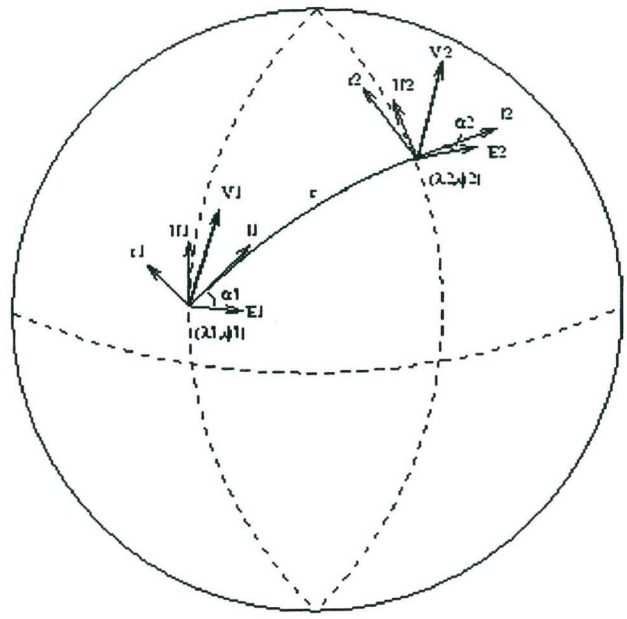

Figure 7.1 Definition of the longitudinal and transverse wind error component

In the spectral domain the background error covariance matrix can be expressed as

$$B = R\Lambda R^{-1}, \tag{7.6}$$

where Λ is a diagonal matrix containing the Eigenvalues of the background error covariance matrix which is defined as

$$\Lambda = \sum_{n,m} diag\left(c_{nl}^{m}, c_{nt}^{m}\right) \tag{7.7}$$

and R is a unitary rotation matrix with the following block diagonal structure structure at each wave number pair (n,m)

$$R_n^m = \begin{pmatrix} \cos\theta_n^m & -\sin\theta_n^m \\ \sin\theta_n^m & \cos\theta_n^m \end{pmatrix}, \quad \theta_n^m = \arctan\frac{n}{|m|}. \tag{7.8}$$

The coeficients c_{nl}^{m}, c_{nt}^{m} are determined by error covariance functions, which are functions of distance only. These error covariances are usually determined empirically. In 2D-VAR the covariance functions consist of a constant variance, due to homogeneity and isotropy, and quasi-geostrophic structure functions (error correlation functions, fig. 7.2) (Buel, 1972).

The spectral implementation of the background term requires that in grid point space the control variable is defined on a so-called "extended grid" (see figure 7.3) to avoid that the periodicity of Fourier Transform affects the solution on the grid near the location of observations

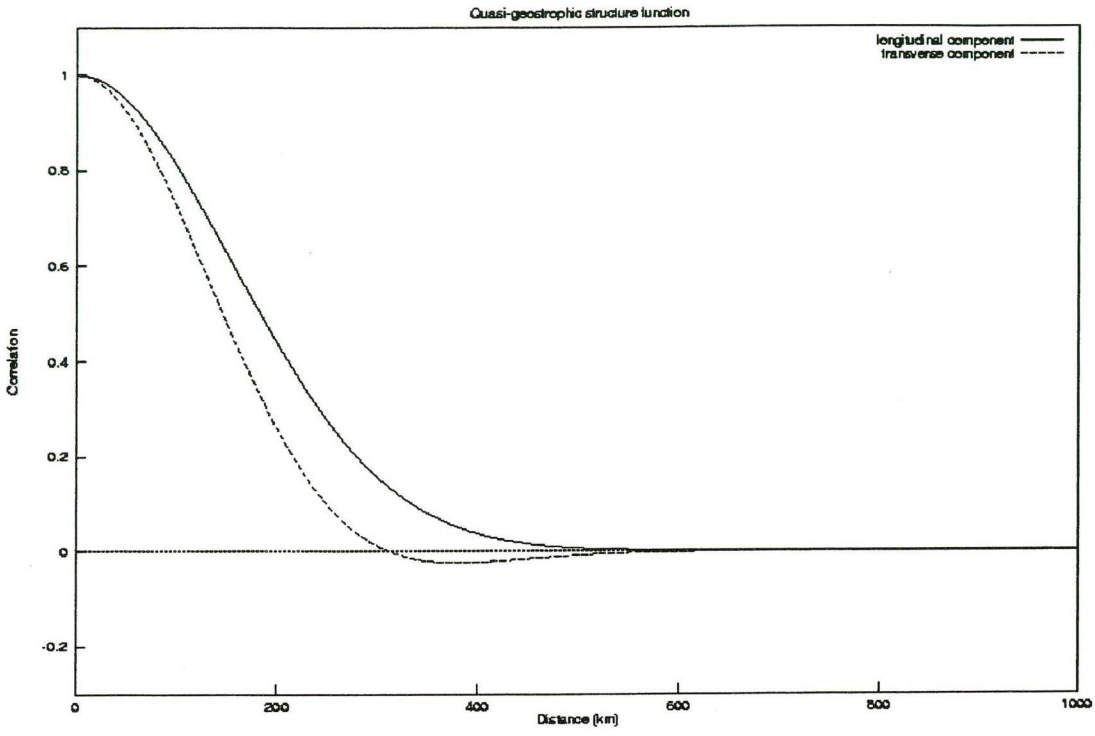

Figure 7.2 Structure functions for the longitudinal and transverse wind error component

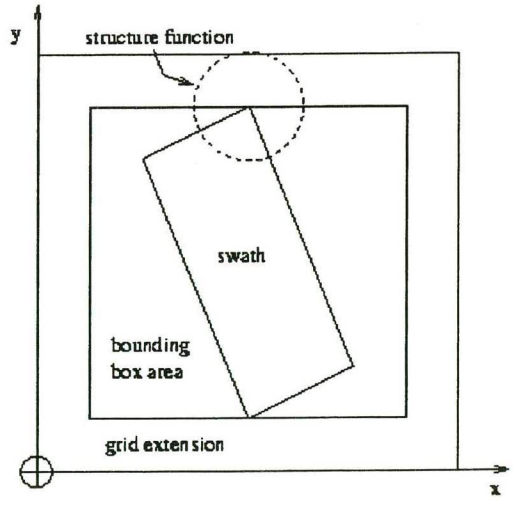

Figure 7.3 The extended grid constructed around the bounding box that holds the observations

To make the minimisation proces more robust, preconditioning is applied by introducing a new variable

$$\delta \underline{z} = \Lambda^{-\frac{1}{2}} R^T \delta \underline{x} \tag{7.9}$$

The cost function to be minimised is reformulated as

$$J = \delta \underline{z}^T \delta \underline{z} + J_o^{SCAT} \tag{7.10}$$

The gradient of the cost function, which is required in the minimisation, becomes

$$\nabla_{\delta \underline{z}} J = \nabla_{\delta \underline{z}} J_b + \frac{\partial \delta \underline{x}}{\partial \delta \underline{z}} \nabla_{\delta \underline{x}} J_o^{SCAT} = 2\delta \underline{z} + \Lambda^{\frac{1}{2}} R^T \nabla_{\delta \underline{x}} J_o^{SCAT} \tag{7.11}$$

In the computation of the cost function, J_o^{SCAT} is evaluated in grid point space for which

$$\delta \underline{x} = R\Lambda^{\frac{1}{2}} \delta \underline{z} \tag{7.12}$$

is needed which requires convolution and an inverse Fourier Transform. The subsequent computation of the gradient of J_o^{SCAT} requires a forward Fourier Transform and again convolution. With the implementation of 2D-VAR in this way the necessity of having to apply deconvolution and the explicit specification of the B-matrix in grid point space are avoided. Also the solution increments in the minimisation are expressed in terms of the spatial structure of the error covariances.

As discussed in chapter 6, the observational term in the cost function J_o^{SCAT} is

$$J_o^{SCAT} = \left[\sum_{i=1}^{N} J_i^{-p} \right]^{-1/p} \tag{7.13}$$

in each observation point with

$$J_i = -2 \ln P\left(\mathbf{V}^i \middle| \delta \underline{\mathbf{x}}\right) = \frac{(H(u) - u_i)^2 + (H(v) - v_i)^2}{\varepsilon_{si}^2}, \tag{7.14}$$

where $\mathbf{V}^i$ is a wind vector solution, u_i, v_i are the (observation-minus-background) wind component increments, H is an interpolation operator that maps the control variables onto the observations and ε_{si} is the standard deviation of the expected total mean component wind error for scatterometer winds that currently is defined by ε_s = 1.8 m/s. The parameter p has the value of 4. The gradient of the observational term at each observation point is

$$\nabla_{\delta \underline{x}} J_o^{SCAT} = \sum_{k=1}^{N} J_k^{-(p+1)} \left[\sum_{i=1}^{N} J_i^{-p} \right]^{-(1+1/p)} \frac{\partial J_k}{\partial \delta \underline{x}} \tag{7.15}$$

To define solution probability (as in chapter 6) the expected value <MLE> for 100-km resolution scatterometer data was obtained according to the procedure described by Portabella and Stoffelen (2000). The <MLE> as a function of wind speed and WVC number is presented in figure 7.2. The expected MLE was computed as a function of rank-1 wind speed and SWVC number with 200 orbits of observed Seawinds data averaged to 100-km resolution. We filtered the surface twice to

obtain figure 7.4 in order to reduce sampling noise. The filtering procedure was identical to that described by Portabella and Stoffelen (2000).

After minimisation the analysis is obtained from

$$\underline{x}_a = \underline{x}_b + \delta\underline{x}_a \tag{7.16}$$

which constitutes the best estimate for the surface wind field given the background field, the observations, and the objective function.

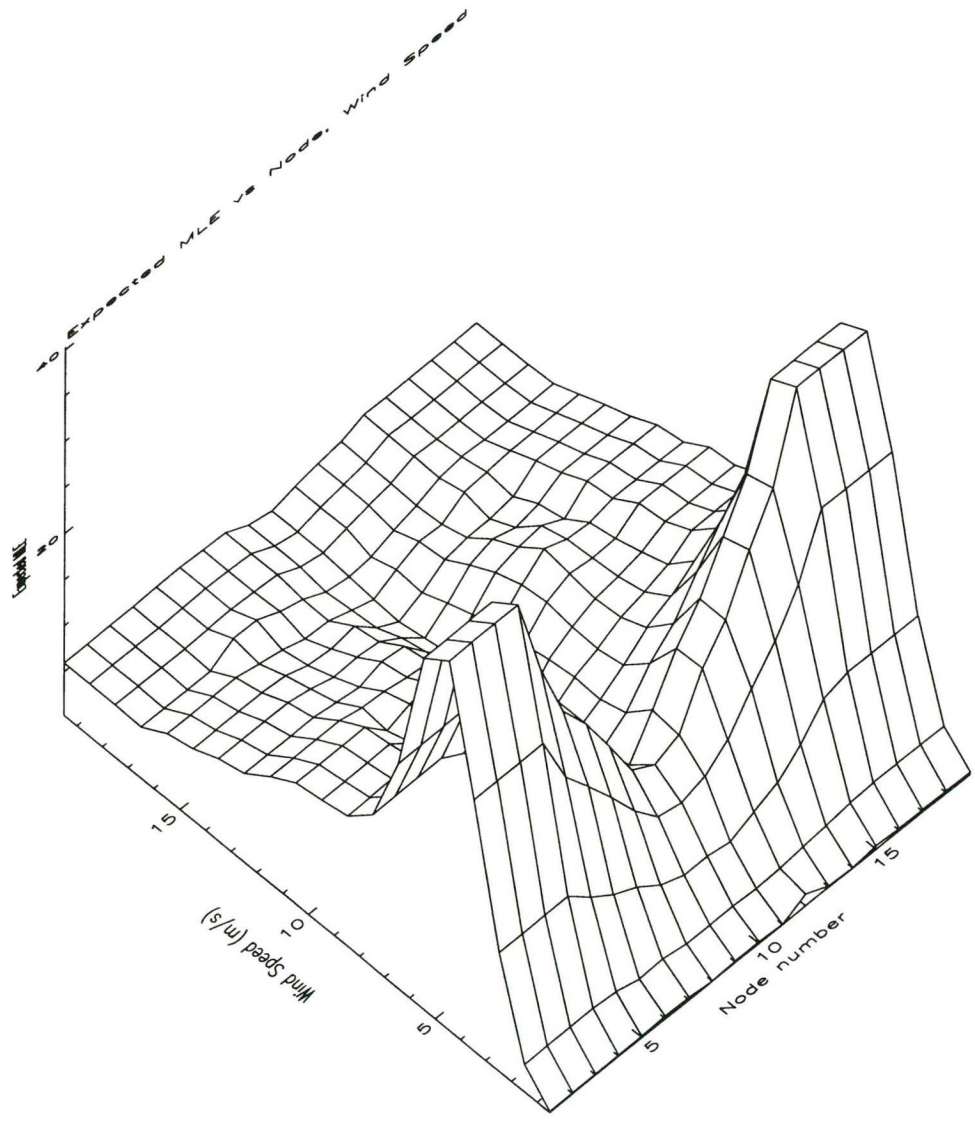

Figure 7.4 The mean MLE surface used for normalisation.

7.2 QUALITY OF THE AMBIGUITY REMOVED WINDS

To illustrate the quality of the 100-km winds we present a case of a storm in the Atlantic region west of Ireland. To be able to compare the 25-km SeaWinds product with the KNMI 100-km product we thin the JPL winds provided by NOAA to 100 km. Figures 7.5a and 7.5b show the JPL wind product and the KNMI 100-km product respectively of this storm on the 28th of September 2000. The red arrows represent the QuikSCAT winds in the products. The sky blue arrows represent a HIRLAM 3hr forecast. The grey-scaled infrared cloud image is from METEOSAT.

The thinned JPL product and the KNMI 100-km product show that at the eye of the storm the centre of vorticity in the surface wind is somewhat shifted to the East compared to the rotation higher up in the atmosphere, as depicted by the cloud structure. The saddle point between the center of the storm and a second low to the North is well defined in the JPL product but poorer in the KNMI 100-km product. The intensity of the secondary low at 15W and 60N in the KNMI product is lower than in the JPL product because of the inherent smoothing, but possibly also because of improved rain elimination. From figures 7.5a-b we can conclude that for this meteorologically significant case with a well-defined structure of the wind field, important features present in the 25-km product are generally preserved in the 100-km product.

In fig.7.6a-b we show a typical tropical case with more moderate and low winds. In figure 7.6a, the JPL winds show a general preference to blow across-swath and to a lesser degree along-swath. Moreover, some erratic large wind vectors appear that are most likely caused by rain (Portabella and Stoffelen, 2000). The KNMI product in figure 7.6b has cured to a large degree both the directional preference and the erratic speed variations. This is fairly typical in the tropical area, thus indicating an improved performance at low and moderate wind speeds.

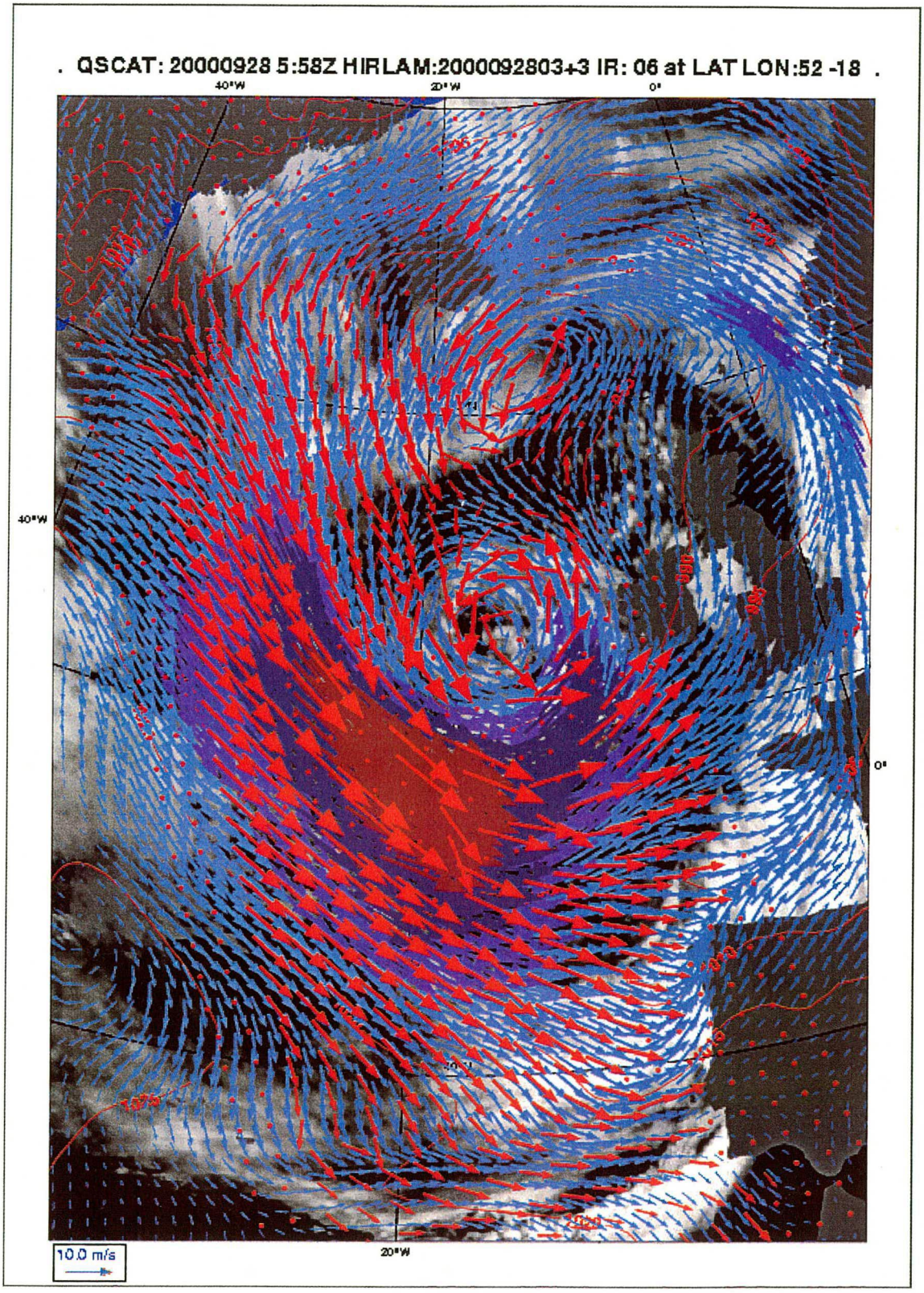

Figure 7.5a The JPL wind product of an Atlantic storm on september 28 2000 thinned to 100 km resolution (red arrows). For reference a MeteoSat infrared image is used as background (grey-scale) and the HIRLAM winds (blue).

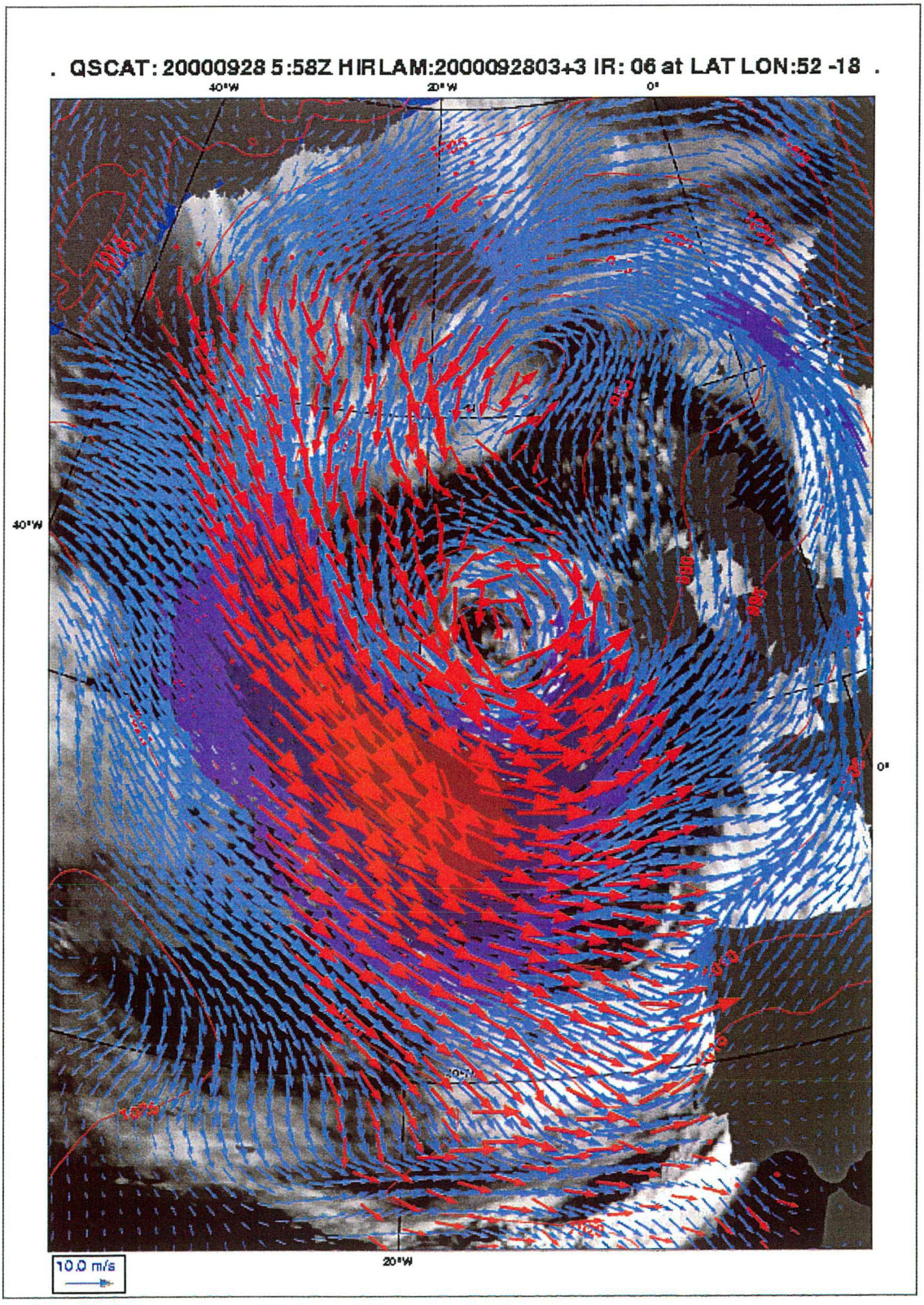

Figure 7.5b As 7.5a, but the KNMI 100 km wind product of the Atlantic storm on september 28 2000.

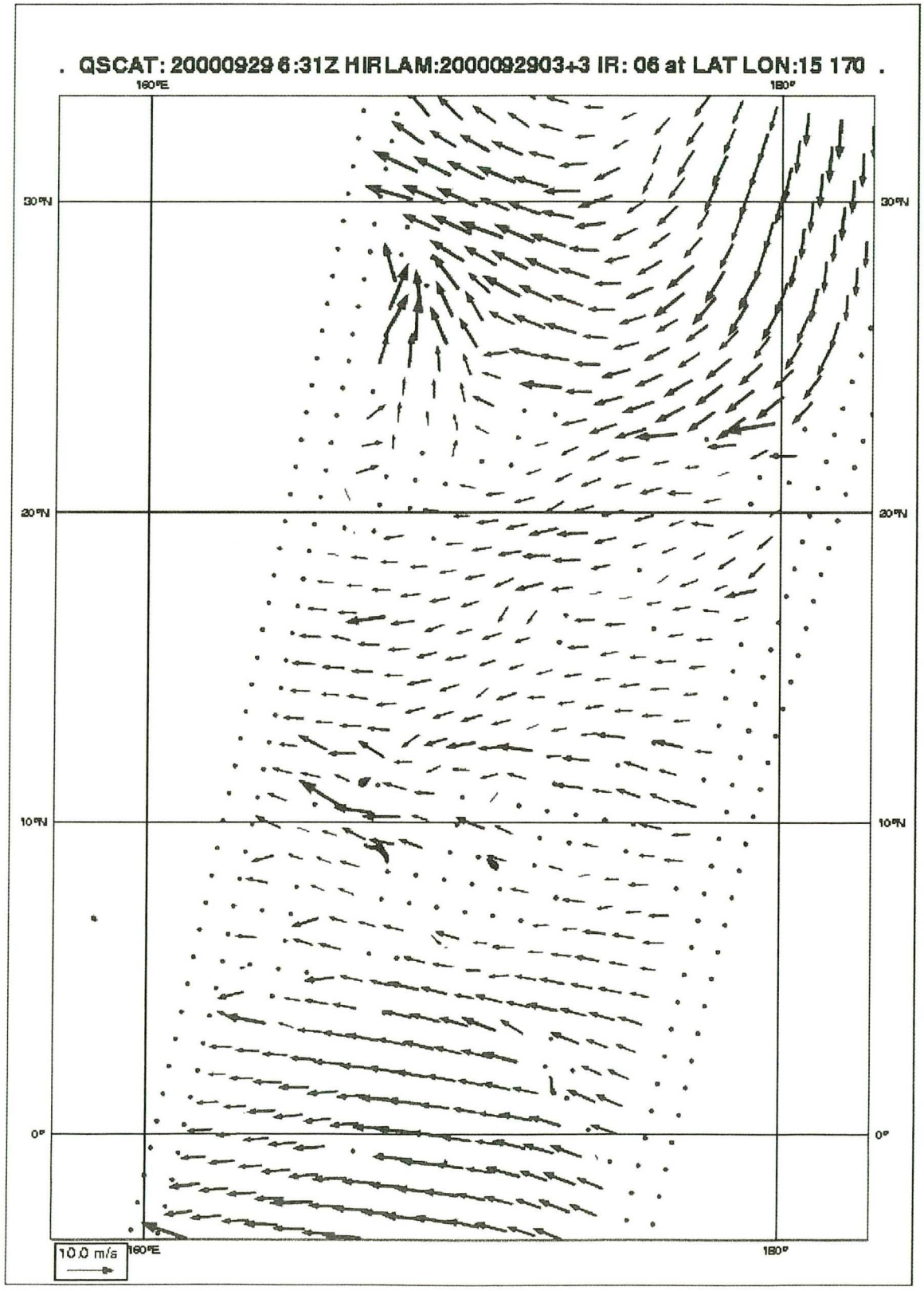

Figure 7.6a The JPL wind product of a tropical area on september 29 2000, thinned to 100 km.

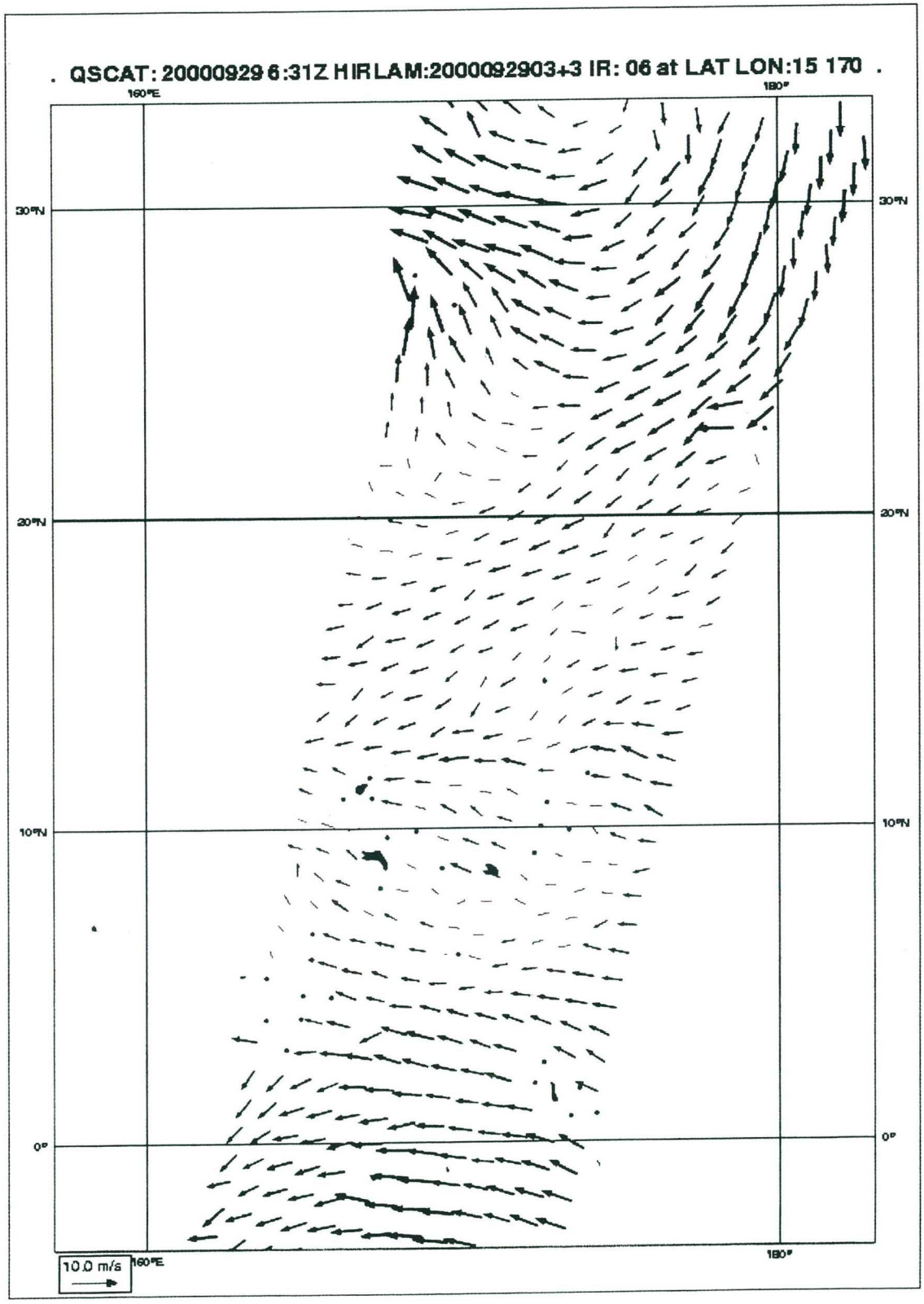

Figure 7.6b As 7.6a, but the KNMI 100 km wind product.

8 QUALITY ASSESSMENT

8.1 OBJECTIVE ANALYSIS

To assess the quality of the retrieval and the ambiguity removal a comparison was made between the JPL 25-km BUFR wind product thinned to 100-km and the KNMI 100-km wind product. For the comparison wind speed, wind direction and wind components were computed for an independent reference and both the thinned JPL product and the 100-km KNMI product

The comparison with the independent reference was carried out for the closest vector solution to the reference, for the rank 1 solution, and for the AR selected wind solution. A direct comparison was done for the rank 1 and selected solutions. In the thinned JPL product the 25-km wind closest to the centroid of the 100-km SWVC was used. The comparison was carried for the SWVC's in the sweet part of the swath where the best quality is expected.

The reference was the ECMWF analysis of the 10-m wind. The analysis wind has been interpolated both in space and time to the location and observation time of the scatterometer measurements. The ECMWF does not assimilate SeaWinds scatterometer winds and both are thus independent.

The wind speed, wind direction and wind components were accumulated in two-dimensional histograms for the measurements on days 252 to 255 of the year 2000. Figures 8.1 show density-contoured plots of the two-dimensional histogram of KNMI versus ECMWF for the (a) closest-to-reference, (b) the rank 1 and (c) the selected wind solutions. Figures 8.1d-f show the same plots for thinned JPL versus ECMWF.

If we consider the two closest-to-reference plots (figures 8.1a and 8.1d) we notice that both products have similar standard deviation and small systematic differences with ECMWF for the direction distribution. The JPL product has a somewhat larger systematic speed difference for high wind speeds than the KNMI product. As a result of the speed difference the component distributions are somewhat rotated in the JPL product. Remarkable is the small number of realisations of wind speed under 2 m/s in the KNMI wind product. This phenomenon is probably related to the inversion scheme and requires further study. The contours in the upper left and lower right corners in the direction plots are due to the periodicity of the wind direction domain. As such, these parts of the distribution have been taken as close-to-zero differences in the computation of the statistics.

Looking at the JPL differences between the closest-to-reference and the rank 1 histograms (8.1d and 8.1e) it is evident from the distribution peaks around the lines of 180 degrees deviation in the direction plot that the JPL products have a directional ambiguity problem. The error in the JPL wind direction has increased significantly in the rank-1 plots due to this ambiguity problem. The ambiguity problem further results in the spikes perpendicular to the diagonal in the component distributions. In the KNMI product (8.1b) the rank-1 ambiguity problem is much reduced. The statistics show that the systematic wind speed difference and the standard deviation in the wind direction distribution of the rank-1 solution of the KNMI product are smaller compared to ECMWF than those of the thinned JPL product. This gives a strong indication that the retrieval at 100-km improves the quality of the rank-1 solution at the ECMWF model resolution.

Comparison of the density-contoured histograms for the distributions of the selected solutions (8.1f) with those for rank 1 (8.1e) show that the direction distribution has been improved considerably by the JPL ambiguity removal. The distribution peaks around the 180-degree deviation

lines have been removed. To a lesser extend (compare 8.1c and 8.1b) this is also the case in the KNMI product.

If we consider the solution distribution among ranks for the selected solution for all NSCAT-like nodes for both products, tables 8.1a-b show that they are quite similar. Given the higher quality rank-1 solution, KNMI should have a lower standard deviation in the wind direction difference than JPL. Yet the JPL wind direction difference standard deviation is smaller. Therefore, the ambiguity removal in the JPL product is more effective and there seems room for improvement for AR in the KNMI product.

A reason for the lower AR score in the KNMI product could lie in some of the numbers provided in tables 8.1a-b, which show that the number of cases with 4 solutions in the KNMI product is high compared to that in the JPL product. To understand the consequences of these differences, the directional distribution patterns should be compared, which requires further study. Moreover, since JPL changed the GMF it is inverting in spring 2000, there is another difference between JPL and KNMI (old GMF) products than solely due to resolution. By recomputing the 25-km product at KNMI the precise effect of the GMF in the solution pattern should be investigated.

JPL	#of solutions	1	2	3	4	all
	#of nodes	41	32828	33178	32369	98416
Selected rank		(%)	(%)	(%)	(%)	(%)
1		100	92	82	75	83
2		0	7	14	19	13
3		0	0	3	4	2
4		0	0	0	1	0

Table 8.1a Solution distribution among ranks for the JPL wind product

KNMI	#of solutions	1	2	3	4	all
	#of nodes	20	14610	22306	55390	92326
Selected rank		(%)	(%)	(%)	(%)	(%)
1		100	98	89	77	83
2		0	1	7	14	10
3		0	0	2	4	3
4		0	0	0	3	1

Table 8.1b Solution distribution among ranks for the KNMI wind product.

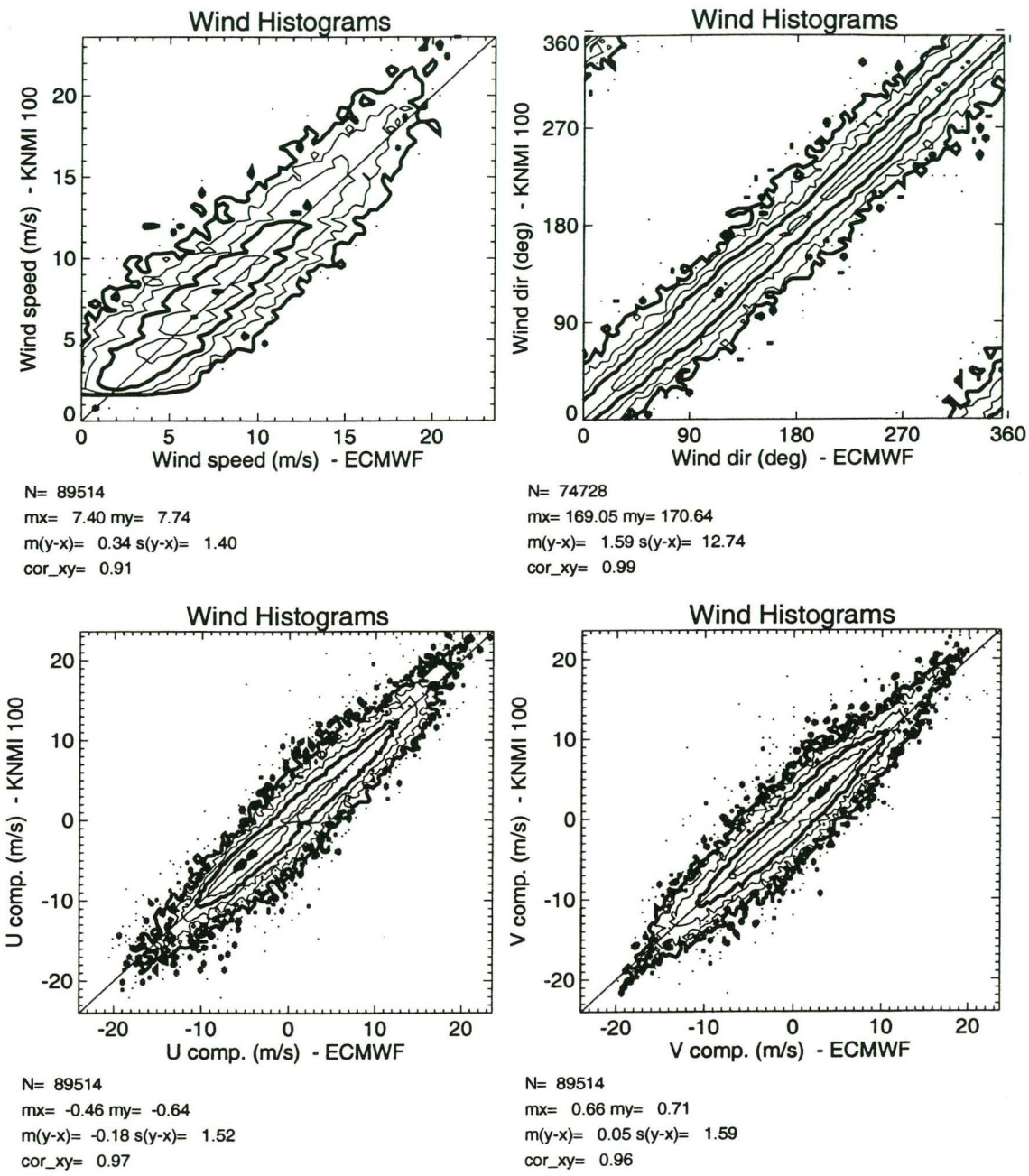

Figure 8.1a: Wind speed, wind direction and wind component distributions of the KNMI solution closest to ECMWF versus ECMWF.

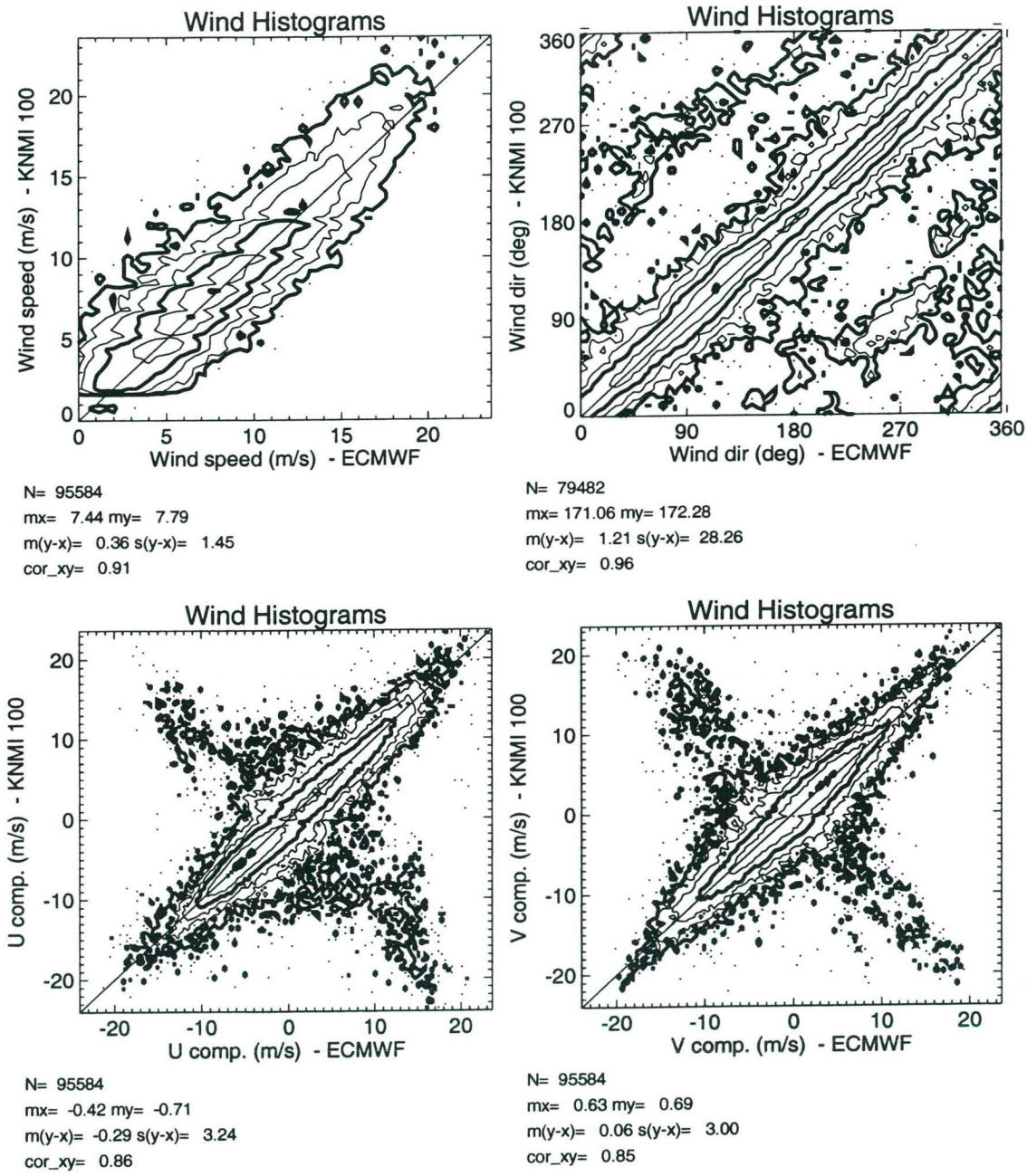

Figure 8.1b: Wind speed, wind direction and wind component distributions for the rank 1 solution of the KNMI product versus ECMWF.

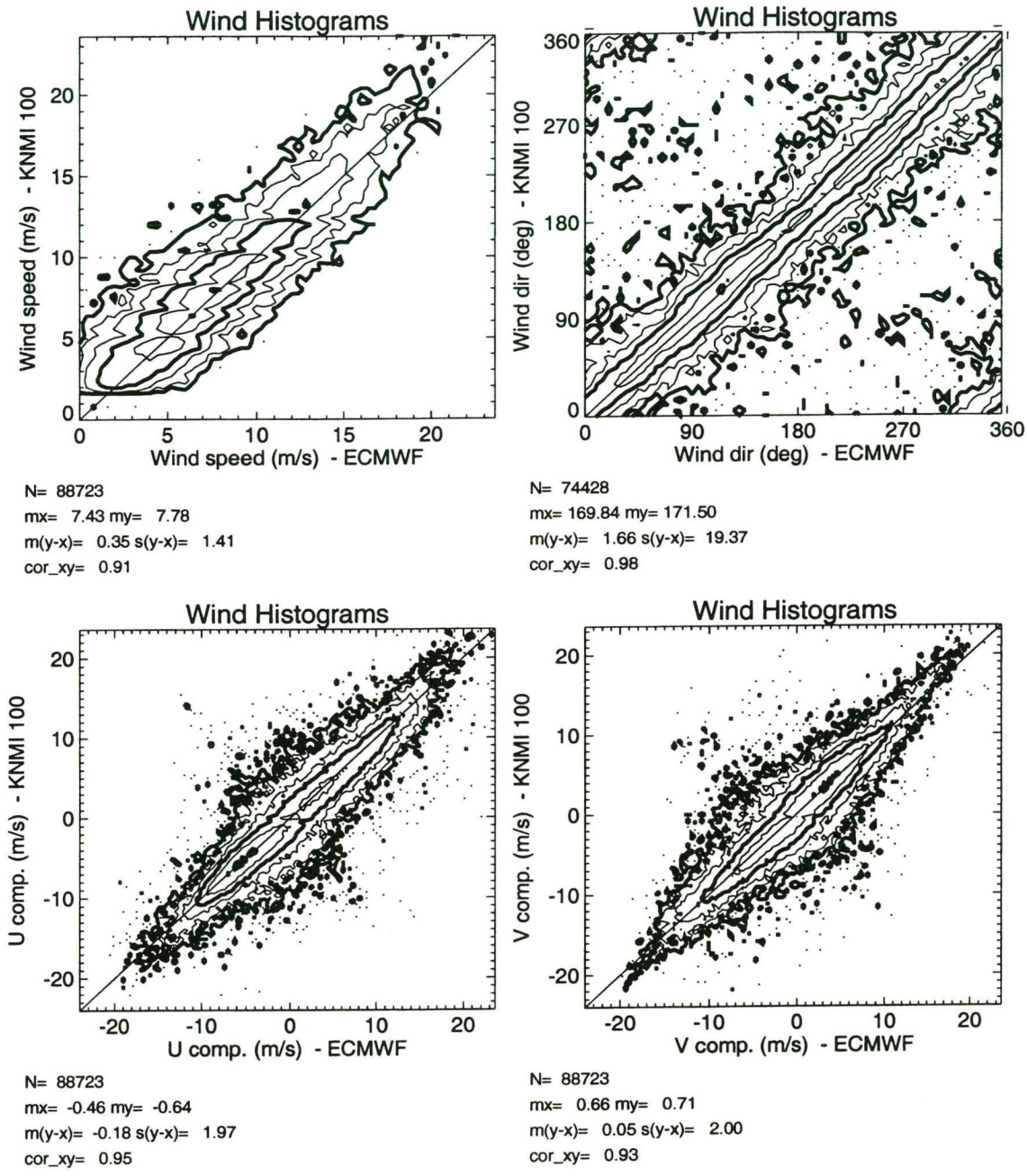

Figure 8.1c: Wind speed, wind direction and wind component distributions for the selected solution of the KNMI product versus ECMWF.

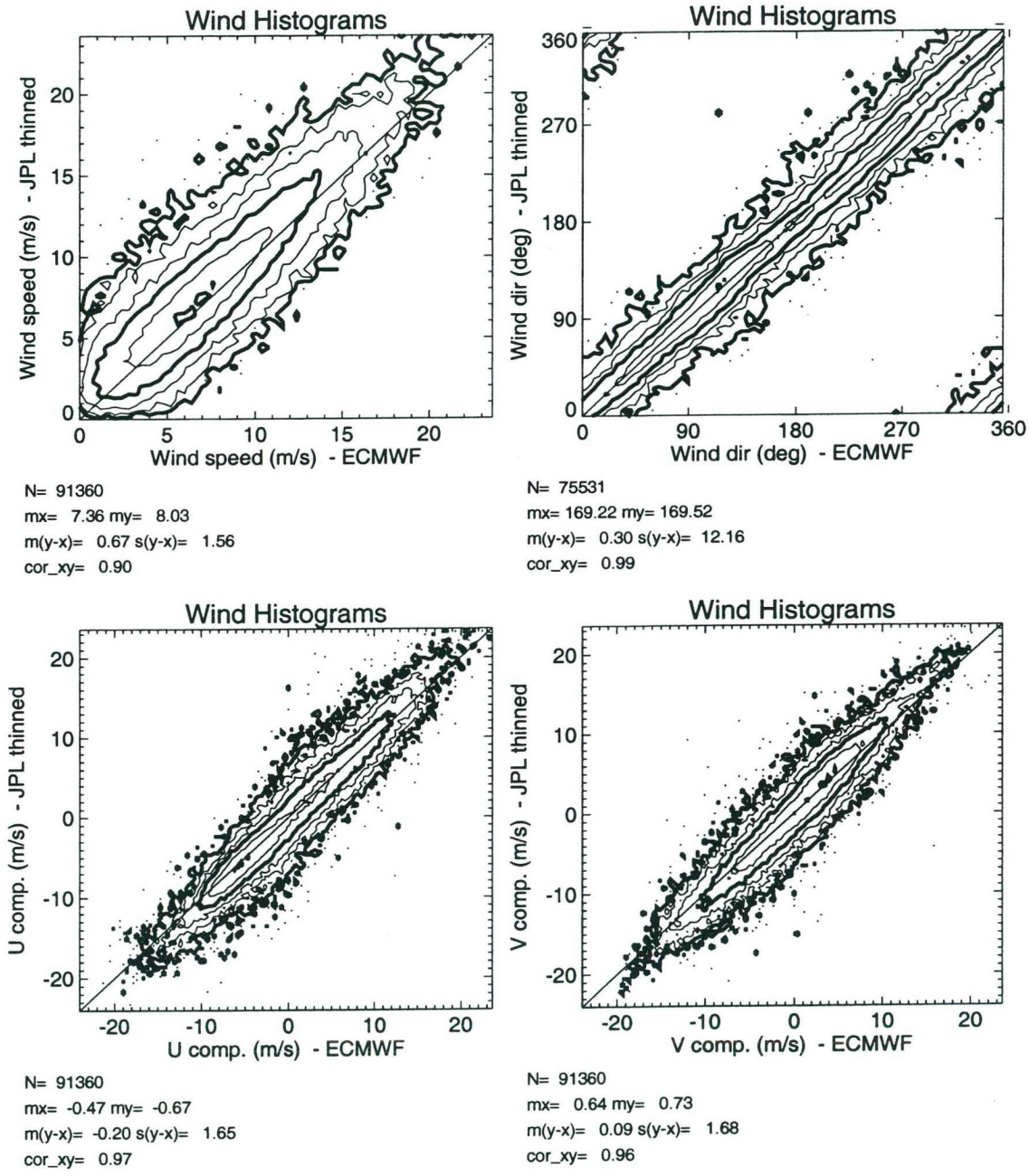

Figure 8.1d: Wind speed, wind direction and wind component distributions of the JPL solution closest to ECMWF versus ECMWF.

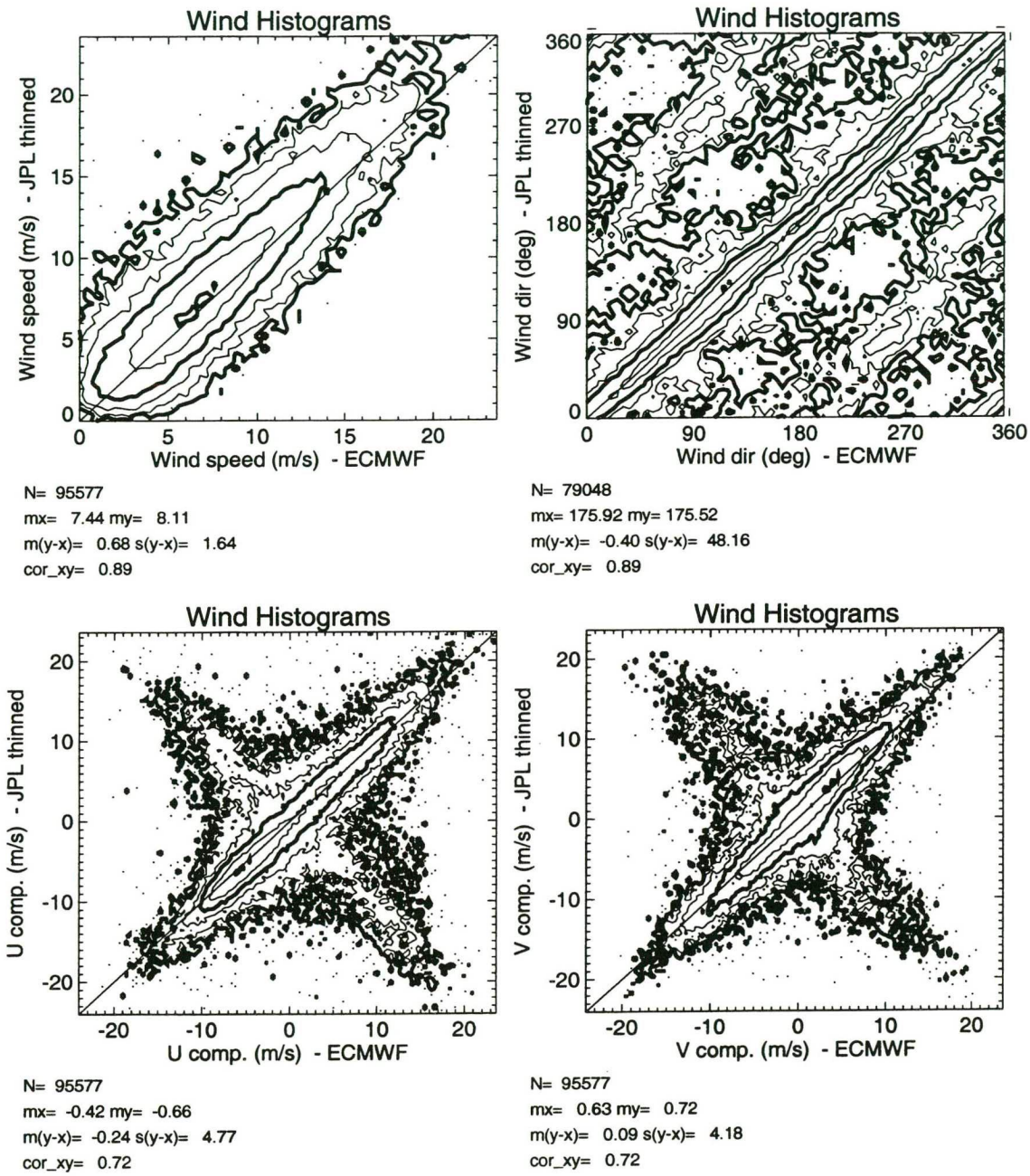

Figure 8.1e: Wind speed, wind direction and wind component distributions of the rank 1 solution of the thinned JPL product versus ECMWF

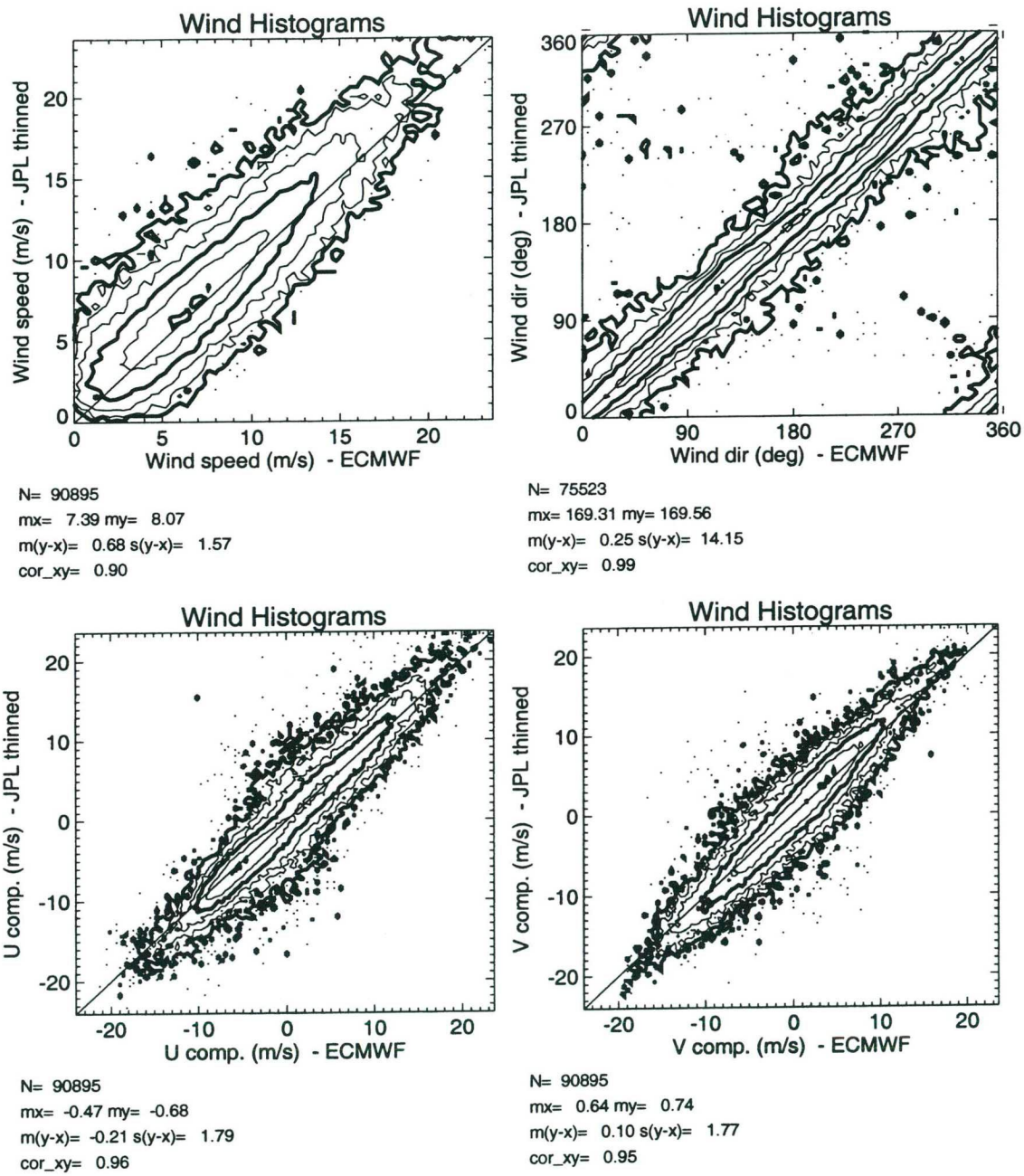

Figure 8.1f: Wind speed, wind direction and wind component distributions of the selected solution of the thinned JPL product versus ECMWF

8.2 SUBJECTIVE COMPARISON

8.2.1 VALIDATION PROCEDURE

In the period of October 1st 2000 to January 1st 2001 a validation procedure was carried out in which the 100-km QuikSCAT product of KNMI was compared with the original 25-km NOAA QuikSCAT product. During the validation effort the on-duty meteorologist received an e-mail notifying him/her when significant changes were present in the KNMI product between the QuikSCAT observations and NCEP model output for the 10m wind, which was used as reference. The mail also referred the meteorologist to web pages where the wind products were shown. At first the reference for the NOAA product was the web site at NOAA (cf. http://manati.wwb.noaa.gov/quikscat). Because of frequent non-availability of the wind products on the NOAA website however it was decided to create a thinned 100-km NOAA QuikSCAT product based on the original data. From December 4th onwards this product was presented on the local web page along with the KNMI product.

The meteorologist was asked to classify the meteorological conditions, to determine the usefulness of the wind products, to compare JPL and KNMI, select the better product, and report his/her findings on a form that was issued in advance (cf. appendix A).

8.2.2 RESULTS

The findings have been compiled into tables. From the tables a score matrix was derived (table 8.3). Reports were used in the statistics if usefulness and the selection of the better wind product were mentioned. Scores ending on .5 result from assigning a particular case to two classes by the meteorologist.

Judgement	Classification				Total
Better	1[a]	2[b]	3[c]	4[d]	
1. KNMI	2	2.5	0.5	1	6 (8.8%)
2. NOAA	7.5	9	12	1.5	30 (44.1%)
3. Neither	11.5	12.5	5.5	2.5	32 (47.1%)

Table 8-3 : The score matrix

The scores show that the quality of KNMI product compared to the NOAA product is inferior for use in synoptic weather forecasting. In almost half of all cases there is however no important difference between the products.

In the beginning of December the quality control for the KNMI wind product was altered temporarily for over a week. Information from NOAA on rain detection was included. This resulted in a noticeably higher level of rejection of wind observations. The meteorologists, who were not

[a] developing or decaying weather system, saddle point.

[b] developed system with sharp pressure gradient(s).

[c] sharp fromt, ridge or trough

[d] different namely ...

notified of the change did notice it and mentioned it in their reports. Reports from December indicate that the lack of winds in the KNMI product was reason for the meteorologist to favour the NOAA product.

8.2.3 USEFULNESS OF THE WIND PRODUCTS

From the report form it follows that in 15.5 % of cases the wind products are considered as essential information, in 48.8% as important and in 35.7% of cases rated as of little use. It is apparent that a 100-km scatterometer wind product has added value for synoptic meteorological analysis. The main reasons mentioned are:

- More and better information on the detailed structure of the wind field
- Accurate estimation of the position and movement of low pressure systems
- Positioning of fronts, troughs and ridges
- The great advantage of a large coverage;
- Confirming/refuting model forecasts/analysis

During the current validation procedure we experienced difficulties that have hampered a smooth execution of the work that had to be done. The following may be improved

- Product quality, see section 8.1;
- For use in synoptic meteorological analysis by a meteorologist it appears better to develop a 50-km product;
- The way information is presented in terms of geographical projection, data resolution, symbols (wind vectors/barbs) may be improved;
- The easy accessibility through the use of a clickable map is important to control the abundance of wind products with which the meteorologist is confronted;
- Untimely availability of the wind products renders them useless in many cases for the meteorologists. Familiarity with the products should be increased through user support.

9 MONITORING

The last but not least important bit of the SeaWinds processing chain is the product monitoring. Product monitoring is implemented to guarantee that the products distributed do not suffer a common problem in the instrument functionality or data processing. In fact, a common problem could lead to serious problems in NWP data assimilation, since the analysis draws to incorrect winds, and as a consequence model forecasts may well be seriously corrupted. The monitoring of ERS data has led to the detection of a handful of cases with unexpected (by the user) instrument behaviour. The monitoring strategy for ERS is to

1. Check that the number of rejected WVC is nominal;
2. Verify that the normalised "distance to the cone" of the accepted WVC is close to unity;
3. Compute the mean and standard deviation of wind speed difference between scatterometer and NWP model; and
4. The mean and standard deviation of wind direction difference between scatterometer and NWP model.

Here we investigate the adaptation of this strategy to SeaWinds. Figure 9.1 depicts the monitoring properties of the JPL SeaWinds product. For a number of variables m it shows

$$\overline{m_n} = \sum_{i=1}^{n} m_i \tag{9.1}$$

where n is the number of data points over which m is averaged. For large n, the $\overline{m_n}$ converges to a fixed number $<m>$ with spread SD(m) as estimated in table 9.1.

Variable m	$<m>$	$<SD(m)>$	Threshold m
Number of rejected WVC [%]	7	3	16
Normalised Residual	0.82	0.1	1.12
Wind Speed [m/s]	7.9	2.1	14.2
SD of speed difference [m/s]	1.7	0.25	2.45
SD Direction difference [deg.]	21	11	54

Table 9.1: Mean, SD and threshold of the number of WVC rejections, mean normalised residual, mean wind speed, SD of wind speed difference between JPL SeaWinds and NCEP, and SD of wind direction difference between JPL SeaWinds and NCEP, estimated from hundred orbits of data. The right column is computed over a quarter orbit of data.

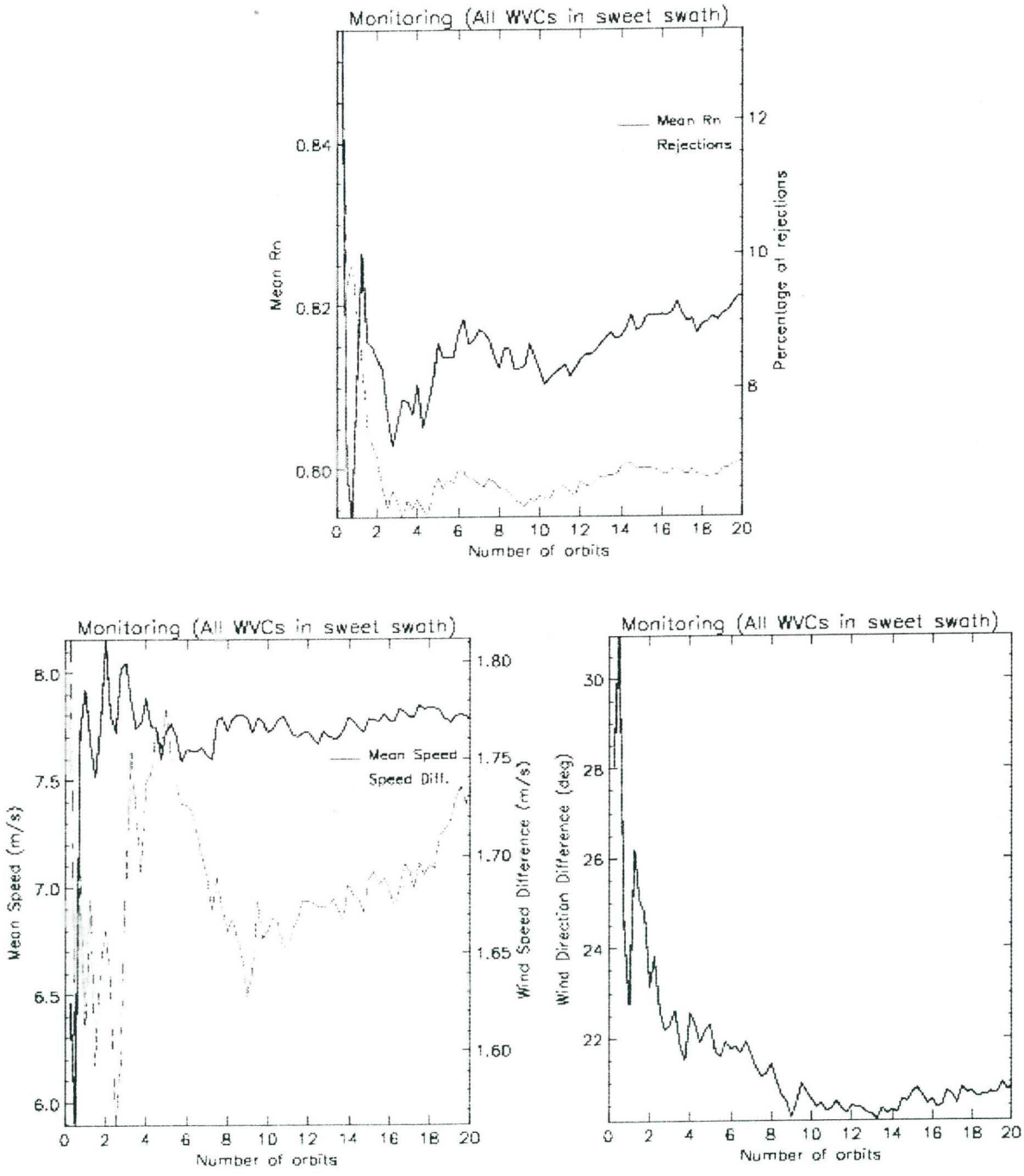

Figure 9.1: .Illustration of the monitoring properties of the SeaWinds instrument and its associated data processing. As a function of an increasing number of orbits we show at the top the number of WVC rejections and mean normalised residual, at the bottom left the mean wind speed and the mean wind speed difference between JPL SeaWinds and NCEP, and at the bottom right the mean wind direction difference between JPL SeaWinds and NCEP. Data volume increases with a quarter orbit on the horizontal.

From table 9.1 and figure 9.1 we note that not all of the monitoring parameters shown are equally valuable. For example, mean wind speed is quite variable from one quarter of orbit data to the next, whereas the SD of wind speed difference with NCEP is much more stable. This is caused by the fact that mean wind speed depends mainly on the geophysical wind regime sampled and not so much on SeaWinds wind quality, whereas the standard deviation of wind speed difference depends on both NCEP and SeaWinds wind quality. Mean wind speed difference between SeaWinds and JPL depends critically on the settings in the NCEP NWP model, which is why we did not use this variable for monitoring. The SD of the difference between NWP model and JPL SeaWinds, on the other hand, is much less sensitive to parameterisation changes in the NWP model.

The SD of wind direction difference is another variable of limited usefulness. If JPL SeaWinds wind directions would be random (no skill) with respect to the NWP wind then the SD of their difdference would be $360/\sqrt{12} = 104$ degrees. The threshold provided in table 9.1 is thus not very sensitive to errors in the SeaWinds product.

The monitoring procedure checks the variables in table 9.1 against their threshold. The threshold is a so-called 3-SD level, where the probability of exceeding one of the thresholds for any one quarter of orbit is about 1%. This percentage is still quite high, so we suggest to flag a quarter of orbit as suspect when three out of five monitoring variables are above the threshold. If we assume that the monitoring variables are mutually independent, then we have achieved a robust monitoring procedure.

SeaWinds data are distributed in batches of about half a revolution. Since some of the orbits contain a lot of land, it makes sense to base the monitoring on a quarter of orbit over the ocean, thereby excluding land and ice points. Over larger amounts of data the threshold can be tightened. Looking at figure 9.1 we note that the variability in $\overline{m_n}$ decreases with increasing n, following by approximation a $\sqrt{n}$ law. This means that in the definition of the threshold as the expected mean plus three times SD(m), the SD(m) term can be made proportional to $1/\sqrt{n}$. We suggest this more critical type of monitoring.

10 CONCLUSIONS AND RECOMMENDATIONS

Within the EUMETSAT-funded NWP Satellite Application Facility, SAF, a SeaWinds processing package is being developed that checks, spatially averages, and inverts backscatter data. After these steps a 2D-VAR ambiguity routine is run to investigate the ambiguity removal properties of the cost function and observation operator as proposed here. After these tests, application in 3D- or 4D-Var (e.g., Courtier et al, 1998) data assimilation systems is a straightforward development.

Following our procedure, we expect that carefully screened, smoothed, and assimilated SeaWinds scatterometer data from QuikSCAT and ADEOS-II have great potential in NWP. We applied a backscatter data averaging to 100 km before inversion, resulting in more smooth wind fields.

We developed tools to visualise SeaWinds measurements in order to qualitatively check the data and the correspondance with the NSCAT2 GMF. It is pointed out how these tools can be refined to provide more quantitative information.

Portabella and Stoffelen (2000) developed a succesful quality control algorithm that eliminates most rain points. The method works poorly in the outer swath where only vertical polarisation information is available. SeaWinds on ADEOS-II profits from AMSR for rain screening, when all parts of the swath can be checked for rain. Work remains to be done to develop procedures to extract high-quality wind information in those swath parts with poor azimuth or polarisation diversity.

A normalised RMS error for wind direction has been defined, which is a more meaningful quality estimator of the wind inversion than existing methods. Existing methods either compute the RMS of ambiguous scatterometer winds by taking

1) the closest solution with respect to to the reference wind; or

2) the selected solution with respect to the reference wind.

The first method is far too optimistic for those schemes that generate a large number of solutions. In this case always a very closeby solution exists. The second method can be too pessimistic on inversion skill, since ambiguity removal errors may dominate the RMS score. The normalised RMS error takes into account the ambiguity patterns in the wind direction skill score computation.

The method of data assimilation of ERS scatterometer data can be generalised to include NSCAT and SeaWinds observations. The asimilation of retrieved winds is the most practicable, since retrieved winds are generally unbiased, and because uncertainties in the background winds and the scatterometer retrievals are well expressed as normal errors in the wind domain. However, in the backscatter domain, these error distributions are skew, irregular, and dependent on the wind (direction), due to the non-linear transformation of these errors from the wind to the backscatter domain. As such, the assumptions generally used in meteorological data assimilation do apply if ambiguous scatterometer winds are assimilated, rather then backscatter data directly.

The generic approach for scatterometer wind assimilation uses the normalised inversion residuals of the solutions and information on the solution pattern to determine the relative probabilities of the wind solutions. The estimated solution probabilities verify very well with the average skill of the ranked solutions.

SeaWinds retrievals exhibit an increased number of wind vector solutions with respect to ERS. However, the rank-1 skill is around 80% and therefore ambiguity removal is less demanding than for

ERS. In objective tests of the performance of 2D-VAR it was found that work remains to be done to refine the validation tests in order to allow separate validation of the GMF, the procedure for its inversion, and the ambiguity removal. What is clear however, is that the KNMI 100-km inverted winds are of better quality than the JPL 25-km product.

A robust monitoring scheme has been defined that acts satisfactorily on a quarter orbit or more of processed winds from SeaWinds.

Challenges remain in the interpretation of the SeaWinds data at higher resolutions, and in those parts of the swath and geophysical conditions where the wind vector is poorly determined by the backscatter measurements available.

We set up at KNMI a SeaWinds scatterometer processing system, with visualisation, inversion, quality control, 2D-VAR ambiguity removal, and validation tools. These tools form a good basis for further development and implementation.

As such, data assimilation experiments can be carried out to test the algorithms in more full meteorological systems, such as 3D-Var or 4D-Var. Moreover, the system can be adapted to work at a resolution of 50 km, where it will probably still provide reliable high-quality synoptic-scale meteorological information of great potential in nowcasting and short-range forecasting by direct presentation to the on-duty meteorologists.

In conclusion SeaWinds provides

- The great advantage of a large coverage;
- Information of acceptable quality on the detailed structure of the wind field
- Accurate estimation of the position and movement of low pressure systems
- Positioning of fronts, troughs and ridges
- Confirmation or corrections of NWP model forecasts and analysis

For the real-time operational application of our products we recommend

- NWP impact of SeaWinds should now be tested at ECMWF and in HIRLAM as planned;
- Further checks on product quality, in particular ambiguity removal may be further improved;
- For use in synoptic meteorological analysis by a meteorologist it appears better to develop a 50-km product;
- The way information is presented in terms of geographical projection, data resolution, symbols (wind vectors/barbs) may be improved;
- The easy accessibility through the use of a clickable map is important to control the abundance of wind products of SeaWinds;
- Untimely availability of the wind products renders them useless in many cases for the meteorologists
- Familiarity with the products should be increased through user support.

11 REFERENCES

Anderson et al, 1999, A Variational data assimilation scheme and its use of meteorological observations, Doctoral dissertation, Dept. of Meteorology, Un. of Stockholm, Sweden, ISBN 91-7153-997-2.

Atlas, R., and R.N. Hoffman, 2000, The Use of Satellite Surface Wind Data to Improve Weather Analysis and Forecasting, in Satellites, Oceanography, and Society, edited by D. Halpern, Elsevier Oceanography Series 63, Elsevier Science, Amsterdam, the Netherlands, ISBN 0-444-50501-6.

Buel, C. Eugene, 1972, "Correlation Functions for Wind and Geopotential on Isobaric Surfaces", Journal of Applied Meteorology, pages 51-59.

Courtier, P., et al, 1998, The ECMWF implementation of three dimensional variational assimilation (3D-Var). Part I: Formulation, Quart. J. Royal Meteorol. Soc. 124, 1783-1808.

ESA, 1999, The atmospheric dynamics earth explorer mission, ESA SP1233(4), ESA/ESTEC, Noordwijk, the Netherlands.

Figa, J., A. Stoffelen, 1999, Towards an Improved Ku-band scatterometer wind product, Final report of the EUMETSAT NSCAT Fellowship, KNMI, de Bilt, the Netherlands.

Figa, J., and A. Stoffelen, 2000, On the Assimilation of Ku-Band Scatterometer Winds for Weather Analysis and Forecasting, IEEE-Transactions on Geoscience and Remote Sensing (special issue on Emerging Scatterometer Applications) **38** (4), pp. 1893-1902.

HIRLAM, 2000, http://www.knmi.nl/hirlam.

Isaksen, L., and A. Stoffelen, ERS-Scatterometer Wind Data Impact on ECMWF's Tropical Cyclone Forecasts, IEEE-Transactions on Geoscience and Remote Sensing (special issue on Emerging Scatterometer Applications) **38** (4), pp. 1885-1892.

Jones, Linwood, and David G. Long, 1999, QuikSCAT Radiometric Calibration and Special Brightness Temperature Product, Proceedings from the QuikSCAT cal/val - early science meeting, 2-5 November 1999, JPL, Pasadena, California.

KNMI satellite section web site. http://www.knmi.nl/onderzk/applied/en/sd_index.html

Leidner, Mark, and Lars Isaksen, 2000, Ku-Band Scatterometer Data Assimilation, paper submitted to the Quarterly J. Royal meteorol. Soc.

Le Meur, Didier, Lars Isaksen, and Ad Stoffelen, "Impact of ERS-1/ERS-2 scatterometer tandem on the ECMWF 3D-var assimilation system", Proc. Of the third ERS symposium – space at the service of our environment, Florence, 17-21 March 1997, ESA special report, ESTEC, Noordwijk, the Netherlands, 1997.

Le Meur, Didier, Lars Isaksen, Ad Stoffelen, 1998, "Wind speed calibration of ERS scatterometer data for assimilation purposes at ECMWF", proc. CEOS Wind and Wave validation Workshop, held at ESTEC, Noordwijk, the Netherlands from 3-5 June 1997.

Lorenc, A. C., 1988, Optimal nonlinear analysis, Quart. J. Royal Meteor. Soc. **114**, pp. 205-240.

Portabella, Marcos, and Ad Stoffelen, EUMETSAT QuikSCAT Fellowship Progress Report, KNMI, de Bilt, the Netherlands, 2000.

Portabella, Marcos, and Ad Stoffelen, 2000, On Quality Control and Rain Detection of SeaWinds, J. Atmosph. Oceanic Technol., accepted.

Rohn, M., G. Kelly, and R. Saunders, 1999, Experiments with Atmospheric Motion Vectors at ECMWF, in Proc. of Fourth International Winds Workshop held 19-23 October 1998, EUMETSAT P24, ISSN 1023-0416, pp. 139-146.

SSMIS, 2000, http://xenon.aerojet.com/Weapon_Systems/Earth_Sensing/SSMIS/

Stoffelen, Ad, 1999, "A Simple Method for Calibration of a Scatterometer over the Ocean", J. Atm. and Ocean Techn. 16(2), 275-282; Appendix A of Stoffelen (1998a).

Stoffelen, Ad, 1998a, "Scatterometry", PhD thesis, ISBN 90-393-1708-9, http://pablo.ubu.ruu.nl/~proefsch/01840669/inhoud.htm.

Stoffelen, Ad, 1998b, "Error modeling and calibration; towards the true surface wind speed", J.Geoph. Res. 103 (C4), 7755-7766; Chapter IV of Stoffelen (1998a).

Stoffelen, Ad, "Calibration and validation in the backscatter domain", proc. CEOS Wind and Wave validation Workshop, held at ESTEC, Noordwijk, the Netherlands from 3-5 June 1997.

Stoffelen, A. C. M. and D. L. T. Anderson, 1997a, Scatterometer Data Interpretation: Measurement Space and Inversion, J. Atmosph. and Ocean Techn. 14 (6), 1298-1313; Chapter II of Stoffelen (1998a).

Stoffelen, A. C. M. and D. L. T. Anderson, 1997c, Ambiguity removal and assimilation of scatterometer data, Q. J. Roy. Meteorol. Soc., 123, 491-518; Chapter V of Stoffelen (1998a).

Stoffelen, A.C.M. and D.L.T. Anderson, "Wind retrieval and ERS-1 radar backscatter measurements", Adv. Space Res. 13 (5), pp. (5)53-(5)60, 1993.

Stoffelen, Ad and Paul van Beukering, "The impact of improved scatterometer winds on HIRLAM analyses and forecasts", BCRS study contract 1.1OP-04, report published by BCRS, Delft, The Netherlands, and HIRLAM technical report #31, published by IMET, Dublin, Ireland, 1997.

Vries, de, John, and Ad Stoffelen, 2000, 2D variational ambiguity removal, Project report for the BCRS, KNMI, de Bilt, the Netherlands.

Wentz, Frank, Deborah Smith, and Carl Mears, 1999, Rain and the QuikSCAT winds, Proceedings from the QuikSCAT cal/val - early science meeting, 2-5 November 1999, JPL, Pasadena, California.

WMO, 2000, meeting on French Christmas storms, Meteo-France, Paris, January 2000.

12 ACRONYMS

2D-VAR	2-dimensional AR
3D-Var	3-dimensional variational meteorological analysis
4D-Var	Variational meteorological analysis in space and time
ADEOS-I	Advanced Earth Observation System (1996-7)
ADEOS-II	Advanced Earth Observation System (2002)
AMSR	Advanced Microwave Instrument on ADEOS-II
AR	Ambiguity Removal
ASCAT	Advanced scatterometer on METOP
BCRS	Beleidscommissie Remote Sensing (Dutch)
BUFR	Binary Universal Format Representation
ECMWF	European Centre for Medium-range Weather Forecasts
ERS	European Remote Sensing Satellite
ESA	European Space Agency
EUMETSAT	European Organisation for the Exploitation of Meteorological Satellites
GMF	Geophysical Model Function
GMT	Greenwich time
HH	Horizontal polarisation emitted-Horizontal received
HIRLAM	HIgh-Resolution Limited-Area Model
JPL	Jet Propulsion Laboratory
KNMI	Royal Netherlands Meteorological Institute
METOP	Meteorological Operational satellite (2003)
MLE	Maximum Likelihood Estimator
NASA	National Aeronautics and Space Administration (USA)
NCEP	National Centre for Atmospheric Prediction (USA)
NOAA	National Oceanographic and Atmospheric Administration (USA)
NRMS	Normalised RMS
NRSP	National Remote-Sensing Programme (Dutch)
NSCAT	NASA Scatterometer
NWP	Numerical Weather Prediction
OI	Optimal (statistical) Interpolation
PreScat	Processor of ERS scatterometer data at KNMI
QC	Quality Control
QuikScat	NASA scatterometer mission with SeaWinds
RMS	Root-Mean-Squared
SAF	EUMETSAT Satellite Application Facility
SAG	Science Advisory Group
SD	Standard Deviation
SDE	Standard Deviation of Error
SeaWinds	NASA rotating pencil-beam scatterometer
SNR	Signal-to-Noise Ratio
SSM/I	Special Sensor Microwave Instrument
SWVC	Super WVC

VV	Vertical polarisation emitted-Vertical received
WMO	World Meteorological Organisation
WVC	Wind Vector Cell

13 ACKNOWLEDGEMENTS

We acknowledge NASA and NOAA for providing the QuikSCAT data and help using it, and the project and science teams for their inspiring meetings. The collaboration with ECMWF, and more in particular Mark Leidner, on visit from AER, and Lars Isaksen has proven very fruitful. EUMETSAT supports our activities within the context of the NWP SAF and by providing an EUMETSAT fellowship. This report has been written to finalise a work plan funded by the Dutch BCRS.

APPENDIX A:
BEOORDELINGSFORMULIER SEAWINDS PRODUKT

(S.v.p. een formulier per bericht)

DTG:
Bericht No:
Meteoroloog:

A. CLASSIFICATIE

Zou je deze situatie kenmerken als (omcirkelen s.v.p.):
1. ontwikkelend of opvullend systeem, zadelvlak;
2. ontwikkeld systeem met scherpe drukgradient;
3. scherp front, rug, of trog;
4. anders, namelijk .....

B. WAT KUN JE ER MEE DOEN?

Is het produkt waardevol en bruikbaar voor de meteorologische analyse:
1. Hoe zou je het kunnen gebruiken?
2. Voegt het produkt:
    a. essentiele informatie;
    b. belangrijke gegevens; of
    c. weinig

toe aan de bestaande analyse (omcirkelen s.v.p.)?

C. VERGELIJKING MET NOAA/NASA 25-KM PRODUKT:

1. Hoe is het KNMI-produkt vergeleken met het NASA/NOAA produkt:
    a. KNMI beter;
    b. NOAA/NASA beter;
    c. geen noemenswaardig verschil in kwaliteit?
3. Is er een belangrijk verschil in het gebruik van de KNMI en NOAA/NASA produkten?

D. EVENTUELE OPMERKINGEN

The User Support Programme 1996-2005 (USP-2) is implemented under the responsibility of the Netherlands Remote Sensing Board (BCRS) and the Space Research Organization of The Netherlands (SRON).

The objectives of the USP-2 are: to support Dutch users of information from future European earth observation systems in the development of applications for operational and scientific use; to develop the required national infrastructure and to support users in developing countries with applications for the purpose of sustainable development, in connection with activities carried out by ESA and EUMETSAT.

The USP-2 is financed from the national space budget. During the period 1996-2000 the USP-2 element under the responsibility of the BCRS is executed in connection with the National Remote Sensing Programme 1996-2000.

Publication of:

Netherlands Remote Sensing Board (BCRS)
Programme Bureau
Rijkswaterstaat Survey Department

P.O. Box 5023
2600 GA Delft
The Netherlands
Tel.: +31 (15) 269 11 11
Fax: +31 (15) 261 89 62
E-mail: p.b.bcrs@mdi.rws.minvenw.nl
BCRS homepage: http://www.minvenw.nl/rws/mdi/bcrs